12-2020

A Comparison of Methods to Measure Crop Water Use in South Carolina

Andrew C. Ewing
Clemson University

A COMPARISON OF METHODS TO MEASURE CROP WATER USE IN SOUTH CAROLINA

A Thesis
Presented to
the Graduate School of
Clemson University

In Partial Fulfillment
of the Requirements for the Degree
Master of Science
Biosystems Engineering

---

by
Andrew C. Ewing
December 2020

Accepted by:
Dr. Tom O. Owino, Committee Chair
Dr. Dale E. Linvill
Dr. José O. Payero
Dr. Diana C. Vanegas

ABSTRACT

The objective of this thesis was to compare cost-effective methods of measuring crop water use, known as evapotranspiration (ET), in South Carolina's humid climate. The methods analyzed were the surface renewal method (SR), the Eddy Covariance method (EC), large in-field weighing lysimeters, a newly developed pressure differential device (PDD), a Class A Evaporation pan, and the Penman-Monteith equation. In the first chapter, ET measurements obtained by SR were compared to ET measured by EC and weighing lysimeters. For reference, EC and SR track the energy budget to estimate ET, while the weighing lysimeters used in this study are box-like containers measured continuously for mass changes attributed to water gained or lost. Great agreement was observed between the surface renewal and EC methods ($R^2 \geq 0.89$), while agreement was weak or inconsistent between the surface renewal method and lysimeters. In the second chapter, a PDD was designed, fabricated, and tested in its ability to measure ET. Despite the PDD and its neighboring weighing lysimeter showing agreement in profile moisture changes, inferred PDD ET measurements showed little agreement with the lysimeter ($R^2 < 0.2$). The PDD appeared to be affected by a delay in measuring rainfall, among other factors, in comparison to the lysimeter. The study suggests that the PDD may not suit ET measurement but could be useful for subsoil measurements in other fields of study. In the third chapter, the Penman-Monteith equation and a Class A Evaporation Pan were analyzed. The two methods measured reference evapotranspiration (ET_o), and showed good agreement with each other ($R^2 = 0.95$). The results of the ET_o comparison were further used to develop pan coefficient values (K_p) and compare these to K_p values estimated from

equations recommended by the Food and Agriculture Organization (FAO). No significant difference was found in the K_p comparison. The Penman-Monteith ET_o measurements were then used a third time with weighing lysimeter data from the cotton field to develop a crop coefficient curve (K_c). The obtained K_c values were compared to FAO recommended K_c values, showing no significant difference. The study suggests that FAO recommendations for ET_o measurement, K_p estimation, and K_c values do apply to South Carolina.

DEDICATION

Thank You, God, for everything. This is Your Thesis.

ACKNOWLEDGMENTS

I want to thank a number of people who contributed to this effort. First, thank you, Becky Davis and Bayleah Cooper, for all of your help in the field and advice doing research work. Second, thank you, Committee, for your support and guidance in this process: Dr. Diana Vanegas, Dr. Christophe Darnault, Dr. Dale Linvill, Dr. José Payero, and our committee chair- Dr. Tom Owino. Third, thank you Dr. Kosana Suvočarev and Dr. Liyi Xu for your help with the Surface Renewal analysis. Fourth, thank you, Robert Cornell, of Missouri Northern Pecan Growers, Colby Cofield, Derek Coleman Justice, Michael Ewing, Doug Allen, and Clint Thackery in helping with the design and fabrication of a pressure differential device. In addition, thank you, Dr. Mike Marshall, Cash, Kinley, Trevor, and fellow Master's student Stewart Bell for your work in the cotton fields and supplying the needed information to write this Thesis. Lastly, thank you to Grandma Darline and Grandpa Don for your editing skills and input in writing this Thesis. Without each of you, this would not be accomplished.

Sincerely,

Drew

TABLE OF CONTENTS

Table of Contents (Continued)

Page

LIST OF TABLES

List of Tables (Continued)

Table Page

LIST OF FIGURES

List of Figures (Continued)

List of Figures (Continued)

Figure Page

DEFINITIONS

3D – Three Dimensional
Cas. – Castellví Method
EC – Eddy Covariance Method
ET – Evapotranspiration
ET_o – Standard Reference Evapotranspiration
FAO – Food and Agriculture Organization of The United Nations
K_c – Crop Coefficient
K_p – Evaporation Pan Coefficient
PDD – Pressure Differential Device
REC – Research and Education Center
SR – Surface Renewal Method
UGA – The University of Georgia

INTRODUCTION

Cotton is among the most valuable agricultural field crops in South Carolina. As the #2 grossing crop in the state, cotton made up nearly 20% of the state's crop revenue in 2017 at $169,107,000 (USDA-NASS, 2018). A key parameter of interest in growing these field crops is overall crop water use. Traditional methods of estimating crop water use center around the evapotranspiration (ET) rate, which encompasses the total evaporation and transpiration of water vapor by the crop and surrounding soil (Rosenberg, 1974, p. 159). Since ET is largely impacted by relative humidity, solar radiation, air temperature, and wind speed, there is potential for region-to-region variability in the actual ET rate of a specific crop (Lu et al., 2005). A stated interest of researchers and farmers is to better understand the actual crop water use rates for cotton in South Carolina. This will be the main objective of this Thesis, with a sub-objective of testing practical, accurate, and cost-effective ET measurement methods.

As part of its efforts to help improve the capabilities of its agricultural sector, South Carolina has created several Research and Extension facilities throughout the state in partnership with Clemson University and its Extension Agency--Clemson Public Service and Agriculture. Among these facilities is the Edisto Research and Education Center near Blackville, SC. At this facility, a team of around 25 individuals is employed full-time to conduct research and extension programs on the facility's 2,000+ acres.

This thesis has three chapters, each describing a separate study that employed a low-cost ET measurement method in comparison to one or more standard measurement methods of ET. The objectives of each chapter are detailed as follows.

Chapter One:

1. To test the surface renewal method's performance in estimating ET of a cotton crop as compared to the ET measured by a weighing lysimeter and by the Eddy Covariance method.

Chapter Two:

1. To develop, fabricate, and test a pressure differential device (PDD) for determining crop ET.
2. To compare the performance of the PDD in measuring crop ET with ET measurements from a lysimeter

Chapter Three:

1. Compare ET_o measurements obtained from a Class A evaporation pan with those obtained using the Penman-Monteith equation.
2. Develop Pan Coefficient (K_p) values based upon the Penman-Monteith ET_o comparison.
3. Develop a crop coefficient curve from lysimeter data for a cotton crop growing in the southeastern humid climate.

REFERENCES

Lu, J., Sun, G., McNulty, S. G., & Amatya, D. M. (2005). A comparison of six potential evapotranspiration methods for regional use in the southeastern united states. *JAWRA Journal of the American Water Resources Association, 41*(3), 621-633. doi:10.1111/j.1752-1688.2005.tb03759.x

Rosenberg, N. J. (1974). *Microclimate: The biological environment*. New York: Wiley.

USDA-NASS. (2018). *2017 south carolina state agriculture overview* USDA-NASS. Retrieved from https://www.nass.usda.gov/Quick_Stats/Ag_Overview/stateOverview.php?state=SOUTH CAROLINA

CHAPTER ONE

EVALUATION OF THE SURFACE RENEWAL METHOD FOR MEASURING CROP EVAPOTRANSPIRATION IN SOUTH CAROLINA

Introduction

The surface renewal method was first applied to micrometeorology in the early 1990's (Paw U et al., 1995) after it was observed that structured ramp patterns could account for a majority of the momentum and heat transfer in and above a forest canopy (Gao et al., 1989). The method itself is a simpler version building upon similar work done in other fields around the renewal process. The renewal process used in this paper is when air parcels come into contact with the crop canopy, heat up, and then are ejected away from the canopy, only to be renewed by other cooler air parcels that sweep down and take their place (Paw U et al., 1995). Through tracking air temperature at high-frequency time intervals, one can observe these air parcels ejecting in a ramp-like fashion. The ramp-like shape of ejection is referred to as surface ramps, and its trajectory is determined by the amount of heat contained in the air parcel. Through continuously measuring the air temperature, a flux of sensible heat over time can be calculated. This sensible heat flux can then be combined with measurements of net radiation and soil heat flux, using the Energy Budget method, to estimate the flux of energy associated with water leaving the canopy as a vapor. This energy flux associated with lost water vapor is referred to as the latent heat flux. By the use of a thermodynamic specific heat value, one can use the latent heat flux to quantify the mass of water leaving the crop canopy over time, known as Evapotranspiration (ET).

The advantages of using the Surface Renewal method is that the equipment necessary for measurement is typically more affordable (Suvočarev et al., 2019) and has been to shown to perform well under relaxed fetch conditions compared to the Eddy Covariance method (Haymann et al., 2019; Paw U et al., 1995).

The objective of this study was to test the surface renewal method's performance in estimating ET of a cotton crop as compared to the ET measured by a weighing lysimeter and and by the Eddy Covariance method. This comparison had previously been mentioned as a beneficial area of further study in addition to the use of Eddy Covariance over a cotton crop in a humid environment (Suvočarev et al., 2019). Other studies have had success comparing the Surface Renewal method with weighing lysimeters to measure ET. These were compared using a short grass canopy and grapevines growing in a vineyard (Parry et al., 2019; Castellví and Snyder, 2010a).

A sub-objective of this study was to test the practicality for farmers of using the Surface Renewal method for agricultural water management.

Background

Energy Budget

Before focusing on the Surface Renewal method, the Energy budget first needs to be understood. The Energy budget method measures net incoming energy and tracks where it is transferred at the soil-crop-air interface as indicated in **Figure 1.1**.

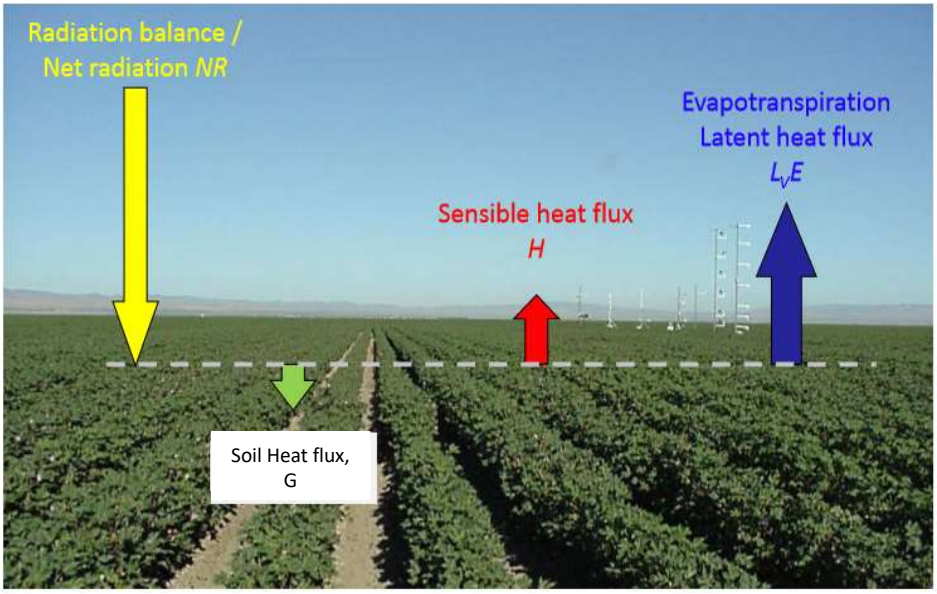

Figure 1.1. Energy Budget Variables

Modified from (ETH Zürich, n.d.)

In **Figure 1.1** , there is one energy source and three energy sinks. The energy source is Net radiation, which is the amount of energy retained from incoming solar radiation after accounting for energy losses such as albedo (reflected solar radiation) and the earth's emission of long-wave radiation back out into the atmosphere. The three sinks are Soil Heat flux, Sensible heat flux, and Latent heat flux. Soil Heat flux is the amount of energy that goes into heating up the soil and soil-water. Sensible heat flux is the amount of energy that goes into heating up air particles. Lastly, Latent Heat flux is the amount of energy that turns water into vapor. The one-dimensional energy balance equation is as follows:

$$R_n = G + H + L * E \tag{1.1}$$

where
R_n = Net radiation (W/m^2)
G = Soil Heat Flux (W/m^2)
H = Sensible Heat Flux (W/m^2)

L = Latent heat of vaporization (kJ/kg)
E = Mass transport rate at which water is evaporated and transpired ($\frac{\text{kg}}{\text{m}^2\text{s}}$)

In **Equation 1.1**, it is assumed that the energy retained by photosynthesis and other miscellaneous processes is less than the standard error of measurement, and therefore considered negligible (Rosenberg, 1974). By manipulating **Equation 1.1**, the volume of water lost can be calculated as:

$$E = \frac{R_n - G - H}{L} \tag{1.2}$$

The measurement of total soil heat flux is done using **Equation 1.3,** below, for each set of soil measurement equipment. **Equation 1.3** comes from a Surface Renewal datalogger program designed by a research team at the University of California, Davis (Shapland et al., 2013) who cite de Vries (1963) and Jensen, Burman, and Allen (1990) in deriving the equation.

$$G = (0.837 * \rho_{soil} + 4.19 * \theta) * 10^6 * \left(\frac{\Delta T}{t}\right) * d + P \tag{1.3}$$

where
G = Soil Heat Flux (W/m^2)
ρ_{soil} = Soil Bulk Density (Mg/m^3)
θ = Volumetric Water Content (m^3/m^3)
ΔT = Change in Soil Temperature in last 30 minutes (˚C)
t = Time elapsed (s)
d = Depth of measurement for Soil Heat Flux plates (m)
P = Heat Flux measurement taken from Soil Heat Flux plate (W/m^2)
0.837 = Specific Heat of Soil ($\frac{\text{J}}{g*^{\circ}\text{C}}$)
4.19 = Specific Heat of Water ($\frac{\text{J}}{g*^{\circ}\text{C}}$)
10^6 = Conversion factor of $\frac{\text{Mg}}{m^3}$ to $\frac{\text{g}}{m^3}$ for bulk densities of soil and water

Surface Renewal Method

The Surface Renewal method is similar to other Energy Budget methods, such as the Eddy Covariance method, but differs in how it measures energy flux of sensible or latent heat. The methodology focuses on measuring individual air parcels as they are ejected from the crop canopy. To illustrate the surface renewal process, **Figure 1.2** is shown below:

Figure 1.2: Illustration of Surface Ramp

In **Figure 1.2,** the red box with red arrows is meant to represent a parcel of air as it travels across a crop field. It can be seen in the figure that the air parcel "sweeps" into the crop canopy and then is "ejected" upwards. This is because sunlight has heated the crop canopy so that it is warmer than the air above it. These conditions are referred to as unstable conditions. Under these conditions, parcels within the canopy will be heated. Since air warmer than its surroundings tends to rise, the air within the canopy would then be ejected

upwards. When air within the canopy ejects, it will be replaced by a cooler air parcel that sweeps in from above to renew the process. The ejection process takes place in a ramp-like structure, which can be measured and is referred to as a surface ramp.

When measured, it is observed that this transfer takes place in batches, rather than a continuous process. By measuring the surface ramps and ejection process at high frequency (e.g. 10 Hz) the surface renewal method can estimate energy fluxes into sensible and/or latent heat. By measuring the air temperature continuously above the crop canopy, a temperature structure similar to that shown in **Figure 1.3** would be observed.

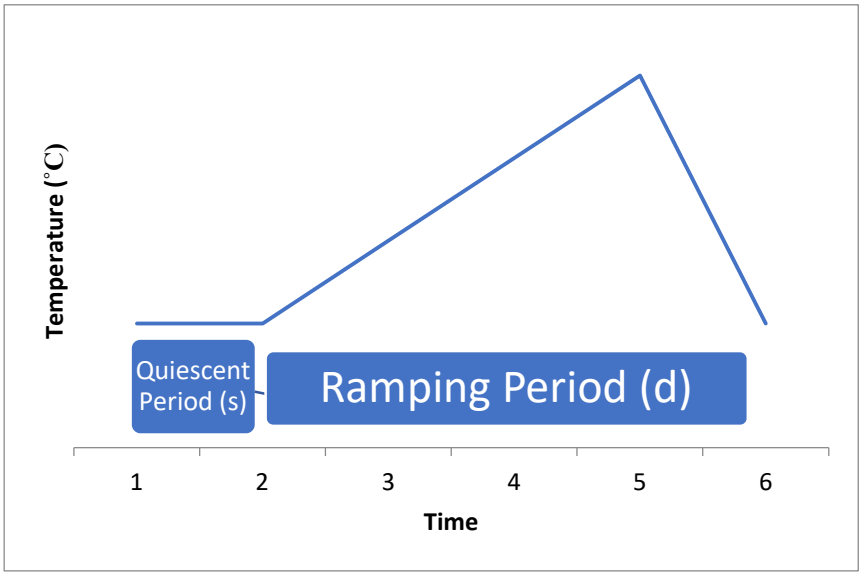

Figure 1.3. Surface Renewal Temperature Time Series

In the illustration, the first two time steps represent a quiescent period of time where no interchange is occurring between the crop canopy and the boundary layer above. Time steps two through five show an ejection of a warmed air parcel out of the crop canopy. The period from time step five to six shows a new cooler parcel of air sweeping in to "renew" the canopy after losing the ejected air parcel.

Through measuring temperature of the air parcels at high frequency, the Surface Renewal method calculates energy fluxes. For this study, we measured the sensible heat flux and estimated the latent heat flux using the residual energy left over from **Equation 1.1.** The sensible heat flux was calculated through ramp structure calculations developed by CW Van Atta (1977) and further applied to the Surface Renewal analysis (Spano et al., 1997; Paw U et al., 1995). The ramp calculations are shown in **Equations 1.4** through **1.11**:

The first step is to calculate the structure function's time lag for the ramp calculations. This is done using **Equation 1.4** below (Shapland et al., 2013):

$$r = \frac{j}{f} \tag{1.4}$$

where
r = structure function time lag (s)
j = # of samples lagged (unitless)
f = sampling frequency (Hz)

With the time lag, the structure function can be calculated for the 2nd, 3rd, and 5th orders from the temperature time series data and the structure function calculation in **Equation 1.5,** below (Shapland et al., 2013).

$$S^n(r) = \frac{1}{m-j}\sum_{k=1}^{m-j}\left[\left(T_k - T_{k-j}\right)^n\right] \tag{1.5}$$

where
S^n = nth order structure function (˚C)^n
r = structure function time lag, defined in **Equation 1.4** (s)
m = total number of points in the time series
j = # of samples included in the time lag
T_k = kth element in the temperature time data (˚C)
n = order being evaluated

Using the structure function and time lag, a calculation of the surface ramp amplitude can be made using **Equations 1.6 through 1.8,** below (Shapland et al., 2013):

$$p = [10 * S^2(r) - \frac{S^5(r)}{S^3(r)}] \quad (1.6)$$

$$q = 10S^3(r) \quad (1.7)$$

$$0 = a^3 + pa + q \quad (1.8)$$

where
a = ramp amplitude (˚C)
p = intermediate variable used for ramp calculation (˚C)^2
q = intermediate variable used for ramp calculation (˚C)^3

In addition, the ramp period can be calculated using **Equation 1.9,** below (Shapland et al., 2013):

$$\tau = d + s = -\frac{a^3 r}{S^3(r)} \quad (1.9)$$

where
τ = ramp period (s)
d = duration of the air parcel heating (s)
s = quiescent period that follows the sweep (s)
a = ramp amplitude (˚C)
r = structure function time lag (s)
$S^3(r)$ = 3rd order structure function ((˚C)^3)

An uncalibrated sensible heat flux is then calculated using **Equation 1.10** (Shapland et al., 2013):

$$H'_{SR} = z\rho c_p \frac{a}{\tau} \quad (1.10)$$

where
H'_{SR} = uncalibrated Surface Renewal sensible heat flux (W/m^2)
z = measurement height of the thermocouple (m)
ρ = air density (1.225 kg/m^3)
c_p = specific heat of air at constant pressure (1004.67 $\frac{J}{kg*^\circ C}$)
a = ramp amplitude (˚C)
τ = ramp period (s)

However, it has been shown that a calibration coefficient is important to include for estimating the true sensible heat, as it corrects for unequal mixing within the air parcel (Castellví and Snyder, 2010b). Therefore, the true sensible heat can be calculated using **Equation 1.11,** below (Hu et al., 2018):

$$H_{SR} = \alpha z\rho c_p \frac{a}{\tau} \quad (1.11)$$

where
H_{SR} = calibrated sensible heat flux (W/m^2)
α = calibration coefficient
z = measurement height of the thermocouple (m)
ρ = air density (1.225 kg/m^3)
c_p = specific heat of air at constant pressure (1004.67 $\frac{J}{kg*^\circ C}$)
a = ramp amplitude (˚C)
τ = ramp period (s)

Once net radiation, sensible heat flux, and soil heat flux have been quantified, the rate of ET can be estimated. By assuming energy balance closure with the use of **Equation 1.2**, the residual amount of energy left over can be attributed to latent heat flux. This latent heat flux is then divided by a latent heat of vaporization constant to calculate the mass of water lost to evapotranspiration.

Eddy Covariance Method

As an additional reference for this study, Eddy Covariance measurements were taken over the cotton canopy. The Eddy Covariance method is another energy budget method useful for the measurement of sensible heat flux, latent heat flux, and ET. This method often needs to be sited higher than the surface renewal method to make sure the Eddy Covariance instruments are in the inertial sublayer to measure the flux of turbulent air currents known as eddies (Burba, 2013). These eddies can be seen when one looks across the surface of the earth on a hot day as unusual swirls of clear air. Since vaporized water and heated air are mixed in a gaseous state when they exit the crop canopy, Eddy Covariance towers often utilize a 3D sonic anemometer and an Infrared Gas analyzer (IRGA) to instantaneously measure the air temperature, the 3-dimensional movements of the eddies, and the density of CO_2 and water vapor to measure ET and other fluxes.

As a reference for this study, we used the Eddy Covariance method to calculate sensible heat flux and estimate the Latent Heat flux as the residual energy left over from **Equation 1.1**. Measurements were taken using a 3D sonic anemometer to measure air temperature and the 3-dimensional movements of the eddies as they rise from the surface. The equations used for the calculation of sensible heat flux involve a two-dimensional rotation correction and tilt-correction, which are laid out in the datalogger program designed by Shapland et. al (2013). The final equation used to calculate sensible heat flux using Eddy Covariance is below, in **Equation 1.12** (Shapland et al., 2013).

$$H_{EC} = \rho_{air} c_p (w' T_s') \quad (1.12)$$

where
H_{EC} = Eddy Covariance calculated sensible heat flux
ρ_{air} = air density (g/m^3)
c_p = specific heat per unit mass of air at constant pressure ($\frac{J}{g*K}$)
w' = instantaneous departure from the mean vertical wind velocity (m/s)
T_s' = instantaneous departure from the mean air temperature measured by the sonic anemometer (˚C)

Like other Energy Budget methods, once net radiation, sensible heat flux, and soil heat flux have been quantified, the rate of ET can be estimated through assuming energy balance closure with **Equation 1.2.** This is done through attributing the residual amount of energy left over as the latent heat flux. This latent heat flux is then divided by a latent heat of vaporization constant to calculate the mass of water lost to evapotranspiration.

Methods and Materials

The measurements for this study took place over two adjacent cotton fields at the Clemson Edisto Research and Education Center (REC) near Blackville, South Carolina (33° 21’ 34” N; 81° 19’ 56” W). The Köppen-Geiger climate classification for the site is Cfa, which classifies the site as temperate (C), fully humid (f), with hot summers (a) (Peel et al., 2007). The equipment utilized includes two in-field weighing lysimeters and two energy budget towers for replication. All measurement equipment was placed in the north cotton field.

Field Management and Dates

Cotton planting in the fields and around the measurement setups was over a couple of weeks, and early growth was inhibited due to lack of rainfall in May and early June. The cotton was planted across the southern field on May 16th with Deltapine variety 1636. The

northern field was planted on May 20th, 2019 with Deltapine variety 1538. Both lysimeters were planted on May 24th. The rows immediately surrounding both lysimeters were unable to be planted mechanically, so they were planted manually on May 25th and 26th. In addition, an area up row 1.5 m WNW of the South Lysimeter was replanted with Deltapine 1538 on June 5th to recover from damage sustained from digging and placing devices used in Chapter 2 of this Thesis. The north field rows were on 0.97 meter (38") spacings for the north field, while the south field was on 0.91 m (36") spacings. No rainfall was received on the sandy soil from 13 May to 4 June. Irrigation did supplement the lack of rainfall, though early growth was still inhibited. Defoliation occurred the week of 15 October. The north field cotton crop was harvested on 11 November. The south field cotton crop was harvested on 8 October. The northern half of the north field, which includes the North Lysimeter, had a deep-tillage rye cover crop grown over the winter and spring leading up to its termination in early May 2019. The rest of the fields had previously been fallow. In the prior year's growing season, 2018, peanuts were grown across the entire north field but had not been harvested due to excess rain during harvest season.

Cotton height measurements were taken regularly throughout the season to account for growth. Measurements were taken twice weekly (Monday and Friday) from the dates of June 10th to September 3rd, with the exception of July 26th. Beginning September 13th, the cotton plant heights were measured each Friday through October 4th. No measurements were taken between September 3rd and 13th. A growth retardant was applied to the cotton plants on August 14th and October 4th. Plant height measurements were discontinued after October 4th, since it was expected that the crop height would not change beyond this date.

It was observed that early cotton growth varied most by row. Therefore, it was decided to measure one cotton plant per row, to account for the variability. The method of measurement consisted of walking a straight path northeast, in a manner perpendicular to the rows, starting from the southernmost row of the north field to the south lysimeter. Each plant encountered would be measured. If a row was missing a plant, the measurement for that row was skipped. The same procedure was followed in the northern half of the north field, where the rye was grown previously, starting at the southernmost row walking to the north lysimeter – perpendicular to the rows. This procedure was followed beginning June 17th. Three plants were measured in each lysimeter to compare lysimeter growth to the field beginning June 21st for the South Lysimeter and consistently for both Lysimeters from July 12th on. A diagram of the layout and each measurement path is shown on the following page in **Figure 1.4**. In total, this amounted to ~17 plants measured in the south path and ~15 plants measured in the north path each measurement date. One of the two field technicians helping with the study, mentioned that the true field edge should have a shorter crop height due to crosswind drying out the field edge faster. An advantage of starting from the south end of both field segments is that it should minimize the influence field edge has on crop height measurements.

Figure 1.4. Paths used for the measurement of Cotton Heights
Modified and Used with Permission from Zoom Earth (Zoom Earth et al., 2018)

In-Field Weighing Lysimeters

Two in-field weighing lysimeters were used as the baseline method of comparison for this study. A weighing lysimeter works by weighing a soil column in regular time intervals. The soil column is held in an inner container, which is filled with soil matching the surrounding field and then oftentimes planted to grow a crop at the same rate as a surrounding field. To help provide a visual reference, **Figure 1.5**, is shown on the following page which includes the cotton plants used in the study.

Figure 1.5. Weighing Lysimeter Planted with Cotton

The goal of the lysimeter is to measure changes in mass in terms of a depth of water evaporated or transpired. It is assumed that changes in mass due to air, plant growth, or soil mass are negligible when measurements are taken in short time intervals. Therefore, changes in mass can be attributed to water gained or lost.

The two in-field weighing lysimeters that were used in this study had been installed in the A12 fields at the Edisto Research Facility. The dimensions of each weighing lysimeter are 1 m wide x 1 m long x 1.5 m deep. The lysimeters are roughly 33 meters away from each other. For reference throughout the study, this southernmost lysimeter will be referred to as the "South Lysimeter", while the northernmost lysimeter will be referred to throughout as the "North Lysimeter". Each lysimeter was calibrated ($R^2 >= 0.9999$) and measured by four CZL301 S Type load cells (Phidgets, Calgary, AB, Canada). Soil volumetric water content measurements were taken at different depths within the lysimeters using an ENVIROSCAN water-content-profile probe (Campbell Scientific, Logan, Utah, USA). An internal gravity drainage system was placed within the device using a perforated PVC pipe installed horizontally along the bottom of the lysimeter. A

vertical riser pipe connects to the perforated pipe, so that a pump can be used at the surface to pump out the water accumulated in the drainage pipe and the riser as needed. To give a better understanding of the weighing lysimeter design, a CAD model of the original design is shown below in **Figure 1.6**. This original design was modified when the lysimeters were moved to the current location in 2018.

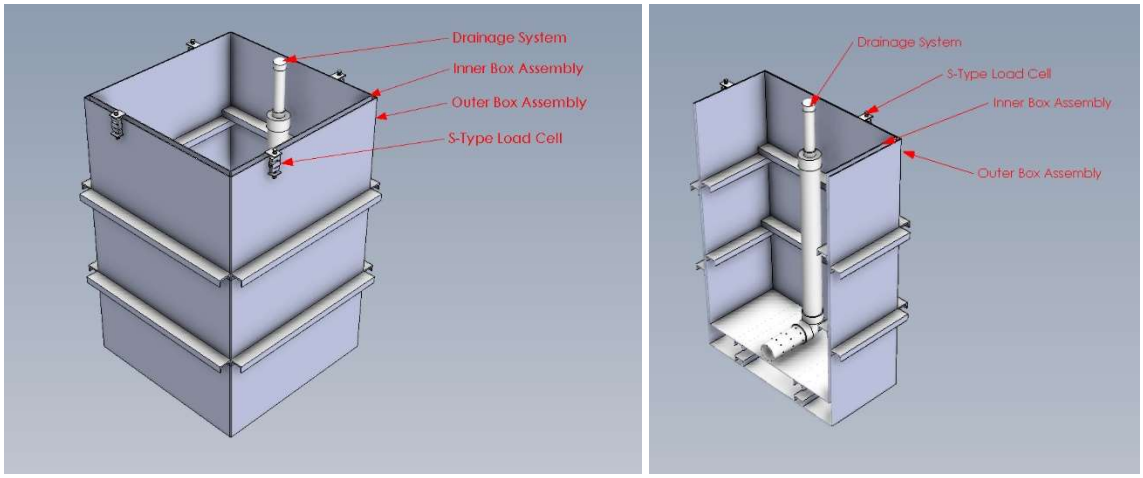

Figure 1.6. Lysimeter CAD Model
Modified from (Justice, Derek C., 2020)

In the study, each lysimeter utilized a Campbell Scientific CR1000X datalogger (Campbell Scientific, Logan, Utah, USA) and output results on 10-minute time intervals. The south lysimeter took a measurement every 5 seconds and output the average of these measurements for each 10-minute interval; whereas, the North Lysimeter output a one-time sampling at the end of each 10-minute time interval. For comparison with the surface renewal measurements, only the values recorded at the beginning of each hour and half-hour were retained from each lysimeter's data. The difference between each successive 30-minute output was computed in terms of mm of water.

In total, it is estimated that the lysimeter equipment used for this study costs roughly $4,215 for each weighing lysimeter. This is based on a 2020 United States Dollar

value by applying the Consumer Price Index inflation from 2001 to 2020 to the estimated cost of building the lysimeter in 2001 (in2013dollars.com, 2020; Fisher, 2003). The total cost per lysimeter includes roughly $2,595 for current datalogger and power equipment costs. The total costs do not include the cost of installing the lysimeter in the field. A more in-depth cost analysis is included in **Appendix K**.

Energy Budget Towers: Surface Renewal and Eddy Covariance Methods

The Surface Renewal methodology employed by the team encompassed using 2 separate energy budget towers for replication. Each tower was sited nearby a weighing lysimeter. The tower sited near the South Lysimeter will be referred to as the South Tower. The tower sited next to the North Lysimeter will be referred to as the North Tower. Both towers were originally sited ESE 1.83 meters of their respective lysimeters, and in the same cotton row as their respective lysimeter. The siting of each tower was chosen with the anticipation that the predominant wind direction would be westerly, so that each tower would measure its lysimeter and the vicinity around the lysimeter. However, the South Tower was moved on July 10th 4.5 m to the East of the South Lysimeter due to lagging growth in the immediate vicinity around the south lysimeter. The lagging growth is believed to be due to compaction from the South Lysimeter's installation the previous year. A layout of the field and ET measurement equipment is shown in **Figure 1.7**.

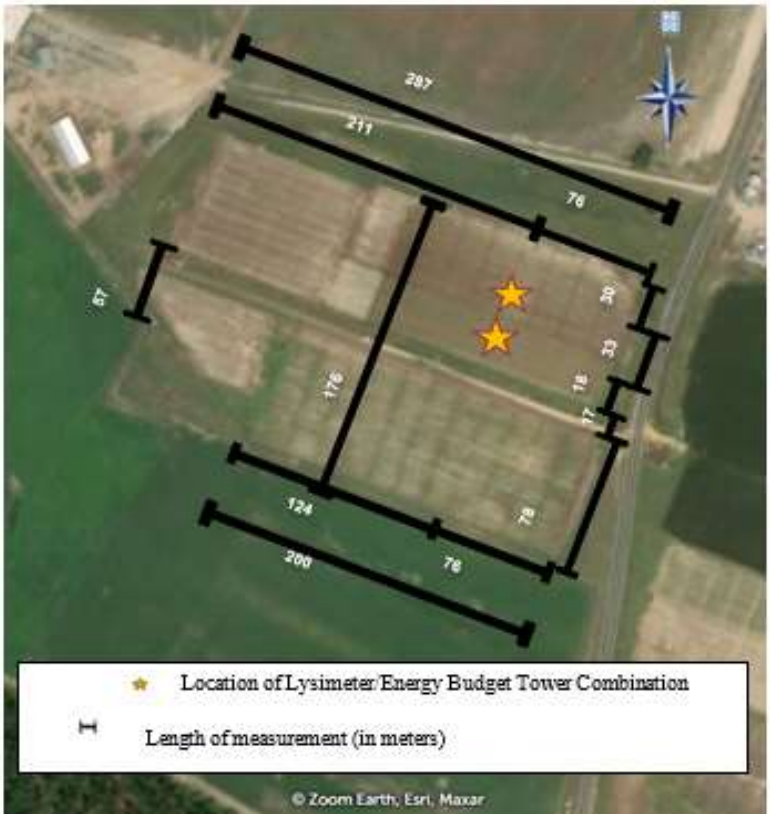

Figure 1.7. Dimensions of Field Layout for Equipment
Modified and Used with Permission from Zoom Earth (Zoom Earth et al., 2018)

Simple dimensions are also included in **Appendix B**, showing the distance to a field edge or field corner for each tower. Manual distance measurements were taken from the field using a Lufkin Hi-Viz MW38 measuring wheel (Apex Tool Group, Sparks, Maryland, USA) and by counting rows. In addition, online measurements were taken using earth.zoom and maps.google.com.

For the study, each tower utilized equipment to track the energy budget. Measurements were taken using a CR1000X datalogger (Campbell Scientific, Logan, Utah, USA). The datalogger ran a program modified from Shapland et. al (2013) to fit the equipment used in this study and to fit the Clemson University Edisto Research and Education Center's fields. Raw turbulent flux and temperature data were recorded at 10 Hz

frequency. Using the Van Atta calculations presented in the Background section, the datalogger calculated ramp characteristics and wrote these to a "PF" table. The programming used negative values to calculate the Surface Ramp characteristics using Van Atta's procedure to allow a wider range of acceptable negative w values during stable boundary layer conditions. A lag time of r = 0.5 seconds was used. These sensible heat calculations were then averaged over a thirty-minute time interval, with the final 30-minute averaged values being submitted to the Energy Balance (EB) table at the end of each ½ hour. The final values submitted to the EB table included sensible heat flux from both the EC and Surface Renewal methods, as well as sonic air temperature and other data concerning air movement. The residual ET calculation was made using a latent heat of vaporization (L) value of 2440 kJ/kg, an air density (ρ) of 1.225 kg/m^3, and a specific heat of air at constant pressure (c_p) of 1004.67 $\frac{J}{kg*^{\circ}C}$. A secondary slow sequence scan was run in parallel with the high-frequency scan. The slow sequence scan sampled all other instrumentation at 5-second intervals. The values from the slow sequence scan were output to the Weather (WX) and Energy Balance (EB) tables on 30-minute time intervals with either an average and/or a one-time sampling for the 30-minute period. A Quality Control (QC) table was output once a day with the maximum, minimum, average, and total values for different variables being measured so that these values could be observed to ensure the equipment was working properly.

Both setups were powered by a 100-Watt solar panel that charged a 12-volt battery. The southernmost battery and solar panel provided power for the south lysimeter, the south tower, and two devices used for a separate study. The northernmost battery and solar panel

provided power for the north lysimeter, the north tower, horizontal wind profile measurements, and two devices not used in this study.

For the Energy Budget tower, the equipment used and measurement heights are shown below in **Table 1.1**.

Table 1.1. Energy Budget Tower Equipment and Measurement Heights

Measurement	Instrument	# Used (per tower)	Height Above or (Below) Soil Surface
Net Radiation (Rn)	Kipp & Zonen NR Lite 2 Net Radiometer	1	2 m
Soil Heat Flux (G)	HukseﬂuxUSA HFP01 Heat Flux Sensors	2 (x2 sets) = 4	(0.08) m
	South Tower: Campbell Scientific CS-655 Soil Moisture and Temperature probe North Tower: Stevens Hydraprobe Soil Moisture and Temperature Probe	1 (x2 sets) = 2	(0.04) m
Sensible Heat Flux (H)	Gill WindMaster 3-D Sonic Anemometer	1	2.6 m
	Campbell Scientific FW3 Type E fine-wire thermocouples	1 x (2 heights) = 2	1.5 m 1.6 m
Solar Radiation (R_s)	Apogee SP-110 Silicon Pyranometer	1	2.1 m
Air Temperature and Relative Humidity	Campbell Scientific CS215 Air Temperature and Relative Humidity	1	~ 1 m
Horizontal Wind Velocity	Adafruit Anemometer Wind Speed Sensor w/Analog Voltage Output (PRODUCT ID: 1733)	1 (x2 heights) = 2	1.5 m 2.1 m

Two devices were used for radiation measurements. An NR Lite 2 Net Radiometer (Kipp & Zonen, Delft, South Holland, The Netherlands) was mounted at 2m above the ground surface to measure net radiation. The net radiometer was mounted at 2m. A secondary measurement was taken for solar radiation using an SP-110 Silicon Pyranometer (Apogee Instruments, Logan, Utah, USA) mounted at a height of 2.1m for both towers.

For the measurement of soil heat flux, the following methodology and equipment were used. For each tower, two sets of heat flux plates and two sets of soil moisture and temperature probes were placed in the soil. One set was placed in the crop row and the other in the middle of two crop rows. For the south tower, each set consisted of two HFP01 Heat Flux Sensors (HukseﬂuxUSA, Center Moriches, New York, USA) and one Campbell

Scientific CS-655 Soil Moisture and Temperature probe (Campbell Scientific, Logan, Utah, USA). For the north tower, each set consisted of two HFP01 Heat Flux Sensors (HukseflUXUSA, Center Moriches, New York, USA) and one Hydraprobe soil moisture and temperature probe (Stevens Water Monitoring Systems, Portland, Oregon, USA). The heat flux plates were placed at a depth of roughly 0.08m in the soil. The soil moisture and temperature probes were placed sideways in the soil profile so that they were halfway between the soil heat flux plates and soil surface. The placement of the heat flux sensors allowed the measurement of heat flux past the depth of 0.08m, while the measurement of both soil moisture and soil temperature allowed the calculation of heat stored above the heat flux plates. As introduced in the background section for calculating the soil heat flux, **Equation 1.3** was used. For the calculation, a soil bulk density of ρ_{soil} = 1.4 Mg/m^3 was used, while the time elapsed was set to 1800 seconds to calculate the change in energy stored over each 30-minute time interval.

The surface renewal measurements took place at two different heights above the soil surface. After an experiment redesign, the measurement heights were placed at 1.5 m and 1.6 m. The lower height, 1.5m, will be referred to as Thermocouple 1 ("T1"). The taller height, 1.6 m, will be referred to as Thermocouple 2 ("T2"). Each height utilized a Campbell Scientific FW3 Type E fine-wire thermocouple (Campbell Scientific, Logan, Utah, USA) for its measurements. Heights for the surface renewal measurements were chosen based upon four decision criteria. First, the concept of fetch was a main consideration. The surface renewal method is able to be deployed at lower heights than the Eddy Covariance method, which allows for less stringent fetch requirements (Castellví,

2012). Second, observations in previous studies had shown higher measurement heights might produce data that was unusable (Paw U et al., 1995) or produce a lower R^2 value (Poblete-Echeverría et al., 2014). Third, from Eddy Covariance reference material, it was noted that a transition between roughness and inertial sublayers would begin about 1.5 m above a bare soil surface (Burba, 2013, pp. 151, 154). This led to anticipation that a sensor height of ~1.5 m would measure in the roughness sublayer for the duration of the season without requiring a change in sensor height, to be more practical.

The Eddy Covariance method utilized a Gill WindMaster 3D Sonic Anemometer (Gill Instruments Limited, Lymington, Hampshire, UK). The height of measurement used for the sonic anemometer was 2.6 m above the soil surface. This height was chosen to best meet the requirements laid out for Eddy Covariance measurements over a short canopy (<2-3 m) while also remaining under the lateral move irrigation system being used for the north field. The requirements involved included: a measurement height (z_{EC}) 1.5 to 2 m above the crop canopy, z_{EC} > 2x the crop canopy height, z_{EC} > 3x the path length, z_{EC} < 1/100 the given fetch (Burba, 2013, p. 154). The sampling rate was 10 Hz for the sonic anemometer.

The estimated equipment cost for the Eddy Covariance method used in this study was $10,295 per tower, which includes about $2,595 for datalogger and power equipment. A more in-depth cost analysis is included in **Appendix K**.

For additional weather data, two other instruments were included on the energy budget tower. Relative humidity and air temperature measurements were taken near the canopy height using a Campbell Scientific CS215 Air Temperature and Relative Humidity

probe (Campbell Scientific, Logan, Utah, USA) mounted in an enclosed solar radiation shield (Campbell Scientific, Logan, Utah, USA) ~ 1 m above the soil surface. In addition, an attempt was made to use a TE525-L Tipping Bucket Rain Gauge (Texas Electronics, Dallas, Texas, USA) for each energy budget tower. However, challenges were experienced with the tipping bucket, so for this study rainfall was determined using each lysimeter directly. The determination of rainfall using the lysimeter was done by using the 2019 rainfall data of the adjacent Edisto Bull Forage Test facility (Sell, 2019) for reference. The Edisto Bull Forage Test facility recorded their rainfall data in 10-minute intervals utilizing a Vantage Pro Weather Station (Davis Instruments, Hayward, California, USA). The 10-minute data were summed to 30-minute and daily total rainfalls to be used as reference in the analysis. With all Surface Renewal equipment included, except the tipping bucket rain gauge, the equipment cost per Surface Renewal tower was estimated to be roughly $7,520. This includes $2,595 for datalogger and power equipment costs. A more in-depth cost analysis is included in **Appendix K**.

The overall cost per tower in this study was lower than the estimates provided in this Thesis chapter. This is because the datalogger and power equipment costs were shared between the three methods of measurement at each measurement site in the field.

Castellví Method

A current challenge of the surface renewal method is that it requires an additional reference measurement to generate a calibration coefficient. This coefficient depends on several factors such as canopy height, crop, measurement frequency, and stability conditions (Hu et al., 2018). The required calibration undermines the purpose of the surface

renewal method being an economical, standalone measurement source for localized ET measurements. To address this challenge, a method has been developed by F. Castellví to provide a calibrated surface renewal measurement based on local factors around the measurement location. The Castellví method comes from a combination of the Monin-Obukhov Similarity Theory and the Surface Renewal method (Castellví, 2004). The practicality for farmers of not needing a calibration interested the research team in testing this method. In addition, a paper focused on a similar wind profile method (Wang et al., 2005), made the research team further interested in the practicality of the Castellví method.

Equipment was installed to measure the additional variables for the Castellví method. Using the north tower, two horizontal cup anemometers (Adafruit Industries, New York City, New York, USA) were installed at 1.52 m (5 ft) and 2.13 m (7 ft) above the soil surface to measure horizontal wind speeds. It was presumed that these two horizontal wind speed measurement heights would allow for the measurement of differing behaviors in the roughness and inertial sublayers for at least part of the growing season (Burba, 2013). A photograph of the horizontal wind speed measurement setup next to the north tower is shown in **Figure 1.8**.

Figure 1.8. Castellví Horizontal Wind Speed measurement

Through collaboration with Dr. Kosana Suvočarev and Dr. Liyi Xu, sensible heat values were calculated using an iterative method (Castellví, 2004). The necessary inputs for the calculations were cotton plant height, horizontal wind speed, and raw 10 Hz thermocouple measurements. In the analysis, it was assumed that the 1.5 m horizontal wind speed measurement height could be applied to both the calculation of T1 (1.5 m) and T2's (1.6 m) sensible heat flux. A height correction was made for T2 post-calculation by dividing each half-hour flux using **Equation 1.14**. This correction was to account for T2's measurement height of 1.6 m above the ground surface.

$$H_{T2} = 1.6 * \frac{H'_{T2}}{1.5} \tag{1.14}$$

where
H_{T2} = Corrected T2 Sensible Heat flux
H'_{T2} = Uncorrected T2 Sensible Heat flux

An additional assumption made was that the horizontal wind speed measurements at the north tower could be applied for the south tower. What influenced this assumption

was that the field was relatively flat, there was a homogenous canopy cover, and the south tower was relatively close in the field (~33 m away).

Gap-Filling Methodology

Gap-filling was completed for the Eddy Covariance sensible heat flux measurements, uncalibrated Surface Renewal sensible heat flux measurements, and the computed Castellví sensible heat fluxes using an online tool supported by the Max Planck Institute for Biogeochemistry (Wutzler et al., 2018). The R-program utilizes the Marginal Distribution Sampling Method for gap-filling (Reichstein et al., 2005), a recommended method for gap-filling EC data. The tool was used only for gap-filling, with both u* filtering and flux partitioning being excluded in this analysis.

Fetch Analysis

A fetch analysis was undertaken to compare surface renewal and lysimeter measurements when the surface renewal method had adequate fetch. The analysis was completed over the season based upon the predominant wind direction for each half-hour. The required fetch was calculated using **Equation 1.15**, presented by Burba (2013) and mentioned in Castellvi's article evaluating the surface renewal fetch requirement (Castellví, 2012).

$$f = 100 * (z - d) \tag{1.15}$$

where
f = fetch requirement
z = sensor measurement height
d = 0.67 * cotton canopy height

The given upwind field distance was calculated for each degree azimuth based on the field measurements mentioned earlier in this section. Calculations were made by subdividing the field into 9 triangles, then using an excel spreadsheet that combined trigonometry and interpolation to calculate the distance from the tower to the field edge for each degree azimuth. A comparison was made for each 30-minute interval to determine if the half-hour's primary wind-direction had adequate upwind distance to meet the fetch requirements based upon the canopy height.

As the field may have inadequate fetch in some directions, the vegetation surrounding the field could influence the measured fluxes. The cotton fields are bordered to the south, the west, and the north by the Edisto Bull Forage test facility, which has different types of grass pasture. To the west of the Edisto Bull Forage Test facility is an evergreen forest and to the south of the Bull Forage pastures is a mixed stand of forest. Across the road from the cotton fields, to the East, is a field that grew corn during the growing season. Also across the road to the northeast is a forest of both mixed and evergreen trees.

Results

The analysis period for this study is from June 26th to November 10th.

Throughout the season various factors caused data to be discarded. For the north tower and north lysimeter, power outages were experienced intermittently overnight in August and September. In addition, a load cell failed on the north lysimeter in October, causing much of October's data to be discarded. For the south tower, a two-week period from August 5th to 21st was omitted due to a recording error during this time.

For the analysis period, the average air temperature near the top of the crop canopy was 24°C, while the average relative humidity was 78%.

Throughout the analysis, drying cycles were used for the periods of comparison. A drying cycle was defined as the period between two soil wetting events, such as rainfall or irrigation events. The use of drying cycles led to the best agreement in comparing surface renewal ET values and the Eddy Covariance and Lysimeter ET values. In all of the analyses, periods determined as soil wetting events were omitted.

Comparison with Eddy Covariance ET

The data for Eddy Covariance and Surface Renewal's ET estimations for each drying cycle are shown in **Figure 1.9**.

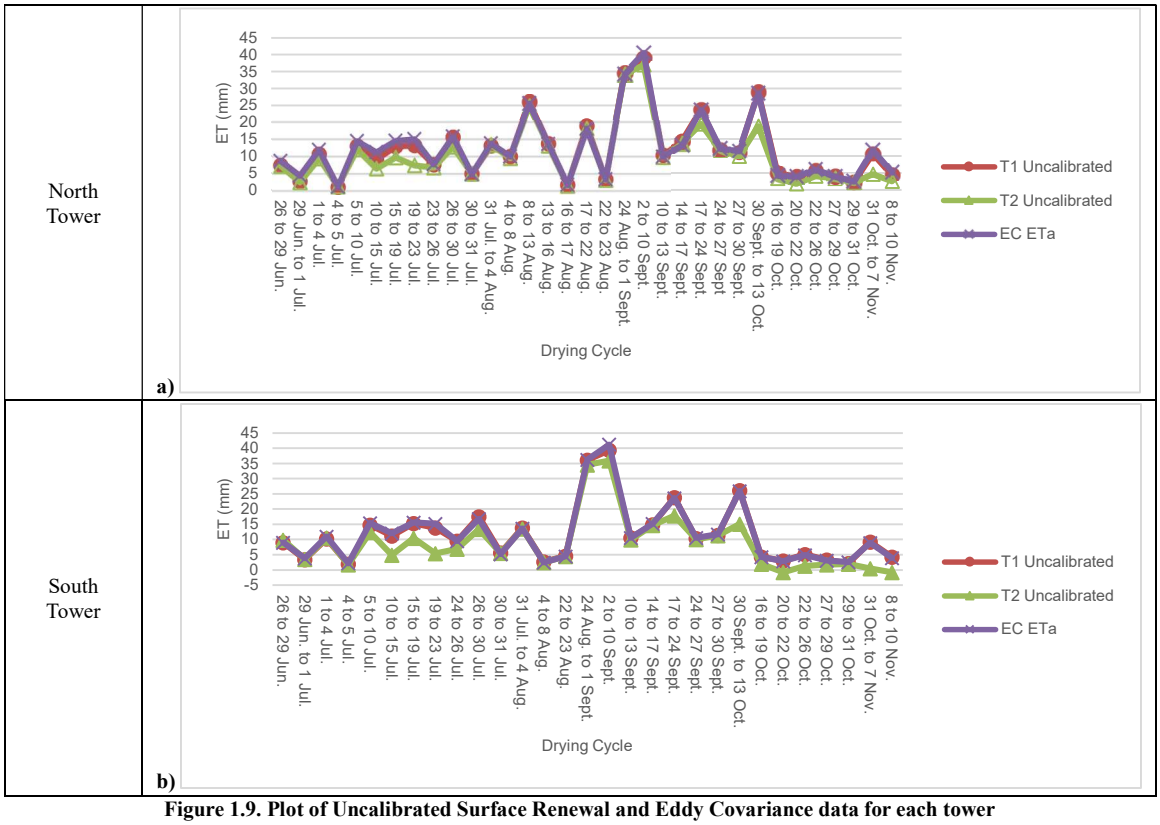

Figure 1.9. Plot of Uncalibrated Surface Renewal and Eddy Covariance data for each tower

When plotted against each other, the uncalibrated surface renewal and Eddy Covariance estimations of ET seem to be in agreement. A further analysis between the two methodologies is shown below in **Figure 1.10**.

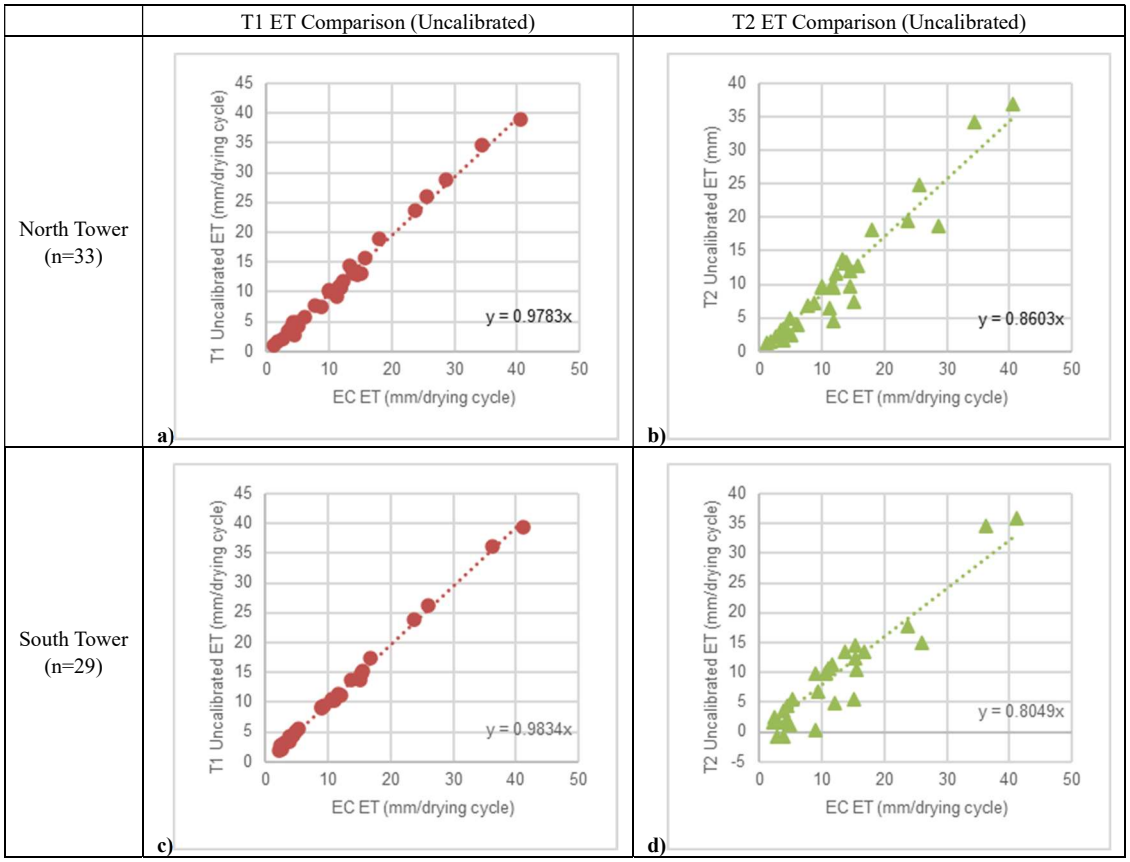

Figure 1.10. Surface Renewal Uncalibrated ET comparison to Eddy Covariance ET

In **Figure 1.10**, it can be seen that T1 has a stronger agreement than T2 with the Eddy Covariance ET values. The R^2 values of both setups for the T1 ET and EC ET comparison are >= 0.99 for both the north and south towers. While T2 ET and the EC ET had R^2 values of 0.93 and 0.89 for the north and south towers, respectively. One notable difference between the two heights is that the sensor that was closer to the crop canopy (1.5 m) showed an almost 1:1 slope with the Eddy Covariance ET values, whereas, the taller sensor height (1.6 m) showed a lower R^2 and underestimated ET based upon the EC ET

estimation. However, it should be noted that the field likely provided inadequate fetch for both the Eddy Covariance and Surface Renewal methodologies.

In addition to the uncalibrated comparison, a comparison was made including the Castellví method for calibrating the sensors. The results of the comparison are shown in **Figure 1.11**.

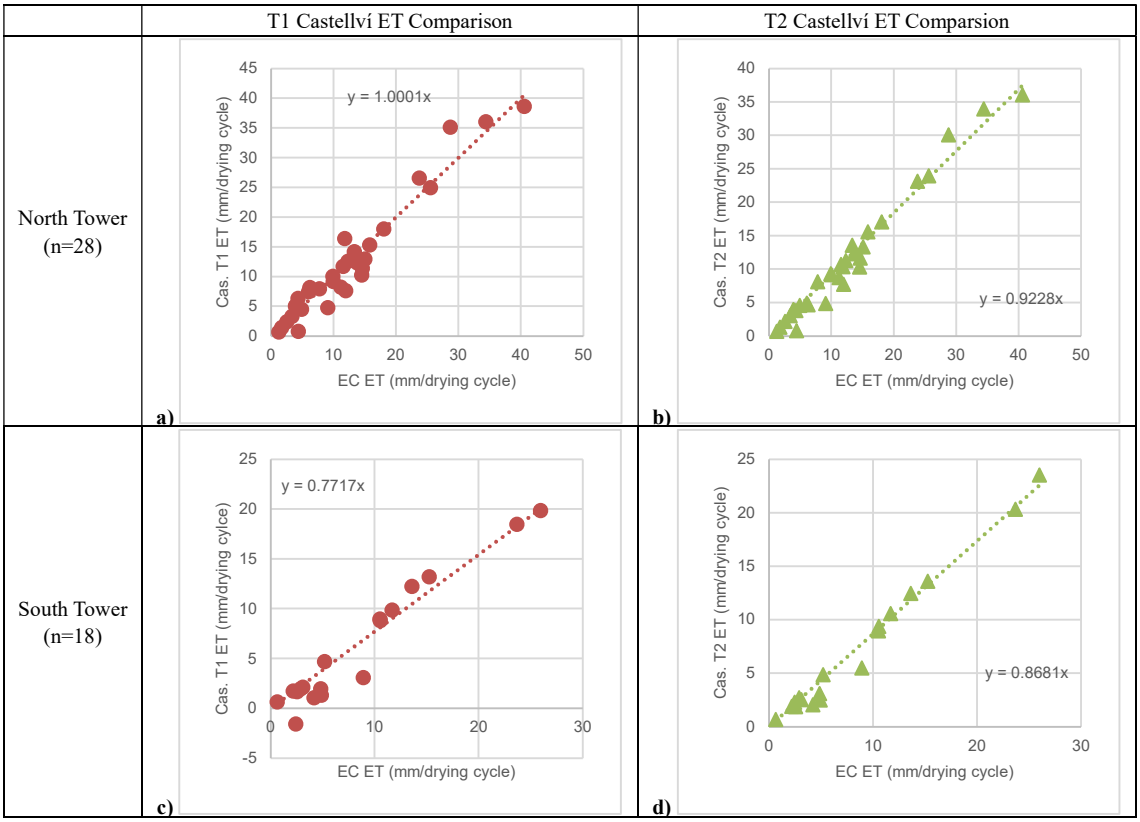

Figure 1.11. Castellví method ET comparison to Eddy Covariance ET estimation

In **Figure 1.11**, it can be seen that the Castellví method consistently underestimated the calibration coefficient compared to the Eddy Covariance method. The slope when comparing the two falls between 0.77 to 1 : 1 (Cas. ET:EC ET) for all towers and measurement heights. A positive result from the use of the Castellví method is that there was strong agreement between the Castellví and Eddy Covariance methods. The R^2 values

for T1 Castellví ET and EC ET were 0.94 for both the north and south towers. The R^2 for T2 Castellví ET and EC ET were 0.98 for the north and south towers.

Comparison with In-field Weighing Lysimeter ET

In comparing the lysimeter and surface renewal measurements, a significant difference (p-value < 0.05) was observed between the lysimeter plant heights and the field on measurement dates in July, August, and September. Therefore, data were excluded from the analysis if the closest measurement date showed a significant difference between the cotton height in the lysimeter versus the cotton height in the field. Using this methodology, the dates 26 June to 17 August and 28 August to 1 September were excluded from the north analysis. The dates of 21 July to 17 August, 28 August to 1 September, and 8 to 16 September were excluded from the south analysis. In the initial analysis below, the data was not filtered for adequate fetch. A plot comparing uncalibrated surface renewal ET to each lysimeter is shown in **Figure 1.12**.

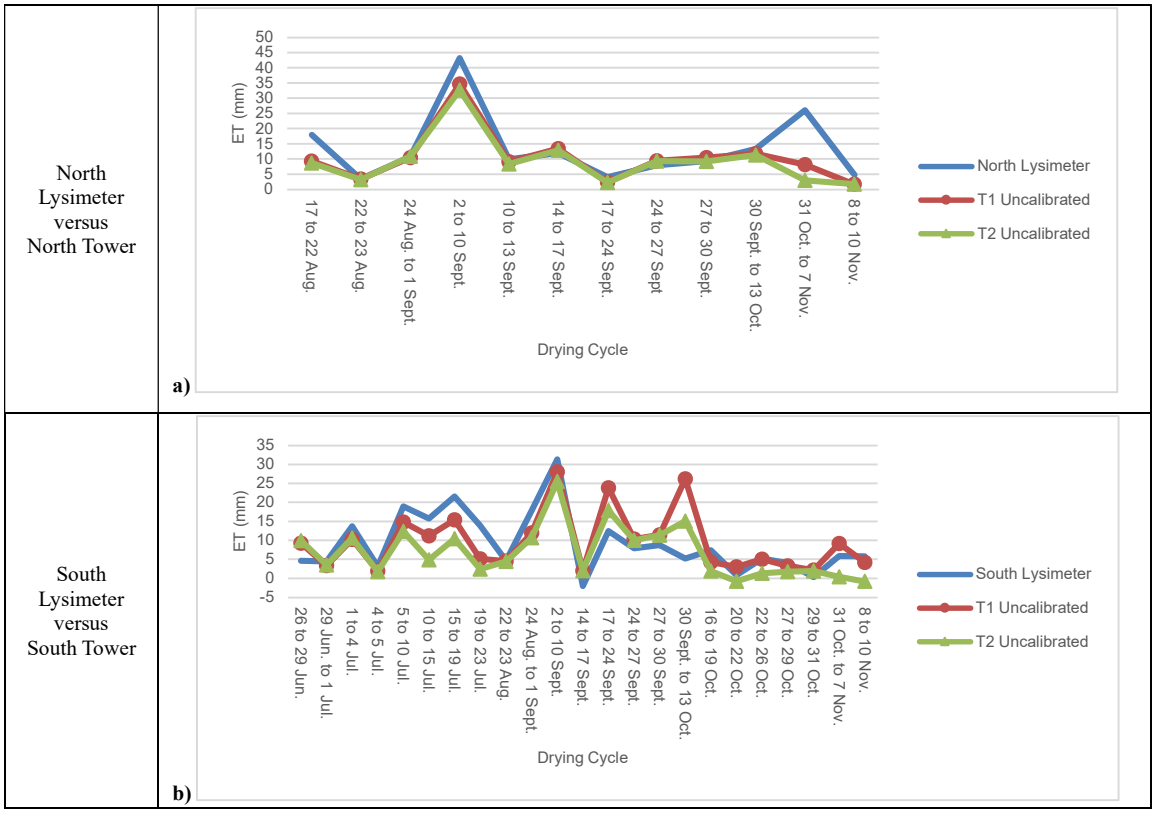

Figure 1.12. Plot of Uncalibrated Surface Renewal ET and Lysimeter ET by Drying Cycle

In **Figure 1.12**, it can be seen that the surface renewal measurements at the north tower track well with the north lysimeter until the last two drying cycles, while the south comparison is more sporadic. Using the data from the comparisons, an analysis was completed to determine the fit between the surface renewal ET estimates and the lysimeter ET measurements. The results are shown in **Figure 1.13**.

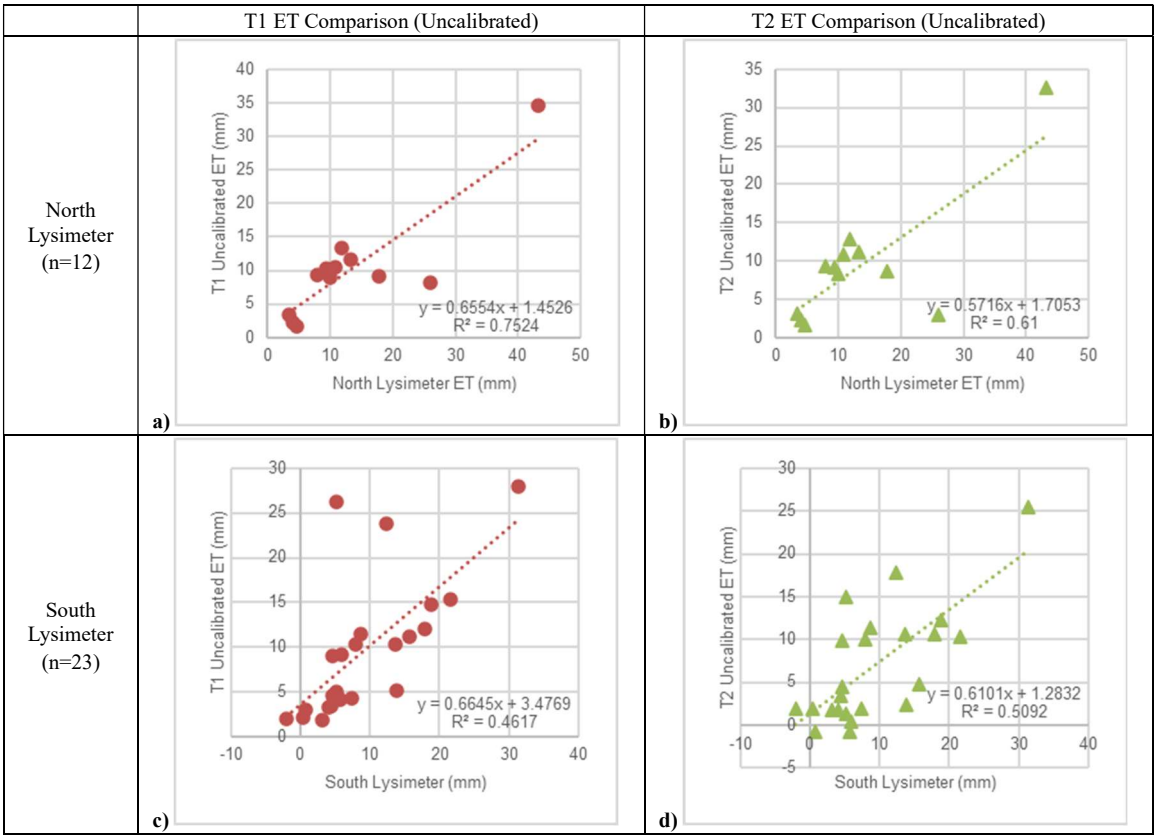

Figure 1.13. Surface Renewal Uncalibrated ET Comparison to Lysimeter ET

As seen in **Figure 1.13**, the agreement between the weighing lysimeters and the surface renewal method is not as strong as the agreement that had been observed between the surface renewal and eddy covariance methods. The T1 ET comparison had R^2 values of 0.75 and 0.46 for the north and south comparisons, respectively. While the T2 ET comparison had R^2 values of 0.61 and 0.51 for the north and south comparisons, respectively. The lack of agreement was concerning. Some reasons for this will be discussed in a discussion section of this paper.

It was hoped that the application of the Castellví method would improve the agreement. **Figure 1.14** shows the comparison of the Castellví method ET values with the lysimeter ET measurements.

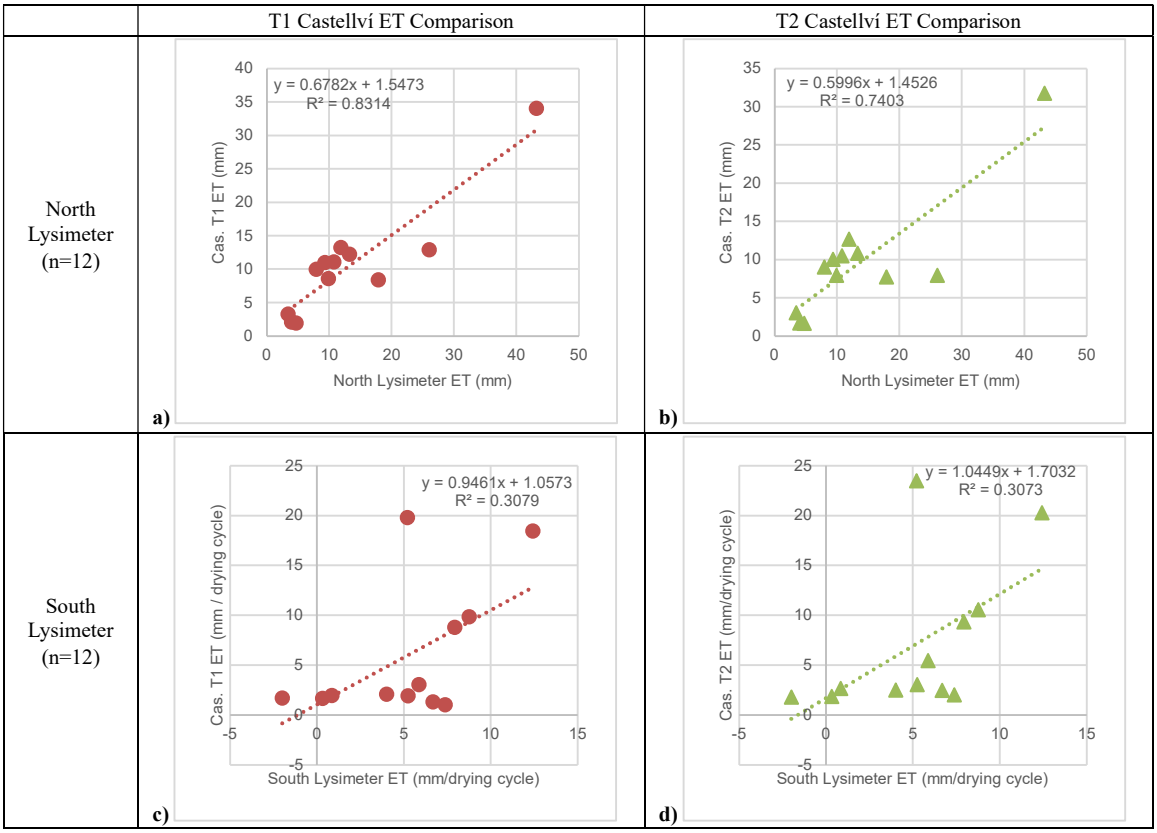

Figure 1.14. Castellví method ET comparison to Lysimeter ET

As seen in **Figure 1.14**, the Castellví method showed mixed results in its performance with each lysimeter. For T1, the Castellví method increased the agreement at the north tower (Uncalibrated T1 = 0.75; Castellví T1 = 0.83) and decreased it at the south tower (Uncalibrated T1 = 0.46; Castellví T2 = 0.31). For T2, the agreement increased at the north tower (Uncalibrated T2 = 0.61; Castellví T2 = 0.74), while decreasing the agreement at the south tower (Uncalibrated T2 = 0.51; Castellví T2 = 0.31).

Based on the data, the correlation between the lysimeter ET and surface renewal ET is weak. This is true for both the uncalibrated ET and Castellví method ET comparisons to the weighing lysimeters.

Fetch Analysis Results

Considering the lower than expected agreement between the surface renewal and lysimeter ET data, a fetch analysis was undertaken to determine if data that only had adequate fetch would improve the ET measurements. The strength of fit between the lysimeter ET and surface renewal ET values is shown in **Table 1.2**. Scatter plots of the analysis are also included in **Appendix D**.

Table 1.2. Lysimeter and Surface Renewal Comparisons with Adequate Fetch

	T1 Uncalibrated ET Comparison	T2 Uncalibrated ET Comparison	T1 Castellví ET Comparison	T2 Castellví ET Comparison
North Lysimeter	0.018 (n=12)	0.0212 (n=12)	0.0287 (n=12)	0.0115 (n=12)
South Lysimeter	0.047 (n=23)	0.0045 (n=23)	0.0007 (n=15)	0.0314 (n=15)

As seen in **Table 1.2**, the fetch analysis shows almost no agreement between both types of Surface Renewal ET calibrations and the lysimeter data. Based on the results, it could be concluded that adequate fetch does not play a role in the surface renewal measurements. However, the research team believes that another factor may have impacted the results. **Figure 1.15** shows the average daily running total of water change measured by the south lysimeter and T1 and T2. In the plot, all rainfall and irrigation data were excluded, as well as any dates with significant differences between lysimeter and field plant heights. The south lysimeter was used for the comparison due to its higher measurement accuracy—from taking the average over 10-minute intervals— and due to it providing more overnight and early morning data throughout the season since it was not affected by power outages. Both of these factors lead to lower variability in the running total below. In

the figure, ET would be negative as it represents water lost, whereas, water gained would be from other sources such as dew.

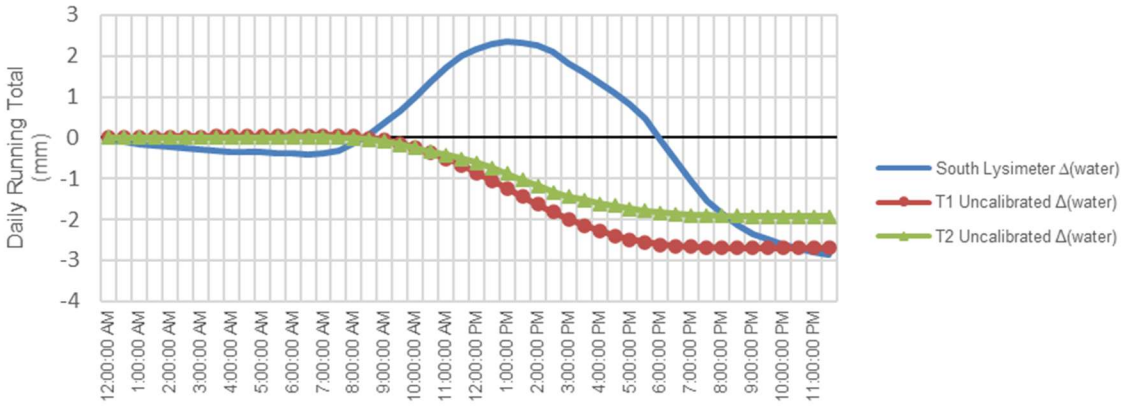

Figure 1.15. Running Total of Day's Change in Water for Lysimeter and Surface Renewal

Seen in **Figure 1.15,** as the day goes along in time, a net increase of ~2mm of water is measured by the lysimeter, while surface renewal measurements do not measure this increase in water. Although the day's net total comes to be a loss of ~3 mm for the South Lysimeter and T1, the diurnal pattern suggests the lysimeter ET and T1 ET may be substantially different. The daily pattern suggests that the south lysimeter's average ET is ~5 mm, with a moisture supply of ~2 mm each morning. From a literature review, it was found that heating can cause steel-walled lysimeters to show a delay in morning ET and an increase in ET during the afternoon (Howell, Terry et al., 1991). In addition, the load cells on the weighing lysimeter are located at the surface which could cause heating effects to influence the measurements. However, field observation leads the research team to believe that condensation on the plant leaf may also be a factor in this diurnal gain of water shown by the lysimeter. An analysis of dewpoint temperature versus

ambient air temperature was undertaken using the CS-215 data near the crop canopy height. However, this analysis has been excluded from this paper as it did not align with field observations when condensation was observed on plant leaves. Further literature review indicates that leaf temperature is an important factor in the formation of condensation (Schmitz and Grant, 2009). For cotton, canopy temperature can vary greatly from the ambient air temperature (Hake and Silvertooth, 1990). In this study, canopy temperature was not measured.

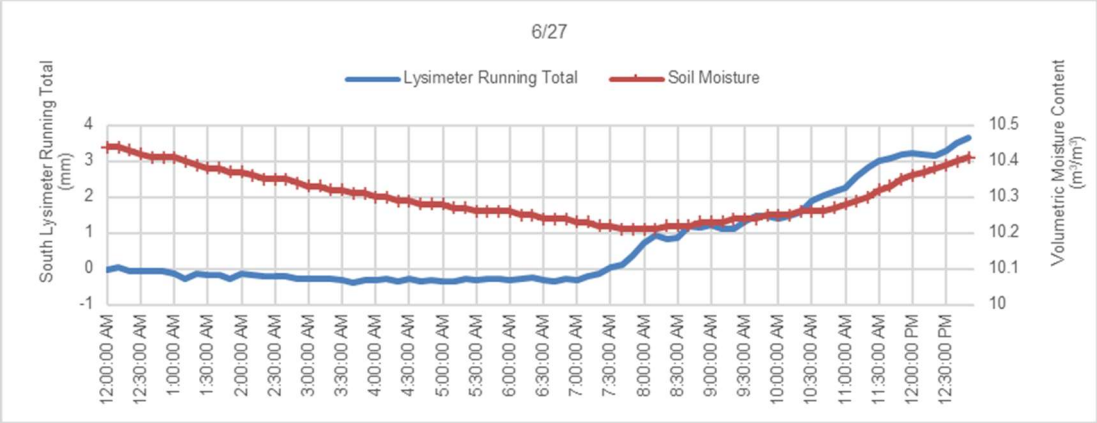

Figure 1.16. Plot of Lysimeter Running Total versus Lysimeter Moisture Sensor at 0.10 m depth

In **Figure 1.16**, it can be seen that both the South Lysimeter and the shallowest measurement of soil volumetric water content increased as time went on throughout the morning hours. It should be noted that both the lysimeter load cells and the soil volumetric water probe could possibly be affected by changes in temperature, which could be a contributing factor. However, the temperature sensitivity of these sensors was not evaluated in this study. The date of the measurements in **Figure 1.16** was chosen to represent a typical day that did not experience a precipitation event. Also, there was no significant difference in plant height compared to the field for this date chosen.

Regardless of the source, the net increases measured in the lysimeter disrupt the ability to filter out data in 30-minute time intervals for the fetch analysis. Therefore, a fetch analysis could not be completed.

Discussion

Comparison with Eddy Covariance ET

For the Eddy Covariance and Surface Renewal ET comparisons, in general, there was good agreement ($R^2 \geq 0.89$) even under inadequate fetch conditions. The best alignment came from T1 when not calibrated (Uncalibrated $R^2 = 0.99$), while, the worst agreement was from the Castellví calibrated T1 values (Castellví $R^2 = 0.94$), which was the measurement height (1.5 m) nearest the crop canopy and in the roughness sublayer for the duration of the growing season. A positive for the Castellví method was that its application did improve both towers' agreement between T2 ET and EC ET (North: Uncalibrated $R^2 = 0.93$ → Castellví $R^2 = 0.98$; South: Uncalibrated $R^2 = 0.89$ → Castellví $R^2 = 0.98$). All of this should be considered in the context that neither measurement had full fetch requirements met.

Comparison with Infield Weighing Lysimeter ET

For the Lysimeter and Surface Renewal comparison, the results varied. In general, decent agreement was seen between the north lysimeter ET and the uncalibrated surface renewal ET estimation (T1 $R^2 = 0.75$; T2 $R^2 = 0.61$). A factor that may have impacted results is that the one-time sampling method taken by the north lysimeter led to a lower sampling accuracy. For the south lysimeter, the agreement was weak for the uncalibrated ET comparison (T1 $R^2 = 0.46$; T2 $R^2 = 0.51$). A potential factor affecting the south

comparison was that plant growth was reduced in the vicinity around the south lysimeter, which was likely due to compaction from the previous year's installation of the south lysimeter.

The application of the Castellví method gave mixed results, mainly dependent on the tower analyzed. For the north tower, the agreement improved for both T1 and T2 when applying the Castellví method (T1: Uncalibrated $R^2 = 0.75$ → Castellví $R^2 = 0.83$; T2: Uncalibrated $R^2 = 0.61$ → Castellví $R^2 = 0.74$). For T2, it improved the agreement for the north site but reduced the agreement for the south site (T1: Uncalibrated $R^2 = 0.46$ → Castellví $R^2 = 0.31$; T2: Uncalibrated $R^2 = 0.51$ → Castellví $R^2 = 0.31$). A potential contributing factor for the south site's low performance with the Castellví method could be that the horizontal wind speed measurements used for calculating the south Castellví ET values were taken 33 m away.

Perhaps the biggest contributing factor for the lysimeter and surface renewal comparison could be fetch, which could not be further analyzed in this study due to the diurnal pattern shown in lysimeter measurements. In this study, the north measurement site was 30 m from the field edge, and the south site was ~18 m from a break in between the two fields where a vehicle service path is located. This break means a discontinuous canopy, which would impact measurements. Being close to the field edge does not allow for wind to normalize its boundary layer flow above the canopy, which commonly causes "edge effect" on vegetation growth and transpiration rates (Allen et al., 2011). Therefore, fetch should be considered in future studies on the site.

Condensation

In this study, diurnal increases from condensation or heating of the measurement equipment played a factor in the comparison of measurements between both lysimeters and the surface renewal method. The surface renewal method did not see this diurnal gain shown by the lysimeters. For the most part, both the energy budget methods and the Castellví method measured limited condensation or none at all, and certainly not to the same degree as each lysimeter.

To better understand if the measurements were realistic for condensation, a literature review was performed. From the literature, it was determined that some diurnal changes in moisture were realistic based upon the results of other studies. A research team in China verified that condensation represented a significant portion of water supply (10.8% of rainfall total) in a subtropical climate that experienced similar weather to this study (July through October growing season with average temperature of 24.8°C and average relative humidity of 79.2%) (Liu et al., 2018). In his literature review on dew, Wallin cited Wegener in reporting dew to be as large as 5 mm/day near 30°S latitude in Brazil (Wallin, 1967; Wegener, 1927). Around that time period, a location at 30°S latitude in Brazil would be classified as Cfa according the Köppen−Geiger Climate Classification (Kottek and Rubel, 2010), which is the same classification as this study's site.

If the diurnal gains shown by the lysimeter are due to moisture condensation, it would be concerning if the surface renewal and the eddy covariance methods do not measure these condensation events to the same degree as a weighing lysimeter. T2 measurements did show some signs of condensation in the form of negative ET for two

drying cycles (see **Figure 1.13d)**, though not in alignment with what the south lysimeter measured. Based on the literature review and the field observations, it would be recommendable to further evaluate the surface renewal method for its ability to measure condensation, especially in areas that rely heavily on condensation for water supply.

Practicality, Accuracy, and Cost-Effectiveness as an ET Measurement

A sub-objective of this thesis was to test practical, accurate, and cost-effective ET measurement methods. From a time perspective, the surface renewal method took hundreds of hours to read reference material, gain an understanding of the concept, become accustomed to the program code and measurement equipment, and then post-process and gap-fill mixing flux data. This time investment may make the surface renewal method more practical for producers with available time and energy to incorporate it into their core operations, or capital to employ a specialist. Due to the calibration factor changing based on the distance between measurement height and the plant canopy height, the method may be most practical over stationary height canopies such as perennial plants. In addition, the surface renewal method in general can be placed nearer to the crop canopy than the Eddy Covariance method. This allows the surface renewal method to be more practical for smaller field sizes than the Eddy Covariance method, by reducing fetch requirements. Lastly, a third advantage of the surface renewal method is that energy budget equipment can be moved in the field, allowing it to be more practical work with than a weighing lysimeter for producers. From a capital perspective, the instrumentation used for the surface renewal method is more affordable than other ET measurement equipment such as the Eddy Covariance method. This study showed that the Surface Renewal performed well

in comparison to the Eddy Covariance method good agreement ($R^2 \geq 0.89$), suggesting that the surface renewal method may be a valid replacement for the Eddy Covariance method.

Conclusion

The surface renewal method was tested to evaluate its performance in comparison to two in-field weighing lysimeters and two Eddy Covariance ET estimates using a residual energy balance measurement. The study was conducted over two adjoining cotton fields in a temperate, humid, hot summer environment and under inadequate fetch conditions. In general, there was strong agreement between the surface renewal's uncalibrated ET measurements and the Eddy Covariance ET measurements ($R^2 \geq 0.89$), with the strongest agreement being between the lowest surface renewal measurement height of 1.5 m and the Eddy Covariance ET ($R^2 \geq 0.99$). The higher measurement height of 1.6 m was improved by the application of the Castellví method to calculate a calibrated surface renewal ET estimate (R^2 =0.98), while the lower measurement height performed worse (R^2 = 0.94). The north lysimeter and surface renewal ET measurements had slightly better agreement ($T1_N$ R^2 = 0.75; $T2_N$ R^2 = 0.61) than the south lysimeter and south surface renewal ET measurements ($T1_S$ R^2 = 0.46; $T2_S$ R^2 = 0.51). Applying the Castellví method further improved the agreement between the north lysimeter and SR ET measurements (Castellví $T1_N$ R^2 = 0.83; Castellví $T2_N$ R^2 = 0.74), but had a negative effect on the agreement of the south measurements. ($T1_S$ Cas R^2 = 0.31, $T2_S$ Cas R^2 = 0.31). Two factors likely impacted the study. First, though surface renewal fetch requirements are not fully known, inadequate fetch could have impacted the study. Second, contribution from an external source thought to be condensation or temperature effects on the lysimeter caused differing diurnal patterns

between the lysimeters and energy budget equipment. Based on this data and a literature review, we recommend that further evaluation be made of the surface renewal method's ability to measure condensation, especially in climates where condensation would be a significant source of moisture supply.

Acknowledgements

Thank you to The South Carolina Cotton Board, The South Carolina Peanuts Board, and the NIFA project SC-1700540 for providing funding to evaluate the Surface Renewal method in this study. Thank you to Becky Davis and Bayleah Cooper for your instrumental contribution in setting up and maintaining field equipment, irrigating, pulling and uploading data regularly, and many other tasks. Thank you Dr. Kosana Suvočarev and Dr. Liyi Xu for calculating Castellví method sensible heat values and for providing guidance and advice. Lastly, thank you Stewart Bell, Dr. Mike Marshall, and Cash, Trevor, and Kinley for your contribution in the field and for providing information to write this Thesis chapter.

REFERENCES

Allen, R. G., Pereira, L. S., Howell, T. A., & Jensen, M. E. (2011). *Evapotranspiration information reporting: I. factors governing measurement accuracy* doi:https://doi.org/10.1016/j.agwat.2010.12.015

Burba, G. (2013). *Eddy covariance method for scientific, industrial, agricultural and regulatory applications: A field book on measuring ecosystem gas exchange and areal emission rates* LI-Cor Biosciences.

Castellví, F. (2012). *Fetch requirements using surface renewal analysis for estimating scalar surface fluxes from measurements in the inertial sublayer* doi:10.1016/j.agrformet.2011.10.004

Castellví, F. (2004). Combining surface renewal analysis and similarity theory: A new approach for estimating sensible heat flux. *Water Resources Research, 40*(5) doi:10.1029/2003WR002677

Castellví, F. (2018). An advanced method based on surface renewal theory to estimate the friction velocity and the surface heat flux. *Water Resources Research, 54*(12), 10,134-10,154. doi:10.1029/2018WR022808

Castellvi, F., & Snyder, R. L. (2010). A new procedure based on surface renewal analysis to estimate sensible heat flux. *Journal of Hydrometeorology, 11*(2), 496-508. doi:10.1175/2009JHM1151.1

Castellví, F., & Snyder, R. L. (2010). *A comparison between latent heat fluxes over grass using a weighing lysimeter and surface renewal analysis* doi:https://doi.org/10.1016/j.jhydrol.2009.11.043

CPI inflation calculator. (2020). Retrieved from https://www.in2013dollars.com/us/inflation/2001

DeVries, D. A. (1963). Thermal properties of soils. In W. R. Van Wijk (Ed.), *Physics of the plant environment* (pp. 382). New York, NY., U.S.A.: North-Holland Publishing Co.

ETH Zürich.*Surface energy balance* ETH Zürich. Retrieved from https://www.ethz.ch/content/dam/ethz/special-interest/usys/iac/iac-dam/documents/edu/courses/climate_systems/Surface-Energy-Balance-Noborder.pdf

Fisher, K. (2003). *Lysimeter work at stoneville, mississippi*. Jamie Whitten Delta States Research Center, 141 Experiment Station Road Stoneville, Mississippi 38776: USDA Agricultural Research Service.

Gao, W., Shaw, R. H., & Paw U, K. T. (1989). *Observation of organized structure in turbulent flow within and above a forest canopy* doi:10.1007/BF00122339

Hake, K., & Silvertooth, J. (1990). *High temperature effects on cotton.* ().National Cotton Council. Retrieved from https://www.cotton.org/tech/physiology/cpt/plantphysiology/upload/CPT-July90-REPOP.pdf

Haymann, N., Lukyanov, V., & Tanny, J. (2019). Effects of variable fetch and footprint on surface renewal measurements of sensible and latent heat fluxes in cotton. *Agricultural and Forest Meteorology, 268*, 63-73. doi:10.1016/j.agrformet.2019.01.010

Howell, T., Schneider, A. D., & Jensen, M. (1991). History of lysimeter design and use for evapotranspiration measurements. Paper presented at the *International Symposium on Lysimetry,* 1-9.

Hu, Y., Buttar, N. A., Tanny, J., Snyder, R. L., Savage, M. J., & Lakhiar, I. A. (2018). Surface renewal application for estimating evapotranspiration: A review. *Advances in Meteorology, 2018*, 1-11. doi:10.1155/2018/1690714

Jensen, M., Burman, R., & Allen, R. (1990). Evapotranspiration and irrigation water requirement. *ASCE American Society of Civil Engineers, 131*

Justice, D. C. (2020). *Weighing lysimeter CAD model.*

Kottek, M., & Rubel, F. (2010). Observed and projected climate shifts 1901-2100 depicted by world maps of the köppen-geiger climate classification. *Meteorologische Zeitschrift, 19*(2), 135-141. doi:10.1127/0941-2948/2010/0430

Liu, X., Xu, J., Yang, S., Zhang, J., & Wang, Y. (2018). Vapor condensation in rice fields and its contribution to crop evapotranspiration in the subtropical monsoon climate of china. *Journal of Hydrometeorology, 19*(6), 1043-1057. doi:10.1175/JHM-D-17-0201.1

Moratiel, R., & Martínez-Cob, A. (2013). Evapotranspiration and crop coefficients of rice (oryza sativa L.) under sprinkler irrigation in a semiarid climate determined by the surface renewal method. *Irrigation Science, 31*(3), 411-422. doi:10.1007/s00271-011-0319-8

Parry, C. K., Shapland, T. M., Williams, L. E., Calderon-Orellana, A., Snyder, R. L., Tha, P. U., Kyaw, & McElrone, A. J. (2019). Comparison of a stand-alone surface renewal method to weighing lysimetry and eddy covariance for determining vineyard evapotranspiration and vine water stress. *Irrigation Science, 37*(6), 737-749. doi:10.1007/s00271-019-00626-6

Paw U, K. T., Qiu, J., Su, H., Watanabe, T., & Brunet, Y. (1995). Surface renewal analysis: A new method to obtain scalar fluxes. *Agricultural and Forest Meteorology, 74*(1), 119-137. doi:10.1016/0168-1923(94)02182-J

Peel, M., Finlayson, B., & Mcmahon, T. (2007). Updated world map of the koppen-geiger climate classification. *Hydrology and Earth System Sciences Discussions, 4* doi:10.5194/hess-11-1633-2007

Poblete-Echeverría, C., Sepúlveda-Reyes, D., & Ortega-Farias, S. (2014). *Effect of height and time lag on the estimation of sensible heat flux over a drip-irrigated vineyard using the surface renewal (SR) method across distinct phenological stages* doi:10.1016/j.agwat.2014.04.006

Reichstein, M., Falge, E., Baldocchi, D., Papale, D., Aubinet, M., Berbigier, P., . . . Valentini, R. (2005). On the separation of net ecosystem exchange into assimilation and ecosystem respiration: Review and improved algorithm. *Global Change Biology, 11*(9), 1424-1439. doi:10.1111/j.1365-2486.2005.001002.x

Schmitz, H. F., & Grant, R. H. (2009). *Precipitation and dew in a soybean canopy: Spatial variations in leaf wetness and implications for phakopsora pachyrhizi infection* doi:https://doi.org/10.1016/j.agrformet.2009.05.001

Sell, S. (2019).
Davis vantage pro weather station - 2019 EDISTO REC WX DATA. Edisto Research and Education Center, 3.5 miles West of Blackville, SC: Clemson University.

Shapland, T.,M., Mcelrone, A., Paw U, K. T., & Snyder, R. (2013). *A turnkey data logger program for field-scale energy flux density measurements using eddy covariance and surface renewal*

Spano, D., Snyder, R. L., Duce, P., & Paw U, K. T. (1997). *Surface renewal analysis for sensible heat flux density using structure functions* doi:https://doi.org/10.1016/S0168-1923(96)02420-3

Suvočarev, K., Castellví, F., Reba, M. L., & Runkle, B. R. K. (2019). *Surface renewal measurements of H, λE and CO2 fluxes over two different agricultural systems* doi:https://doi.org/10.1016/j.agrformet.2019.107763

Suvočarev, K., & Xu Monier, L. (2020). In Ewing A. (Ed.), *Citation recommendation*

Van Atta, C. W. (1977). Effect of coherent structures on structure functions of temperature in the atmospheric boundary layer. *Arch.Mech., 29*, 161-171.

Wallin, J. R. (1967). *Agrometeorological aspects of dew* Elsevier B.V. doi:10.1016/0002-1571(67)90014-3

Wang, A., Jin, C., Diao, Y., Guan, D., & Pei, T. (2005). Estimation of water vapor source/sink distribution and evapotranspiration over broadleaved koreanpine forest in changbai mountain using inverse lagrangian dispersion analysis. *Journal of Geophysical Research: Atmospheres, 110* doi:10.1029/2004JD005227

Wegener, K. (1927). Remarks on spring and autumn dew. *Meteorol.Z., 44*, 188.

Wutzler, T., Lucas-Moffat, A., Migliavacca, M., Knauer, J., Sickel, K., Sigut, L., . . . Reichstein, M. (2018). Basic and extensible post-processing of eddy covariance flux data with REddyProc. *Biogeosciences, 15*(16), 5015-5030. doi:https://doi.org/10.5194/bg-15-5015-2018

Zoom Earth, Esri, & Maxar. (2018). Map of cotton fields used in study Zoom Earth.

CHAPTER TWO

DESIGN, FABRICATION, AND TESTING OF A PRESSURE DIFFERENTIAL DEVICE TO MEASURE EVAPOTRANSPIRATION

Introduction

Evapotranspiration (ET) measurements can be made by instruments known as weighing lysimeters, detailed in Chapter 1 of this Thesis, which measure the mass of a soil column over time and attribute changes in mass to water gained or lost. Though lysimeters are useful in measuring ET, there can be a few downsides to their use. One such downside is that they restrict water movement in the soil column being measured, which can lead to misleading results. With the restriction of water movement in mind, a concept was developed of taking pressure measurements to replace lysimeter ET measurements. This chapter will detail a study applying the concept.

The original idea to use pressure to measure ET was proposed by Dr. Dale Linvill, a retired agrometeorologist and member of this research committee. Dr. Linvill's initial proposal was to measure the pressure above an Evaporation Pan (see Chapter 3) continuously to estimate ET. However, after a literature review on in-field weighing lysimeters, the idea morphed into measuring subsurface pressure to replicate the results of a weighing lysimeter.

The thought process for measuring subsurface pressure for ET measurements builds upon how weighing lysimeters make their measurements. A weighing lysimeter measures changes in mass for ET. Pressure is a measurement of mass times acceleration divided by

an area. For measurements taken using a stationary instrument placed below ground, acceleration due to gravity should be constant and the area measured should be constant. Therefore, changes in pressure should be directly due to changes in mass in the soil. This theoretically could allow pressure measurements to make a similar measurement as the mass changes measured by a weighing lysimeter. With this concept in mind, a pressure differential device was conceived to measure pressure changes in a soil column, which would be assumed to be due to changes in water mass. Following the purpose of the weighing lysimeter, this pressure differential device would be used to measure ET. To test this hypothesis, an experiment was created with the following objectives:

- To develop, fabricate, and test a pressure differential device (PDD) for determining crop ET.
- To compare the performance of the PDD in measuring crop ET with ET measurements from a lysimeter.

Background

Developing, fabricating, and testing a pressure differential device (PDD) for ET

Contributors to the fields of agriculture, hydrogeology, soil mechanics, and soil physics regularly measure pressure as part of measurements for pore water pressure and subsurface stress. Analyses of subsurface stress have revealed differing behaviors in partially saturated and unsaturated conditions compared to saturated conditions (Hillel, 2003). Due to these differing behaviors, this section will seek to provide equations to quantify pressure behavior in saturated, partially saturated, and unsaturated soils.

An important measurement, which the PDD will measure, is total stress. Total stress is measured as the pressure at a particular point in the soil, and represents the total sum of all pressures acting on that point. These pressures come from forces, since pressure is a measurement of force/area. The forces which can contribute to total stress include surface loads, overburden – which is the overlying weight of the profile (Hillel, 2003)—, pore water pressure, cohesion forces (Al-Agha, 2015), and pore air pressure (Borja, 2006).

Historically, in soil mechanics, total stress is distributed into two distinct values of effective stress and pore water pressure by the equation proposed below by Karl Terzaghi in the early 1900's (Terzaghi et al., 1996).

$$\sigma_{total} = \sigma_{eff} + p_w \tag{2.1}$$

Where:
σ_{total} = Total stress (N/m^2)
σ_{eff} = Effective stress (N/m^2)
p_w = Pore Water Pressure (N/m^2)

The effective stress is the pressure on the soil matrix structure itself, while the pore water pressure is a hydrostatic pressure based on the depth of measurement in a water table. This hydrostatic equation will be referenced and given later in **Equation 2.3,** as it applies equally to saturated, partially saturated, and unsaturated soil conditions. **Equation 2.1** is helpful in separating out the stress associated with the soil matrix from the stress associated with water in a soil profile. However, the equation assumes saturated soil conditions and therefore is not robust to be applied to unsaturated conditions (Hillel, 2003, p. 360).

A useful theory for calculating stress above and below water tables is the Rankine Earth Pressure theory (Al-Agha, 2015). The theory is commonly used in the fields of civil

engineering and soil mechanics to predict lateral earth pressure on structures such as retaining walls. In order to calculate the lateral earth pressure, a vertical stress is estimated and then multiplied by a soil-dependent coefficient known as the "transformation factor". An equation for estimating the vertical stress in the vadose zone, which ignores cohesion forces from soil particles, is shown below in **Equation 2.2** (Al-Agha, 2015).

$$\sigma_v = \gamma h + q \tag{2.2}$$

Where:
σ_v = Vertical stress (N/m^2)
γ = Soil unit weight (N/m^3)
h = depth of measurement in soil (m)
q = represents pressure from a distributed load applied at the soil surface (N/m^2)

It is important to note that this equation for vertical stress omits effects from pore water pressure above the water table (Al-Agha, 2015). However, for soil physicists, pore water pressure is important, as it applies to plant-available soil water. To calculate pore water pressure, a hydrostatic equation is often used based on the measurement point in reference to the water table. Above the water table, the value turns negative and is referred to as a pressure potential. The hydrostatic pressure potential equation is given below in **Equation 2.3** (Remson & Randolph, 1962), though it can be used below the water table.

$$\psi = -\rho g z \tag{2.3}$$

where
ψ = hydrostatic pressure potential / hydrostatic pressure (N/m^2)
ρ = density of water (1000 kg/m^3)
g = acceleration due to gravity (9.81 m/s^2)
z = the height of measurement in reference to the water table (m)
(below the water table z is -, above the water table z is +)

Following the equation, it is important to note that the hydrostatic pressure can be both negative or positive in reference to the water table. In the vadose zone, above the water table, the pressure becomes negative and is known as a pressure potential; at the water table, the pore water pressure equals the barometric air pressure (Muir Wood et al., 2000); below the water table, the hydrostatic pressure is a positive pressure. **Equation 2.3** is useful if the water table depth is known. For this study, the water table depth was not be measured, but the behavior of the water table affects the pressure measurements. There are three other key pressure potentials that contribute to the total soil water potential. Among the strongest is the matric potential, which binds water to soil particles using surface tension and its strength is soil dependent. Another potential is the gravitational potential, which is the potential energy associated with a measurement point's vertical position in reference to a set elevation. This is often taken in reference to the soil surface or water table, depending on the direction of the water movement, such as from an infiltration event or a water table rising. Lastly, is osmotic pressure potential, which is the pressure potential exerted from the attractive forces between water and solutes and is usually ignored except in saline soils. The sum of these four potentials is the total soil water potential (Kirkham, 2014).

Compare the PDD to Lysimeter ET measurements

The Pressure Differential Device was compared with an in-field weighing lysimeter designed to measure ET from row crops such as Cotton. For this reason, a literature review

was conducted to better understand the lysimeter design in how it works and understand how this might cause differences in the PDD and lysimeter comparison.

The weighing lysimeter works by containing a mass of soil column within its walls, weighing the mass continually, and attributing changes in mass to changes in water within the soil column. Instrumentation, such as load cells, are used to measure minute mass changes in the lysimeter so that readings can be made in fractions of a mm depth of water. One benefit of a weighing lysimeter design is that it restricts water movement in and out of the device to precipitation and ET, with precipitation coming in and ET going out. This benefit can also serve as a liability, because a weighing lysimeter does not allow water to move naturally in a soil profile. Examples of impacts that might play a role in the measurement of a lysimeter and the comparison seen in this study include:

- The lysimeter has above-surface edges and a gap between the inner and outer box, which prevents runoff. This retains more water in a lysimeter during precipitation events than the field.
- The solid sides of the lysimeter box prevent subsurface lateral flow, which is lateral water movement below ground. This can prevent the lysimeter profile from matching the moisture level of its immediate surroundings.
- The solid bottom of a lysimeter holds water that would otherwise percolate deeper in a field.
    - This can be mitigated by a drainage system installed at the base of the lysimeter inner box; however, regular monitoring must be used to ensure excess water is removed in a timely manner.

- Temperature can affect lysimeters. Temperature can affect micro-lysimeters with 30 cm or less depth by conducting heat down the sides and to the bottom of micro-lysimeters, affecting the evaporation rate of the contained soil column (Evett et al., 1995). The heat conduction depends on the lysimeter wall material as well (Evett et al., 1995; Todd et al., 2000). Historically, it has been recommended to perform lysimeter ET comparisons on 24-hour time intervals, as steel-walled weighing lysimeters have shown delays in morning ET and accelerated ET in the afternoon (Howell, Terry et al., 1991). This is attributed to heat affecting the steel walls and load cells, however, it is possible that condensation could play a factor in this (see Chapter 1).

Because of the restrictions in movement, a lysimeter can have a wetter or drier profile than a surrounding field. Differences in stored water can lead to large deviations in the lysimeter's measurement of ET compared to the ET of the surrounding field (Allen et al., 2011).

Methods and Materials

Developing, fabricating, and testing a pressure differential device (PDD) for ET

Due to the potential for design failure, the team considered 3 designs before making a physical device. The following paragraphs detail the design considerations and iterations taken.

The first option consisted of a raised square box with a bottom that would measure pressure changes by acting much like a diaphragm. An illustration, modelled by William "Colby" Cofield is shown on the following page in **Figure 2.1**.

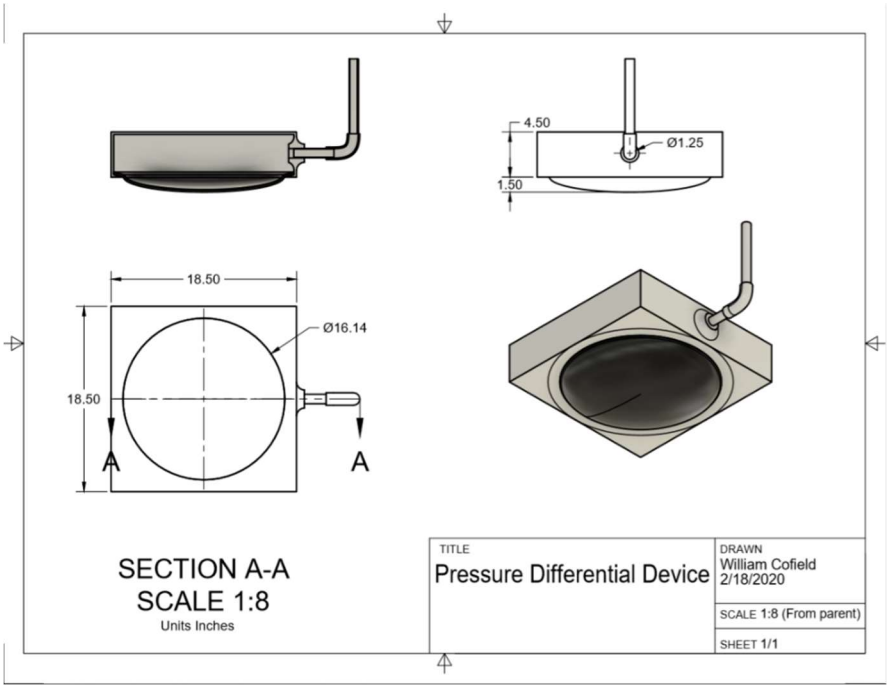

Figure 2.1. First Option Pressure Differential Device Design

(Cofield and Ewing, 2019)

As seen in **Figure 2.1**, the box has a rigid top and non-rigid rubber bottom. The bottom would theoretically deform up and down with changes in the overburden weight. In addition, a riser PVC pipe connects the assembly to the soil surface. All of the assembly would be sealed to be air tight. The theory is that as the overburden changes, the internal volume of the box should change causing the air pressure in the box to change. A sensor would be placed inside the riser to measure the changes in air pressure in the assembly and correlate it with the changing water mass in the profile above. The riser is advantageous in that it allows measurements to take place closer to the surface, which makes maintenance

and replacement of the sensor easier. An additional sensor would be used outside of the assembly at the surface to measure barometric pressure loading and temperature in order to discount these out the assembly's pressure changes.

The main concern with this first design was that the rise and fall of a soil, through soil swelling, would catch the edges of the box and make the box rise and fall with the soil. A moving box might give misleading pressure reliefs and cause the box's internal pressure reading to be useless.

Option 2 consisted of a vertical cylinder with a rubber nitrile bladder on the bottom. This was mentioned as a design similar to a piston accumulator. The design was conceived by Derek C. Justice, an engineer with expertise in designing custom artificial lift systems in the shallow subsoil for the oil and gas industry, with commentary from Michael Ewing, the Thesis author's father and a dairy scientist for the United States Department of Agriculture. The design is illustrated in **Figure 2.2** below.

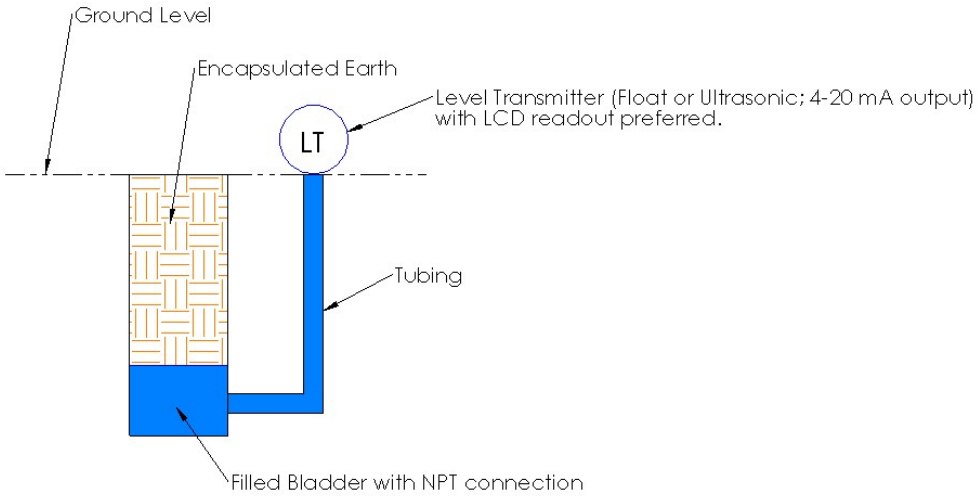

Figure 2.2. Second Option Based on a Piston Accumulator
(Justice, Derek Coleman, 2019)

The advantage of this design is that it still allows for a device to measure pressure changes in the subsoil and pass these pressures back up to the surface for easier measurement and maintenance of instrumentation. The design allows for pressure measurement to be obtained by measuring the height of water in the riser and applying **Equation 2.3**, provided in the background section. There were two main concerns with this design. One concern is that the outer frame still encapsulates the earth to restrict the flow of water movement. The second was that it would not be scalable to measure over a large area, as PVC pipes and bladder sizes are not often comparable in area to a weighing lysimeter of 1 m wide x 1 m long x 1.5 m deep. Dr. Dale Linvill had mentioned that the pressure measurement would need to be taken over a larger area to normalize any local extremes in pressure.

The third option consisted of a deformable pipe laid horizontally in the subsurface that would connect to a riser pipe. The design was initially conceived by Dr. Linvill with two leftover pieces of thin-film PVC from an indoor renovation project. The author of this Thesis had heard a similar idea from Robert Cornell, a designer with Missouri Northern Pecan Growers, LLC of burying a tube to measure changes in water in a soil profile.

Theoretically, the 3rd option avoided the concerns of the 1st and 2nd options. The 3rd option would not provide artificial support, a concern of the 1st option. In addition, theoretically, water flow would not be restricted in the soil column and the length of tube could be scaled for an indefinite distance in a field, like a tile drainage system, to maximize the area measured.

Ultimately the third option was chosen, as it seemingly avoided the concerns of the first two options.

Even with the selection of Option 3, multiple design iterations occurred to improve the design for use in the field. A concern of Device 3.1 was that the thin-film PVC would be too rigid and not be susceptible to measuring minute changes in the soil overburden load. Therefore, a second iteration (Design 3.2) was made using a more flexible hose material. A picture of Device 3.2 is shown below in **Figure 2.3.**

Figure 2.3. Device 3.2 at Dr. Linvill's Dock

Device 3.2 was built using a pool filter supply hose and a 1" PVC pipe as a riser to the surface. Through a trip to Charlotte and commentary from Mr. Doug Allen, water was added to fill the device and distribute pressure changes. Water would theoretically distribute local variances of pressure into one uniform pressure in the tube. In addition, the use of water made pressure changes visible through observing changes in the water column height in the riser. Mr. Allen, who worked in the construction and medical supplies

industries, commented that the device would be similar to burying a Dwyer Mark II manometer.

Device 3.2 was initially tested by submerging the hose part of the device in Lake Hartwell and observing changes in the water height in the riser when waves passed over the submerged device. The testing occurred at Dr. Linvill's Dock in April 2019. The device showed immediate, sizeable responses to lake waves. This encouraged us to continue with the design. An ultrasonic sensor was purchased with the intention of using it for the depth level measurement. However, the ultrasonic sensor purchased was designed to measure only one depth, and therefore was not used in this study. This was an oversight by me, the Thesis author. Despite my error in purchasing a single-depth ultrasonic sensor, I do believe an ultrasonic depth level sensor may work on a similar design in the future. For this study, in the field, Device 3.2 was measured by an eTape (Milone Technologies, Sewell, NJ, USA).

In May 2019, at the Edisto REC, Dr. Payero observed Device 3.2 and added recommendations. Among these recommendations was: increase the tube diameter to increase area the tube measured, use a more deformable material for the tube, and pressurize the entire assembly so that there would be no mold growth within the riser and so that evaporation would not cause decreases in the riser water column height over time. Device 3.3 was developed from these recommendations using materials on hand at the Edisto Research and Education Center, with the exception of the pressure sensors. A CAD model drawing of Device 3.3's concept is shown on the following page in **Figure 2.4**.

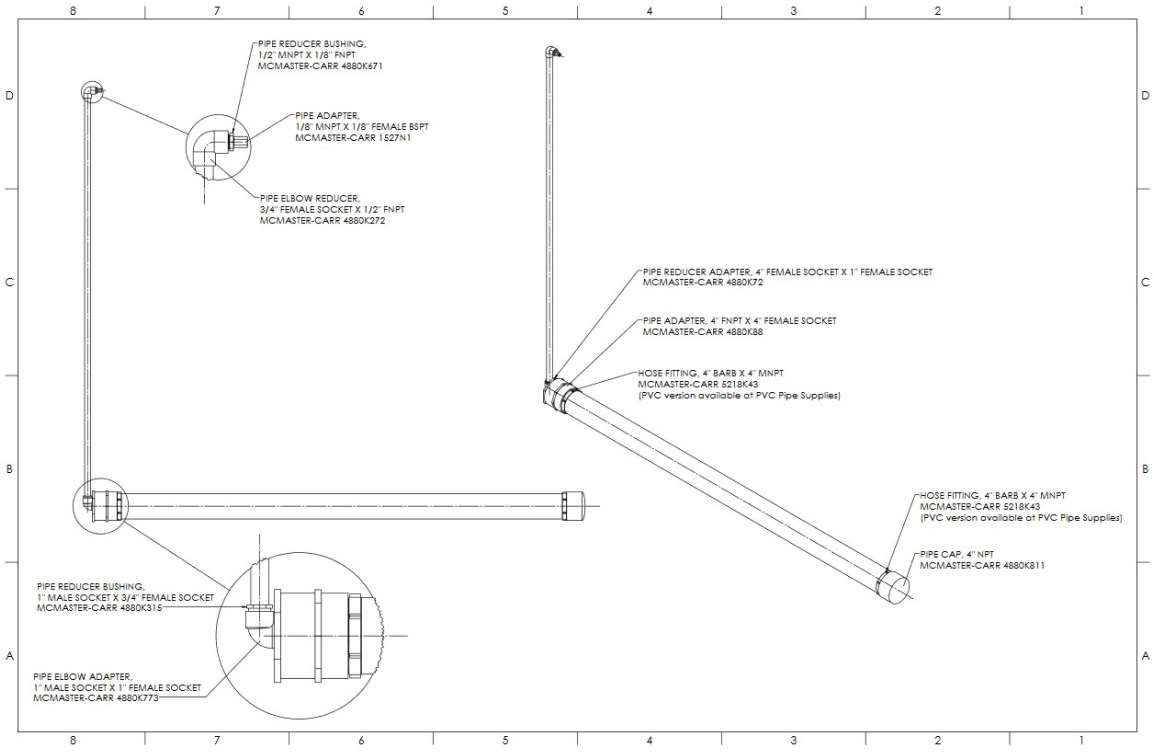

Figure 2.4. Pressure Device 3.3 CAD Model
(Justice, Derek Coleman, 2020)

Device 3.3 is an assembly of a long deformable rubber nitrile tube connected to a ¾" riser PVC pipe that has a pressure sensor near the top. The water within the assembly becomes pressurized upon burial, so that the entire assembly is filled with pressurized water. To measure absolute pressure of Device 3.3, a Nidec Copal P-7100-132A-R1 pressure sensor was chosen. This specific sensor was chosen for its operating pressure of 133.3 kPa (19.33 psi) while still being able to measure barometric pressure as well (101 kPa). Calculations performed using **Equation 2.2** predicted that the pressure range for the device at 1.5 m (5 feet) depth would be close to a range of 121 kPa (17.5 psi) to 131 kPa (19.0 psi). This was done assuming that the soil unit weight would range between γ_{dry} = 12.8 kN/m^3 (1.30 g/cm^3) and γ_{wet} = 19.6 kN/m^3 (2.00 g/cm^3), and the distributed load (q) would be a barometric pressure loading of 101 kPa (14.7 psi) (Beck, 2020). The sensor was

mounted horizontally to avoid air bubbles trapped within the device from rising and interfering with measurements. The anticipated interference from air bubbles would be a pressure drop across an air-water interface. The sensor was calibrated by Dr. Jose Payero and I in an office by recording the linear voltage output for different depths of water in a column filled with water ($R^2 = 0.9983$). This initial calibration led to greater sensitivity in the PDD data compared to the lysimeter. Therefore, the PDD calibration was changed to an empirical calibration that best fit one week's worth of PDD data versus lysimeter data (27 June to 3 July).

A secondary Nidec Copal P-7100-132A-R1 pressure sensor was used at the soil surface next to the PDD to measure the barometric pressure. The voltage output for the barometric pressure was subtracted directly from the pressure sensor voltage output obtained from Device 3.3 for each 10-minute time interval. This subtraction was to account for the noise of pressure due to barometric pressure cycles. It was assumed that the barometric pressure measured at a shallow depth of 1~2 m in the soil could be subtracted at a 1:1 ratio, without a time delay. A literature review over air pressure dynamics suggests that the air pressure at shallow measurement depths in permeable media, such as a sandy soil, can be assumed to be the current barometric pressure and should have a small time delay (Kuang et al., 2013). This trend was also observed in a vadose zone barometric pressure dynamics study at the Los Alamos National Laboratory (Neeper, 2002).

In total, with both sensors included, it is estimated that building the device with purchased material would cost roughly $400. A more detailed presentation of the costs is shown in **Appendix K**.

Both devices 3.2 and 3.3 were installed in the field on 4 June, 2019 1.5 m (5 ft) west of the south lysimeter. The profile was dug to a depth of 1.2 m (4 feet) using a backhoe and then leveled by two people using a rake and shovel. It was intended to bury the devices at a 1.5 m (5 feet) depth; however, a depth of 1.2 m (4 feet) was chosen on the way to installation, as Dr. José O. Payero remembered that the south lysimeter had a history of irregular floating due to a high water-table. It was anticipated that by burying the device at 1.2 m (4 ft) depth, it would be above the water table and avoid measuring within a water table. A second change took place during burial. It was planned to insert the devices sideways at the bottom of the trench into the intact soil wall profile. Upon digging the trench, Bobby Webb, who excavated the trench, stated that OSHA standards do not allow anyone into a 4+ ft deep trench without requiring extra equipment (Occupational Safety and Health Administration, 2005). Therefore, the devices were lowered to the bottom of the open trench and buried manually using shovels. The fact that the devices were not buried under a profile matching the surrounding field may present a potential problem in the trustworthiness of the measurements. On the following page in **Figure 2.5** is a picture of Device 3.2 and Device 3.3 being installed.

Figure 2.5. Devices 3.2 and 3.3 Being Installed in the Field

To better understand the soil and profile type, a Web Soil Survey of the field and its immediate surroundings was performed. The different soil types from the Web Soil Survey are shown below in **Table 2.1**.

Table 2.1. Soil Types from Web Soil Survey Map

Map Unit Symbol	Map Unit Name
DaB	Barnwell loamy sand, 2 to 6 percent slopes
FuB	Wagram sand, 2 to 6 percent slopes
VaA	Orangeburg loamy sand, 0 to 2 percent slopes
VaB	Barnwell loamy sand, 2 to 6 percent slopes
VcB	Neeses loamy sand, 2 to 6 percent slopes

The survey indicated that the location in the field the devices were buried was underlain by Orangeburg Loamy Sand, however, comparison of the soil profile in **Figure 2.5** with each Web Soil Survey's soil profile depths and descriptions leads me to believe

that the devices were buried in a Wagram Sand soil profile. Below, in **Table 2.2**, is part of the Web Soil Survey's description of a Wagram Sand profile.

Table 2.2. Excerpt of Web Soil Survey's Description of Wagram Sand Profile

Typical profile	
Ap - 0 to 9 inches:	Sand
E - 9 to 22 inches:	Sand
Bt - 22 to 79 inches:	Sandy loam
Properties and qualities	
Slope:	2 to 6 percent
Depth to restrictive feature:	More than 80 inches
Natural drainage class:	Well drained
Runoff class:	Very low
Capacity of the most limiting layer to transmit water (Ksat):	Moderately high to high (0.57 to 5.95 in/hr)
Depth to water table:	About 60 to 79 inches
Frequency of flooding:	None
Frequency of ponding:	None
Available water storage in profile:	Moderate (about 6.8 inches)
Interpretive groups	
Land capability classification (irrigated):	None specified
Land capability classification (nonirrigated):	2s
Hydrologic Soil Group:	A
Hydric soil rating:	No

Cotton was planted on June 5th over the devices and surrounding disturbed soil surface.

Sampling of the devices began on June 8th using a CR1000X datalogger that also sampled the south lysimeter. From the dates 8 to 17 June, the sampling consisted of taking a sample every 5 seconds and outputting the average across each 10-minute time period. From 17 to 26 June, a one-time sampling was taken every 10 minutes; however, this led to more noise in the data samples, so on 26 June through the rest of the growing season, the

sampling was changed back to sampling every 5 seconds with the average being reported across each 10-minute time period.

Analysis of the pressure differential device was made for daily ET throughout the season. The ET values are in terms of mm of water. The ET values do have rainfall and irrigation events subtracted directly from each day's total change. The rainfall and irrigation measurements were made using the South Lysimeter in terms of mm of water. The method of determining rainfall and irrigation using the South Lysimeter is outlined in Chapter 1 of this Thesis.

Compare the PDD to Lysimeter ET measurements

For an ET comparison, the South Lysimeter described in Chapter 1 was used for comparison. The lysimeter consists of 2 large steel boxes with one placed within another. The outer box dimensions are 1 m wide by 1 m long by 1.5 m deep. The lysimeter also took samples every 5 seconds and reported the average across each 10-minute time period. For a more complete detail and description of the lysimeter, please see Chapter 1.

A comparison was conducted between the Lysimeter daily ET values and inferred PDD daily ET values for several soil Drying Cycles. A drying cycle was defined as the time between soil wetting events. For the sake of simplicity, for this comparison, the drying cycle ET values were calculated by summing the ET of one or more consecutive days in which no soil wetting event occurred. Therefore, any date with a soil wetting event was discarded from the drying cycle analysis.

For the comparison between the two devices, a linear regression R^2 value was used. In addition, a Spearman Correlation test was performed to determine if the two datasets were correlated with each other using a level of significance of α=0.05.

Results

Due to noise associated with the eTape measurements, Device 3.2's results have been discarded from this study.

Rainfall began after the burial of the device on June 4th as the last two members of the crew were walking out of the field. In the three weeks following burial of the device, 140 mm of rainfall was received at the Edisto Research and Education Center.

Developing, fabricating, and testing a pressure differential device (PDD) for ET

Below, in **Figure 2.6**, is a plot of Device 3.3's inferred ET throughout the season.

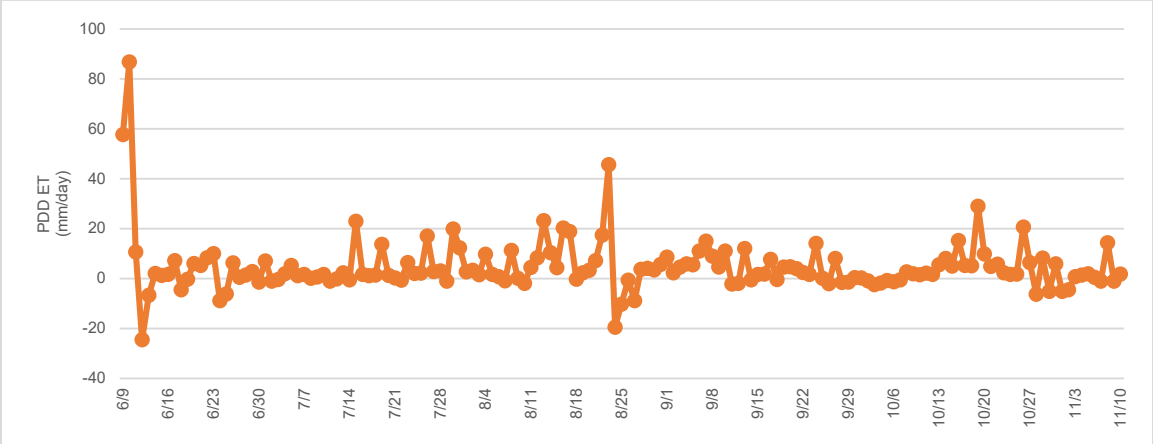

Figure 2.6. Pressure Differential Device ET

Figure 2.6 shows large changes in the PDD's inferred ET in the first week, even with rainfall and irrigation being pulled from the data. It is believed the first week's range of values might be noise from the newly buried profile settling, reorienting, and filling up

with rainfall. Therefore, to gain a better view of the inferred ET data throughout the season, data has been removed to begin the analysis on June 14th in **Figure 2.7**.

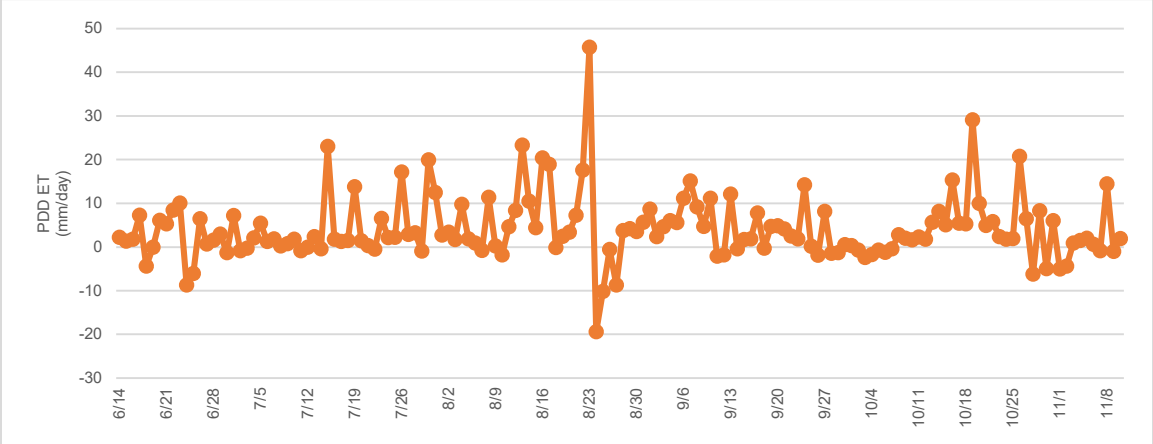

Figure 2.7. Plot of PDD ET from 14 June to 10 November

In **Figure 2.7**, two major findings can be seen. The first finding is that the pressure device showed large changes for most days throughout the season. The ET values ranged between -20 mm and 50 mm, which are unrealistic in scale for daily ET measurements. The second finding is that negative values are observed in the data, suggesting gains in water, even after accounting for rainfall and irrigation. To gain a better understanding of the data in **Figure 2.7**, sample statistics were calculated from the sample set shown. These statistics are shown in **Table 2.3**.

Table 2.3. Sample Statistics of PDD ET from 14 June to 10 November

Sample Statistic	Value
Average	4.1
Median	2.2
Standard Deviation (σ)	7.5

The sample statistics shown in **Table 2.3** show an average inferred daily ET of 4.1 mm/day with a standard deviation of 7.5 mm/day. Typical ET values range anywhere from

0 to 10 mm/day, suggesting the PDD calibrated with this calibration or something similar are in the same range as typical values measured for ET. However, the range of values shown in **Figure 2.7** suggest that, even with a correct calibration, the device was not measuring realistic daily ET values. What was impacting the PDD's measurements may be better known by comparing the device's measurements to a weighing lysimeter.

Compare the PDD to Lysimeter ET measurements

The analysis period for this comparison of the PDD and the South Lysimeter was from 27 June to 10 November. Though measurements began on June 8, the first few weeks of data were discarded from the analysis due to perceived settling in the pressure device profile (9 to 13 June), floating of the south lysimeter due to a high water table (14 to 19 June, 24 to 25 June), and changing sampling methods that effected data on June 26th.

Figure 2.8 shows the results for the analysis period comparing the profile moisture levels measured by the South Lysimeter and PDD.

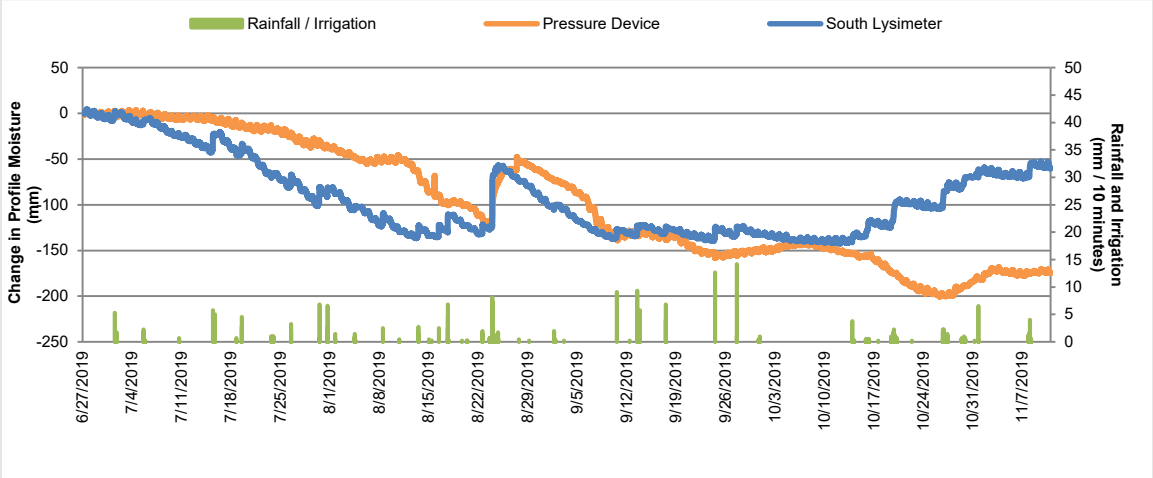

Figure 2.8. Profile Moisture Measurements against Rainfall / Irrigation Totals Included

In the plot, both the pressure device and lysimeter show similar gains and losses throughout the season until mid-October, at which point it appears that the south lysimeter

increases from rainfall while the PDD does not match this behavior. The cotton crop was defoliated about this time in mid-October (see Chapter 1 Methods and Materials), which may play a factor. Though the difference at the end of the season could have had an impact in ET measurements, the results from the first 3.5 months of the 4.5-month (From 27 June to 13 Oct: $R^2 = 0.77$) analysis period show that the PDD was able to track somewhat closely with the lysimeter in making soil profile moisture measurements. However, since the objective of the study was to compare ET measurements, we will turn our attention to this. The comparison of the PDD and lysimeter inferred daily ET values is shown in **Figure 2.9**.

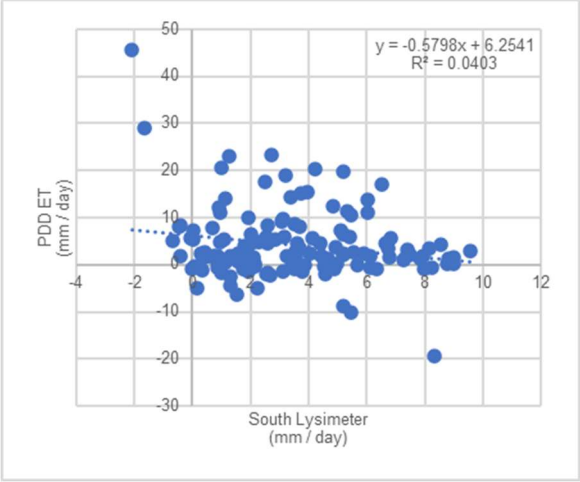

Figure 2.9. Daily ET Comparison between the PDD ET and Lysimeter ET

As seen in **Figure 2.9**, there is almost no agreement between the PDD and South Lysimeter in terms of Daily ET measurement. The Daily ET comparison yields an R^2 of 0.04, with the data not being significantly correlated (r= -0.057; p-value =0.511; N=137).

To see if there was an improvement using Drying Cycles, **Figure 2.10** is given.

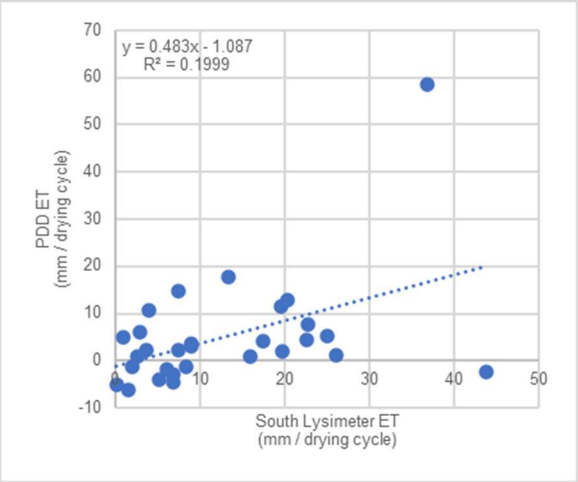

Figure 2.10. Drying Cycle ET comparison

As seen in **Figure 2.10,** when taking this same comparison using just drying cycles, the R^2 improved to 0.20. This improvement is also shown in the Spearman correlation test, which shows a significant correlation when using a level of significance of $\alpha = 0.05$ ($r=0.415$; p-value $=0.025$; $N=29$). However, the linear regression's R^2 value shows that there is still little agreement despite the improvements in regression and correlation between the two methods.

To understand why the inferred ET values differ, a day by day comparison analysis was undertaken using the soil profile moisture level data shown in **Figure 2.8**. This analysis showed that the PDD exhibited four different behaviors in comparison to the lysimeter. These 4 Behaviors are shown in **Figure 2.11.**

Behavior	Example	Dates Observed
1: Same as Lysimeter	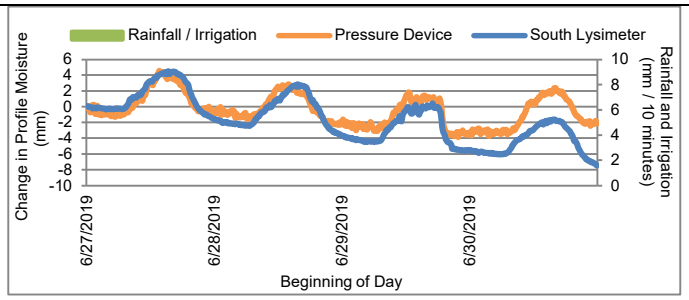	27 Jun to 2 Aug, 15 to 16 Sept, 23 to 25 Oct, 3 to 7 Nov, 10 Nov
2: Settling in the profile	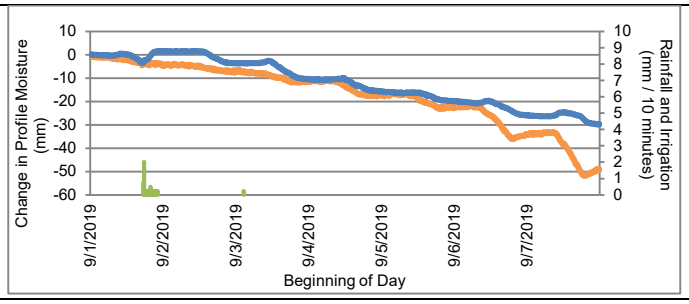	11 to 15 Aug, 19 to 21 Aug, 28 Aug to 7 Sept, 16 to 22 Oct
3: Delay in Rainfall as compared to Lysimeter	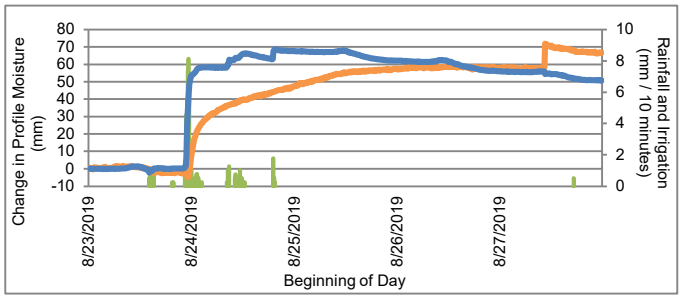	8 to 10 Aug, 16 to 18 Aug, 21 to 27 Aug, 10 to 12 Sept, 13 to 14 Sept, 17 to 18 Sept, 24 to 26 Sept, 27 Sept to 7 Oct, 13 to 15 Oct, 26 Oct to 2 Nov, 8 to 9 Nov
4: Capillary Fringe	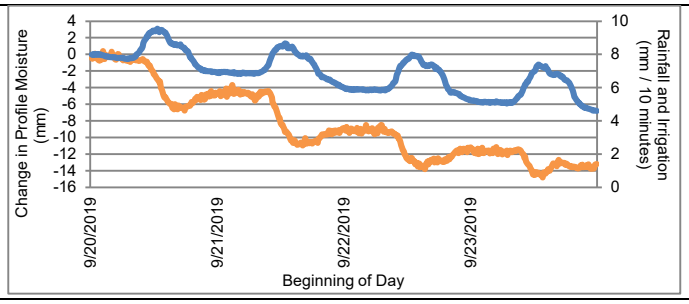	3 to 7 Aug, 8 to 9 Sept, 19 to 23 Sept, 8 to 12 Oct

Figure 2.11. The Four Distinctive PDD vs. Lysimeter Behaviors

The four behaviors are exhibited at different times of the season. The longest-lasting is the first behavior, which matches the south lysimeter's diurnal pattern for the first 38 days of the analysis period. The second behavior shows steep drops in the pressure device moisture level over a relatively short time period, sometimes ignoring rainfall and

at other times being reset by rainfall. The third behavior is a multiple-day delay exhibited by the PDD in measuring rainfall. This third behavior occurs the most often of all the behaviors. The 4th behavior is an inverted diurnal pattern compared to the south lysimeter, often showing moisture gains to the PDD's profile moisture level during late afternoon, evening, and/or overnight hours.

Discussion

Developing, fabricating, and testing a pressure differential device (PDD) for ET

The results of this study suggest that pressure differential device might not be a valid fit for measuring ET. One major finding from the study was that the PDD shows great sensitivity to changes in the profile moisture. This was able to be somewhat diminished by an empirical calibration with lysimeter data; however, this calibration should be improved in future work. An improved calibration might depend upon the device's materials, the effective porosity of the soil, and the soil type. However, optimizing the PDD's calibration was outside of the scope for this study. A second finding was that some of the inferred PDD ET values were negative, suggesting a water gain to the profile, even with rainfall and irrigation totals being removed. This is likely a result of the multiple- day delay the PDD exhibited after rainfall events, seen in Behavior 3.

Compare the PDD to Lysimeter ET measurements

In addition to the results of testing the PDD for ET, the comparison with the South Lysimeter yielded poor agreement in terms of measuring inferred ET. The inferred PDD ET had almost no agreement with the inferred daily ET values of the South Lysimeter. Despite a significant Spearman correlation ($r=0.415$; p-value $=0.025$) when comparing the

two inferred ET values across drying cycles, there was still little agreement when using a linear regression (R^2=0.20). All of this came as somewhat of a surprise as the PDD and lysimeter show similar changes in profile moisture throughout much of the season (June through October).

Four different behaviors in the comparison were observed. The 1st behavior was a matching diurnal pattern seen in both devices. The 2nd behavior was likely settling in the profile of the pressure device, which sometimes ignored rainfall and often did not exhibit the diurnal pattern shown by the lysimeter. The 3rd behavior pattern observed was that the PDD showed a multiple-day delay in measuring rainfall compared to the lysimeter. An explanation of this could be that the delay follows an infiltration curve, which would mean that the PDD was performing correctly and would be an oversight by the lysimeter preventing runoff. Another reason might be due to the behavior analyzed under the Boussinesq equation used for predicting compaction in agricultural soils (Hillel, 2003), which would be a detriment to the PDD. The Boussinesq equation calculates that the nearer the point of measurement in the subsoil is to a surface load, the greater the stress measured. The equation is used for predicting soil compaction from driving equipment in the field. Applied hypothetically to our device: it might be that as a soil wetting front nears the PDD, the pressure measured might increase. In addition to the Boussinesq equation, when the wetting front does arrive, saturation of the soil particles around the device would reduce the effect of negative pore water pressure observed above the water table. The 4th behavior shows moisture gains to the PDD's profile moisture level during late afternoon, evening, and/or overnight hours for some multiple-day periods when the lysimeter does not show

these diurnal gains. This seems to suggest a capillary fringe, where water is pulled upwards from a water table to reach hydrostatic equilibrium in the profile when solar radiation weakens. Given its solid bottom design, the weighing lysimeter would not be able to participate in capillary action.

Based on the order and the dates of the behaviors in relation to one another, the data suggests that the PDD profile was under three different zones throughout measurement: a water table from 27 June to 2 Aug, a transition zone / capillary fringe throughout much of the measurement period from August onwards, and measurements in the vadose zone with no capillary action briefly from 23 to 25 October. Though this is a hypothesis and is not proven. Since volumetric water content measurements were not taken at the PDD depth in the profile, this cannot be verified. Volumetric water content measurements would need to be included in future design analysis to ensure the device's placement is above or in a water table.

Regardless of the behavioral comparisons, the PDD did a poor job of estimating ET as compared to the lysimeter, despite their agreement in measuring profile moisture changes. The device may have been impacted by a number of different factors. The cotton growing on top of the device was planted after the device's burial, which means that the planting date was 2 weeks after the lysimeter. Despite an initial drought and good growth above the PDD, it is possible that the plant heights in the lysimeter and the PDD differed depending upon the point in the growing season. In addition, based on the data, the device could have been impacted by subsurface lateral flow, runoff, capillary action, and a water

table. For future analyses, it might be wise to test the PDD's inferred ET performance within a weighing lysimeter and compare this to the lysimeter measurements itself.

Other Challenges with Design or Future Opportunities

Though the PDD did a poor job of measuring ET, its ability to measure total stress across a distributed distance in the ground may be helpful to other fields of study. In particular, the fields of landslide prediction, poroelasticity, and geotechnical engineering, might serve as future opportunities for the PDD design and future iterations. The measurement of total stress is an important measurement in these fields and the device's ability to measure total stress in a profile could be useful.

The PDD may be more suited for some applications with its current version. First, the device could be used for subsoil total stress measurements, which would be beneficial for verifying theories on subsoil stress in the field of geotechnical engineering or in predicting of land movements. In addition, the device may be useful for measuring large-scale water-storage changes by measuring the loading from water in a profile. A similar technique has been used for measuring regional water-storage changes through the use of aquifers that serve as natural geologic weighing lysimeters (Bardsley and Campbell, 2000). Lastly, the PDD may be useful for verifying theoretical total and effective stress computations in the field of poroelasticity; however, if applied, the PDD would likely need additional measurements of soil volumetric water content and pore water pressure at the same depth (Borja, 2006).

In order to help with future use or application of the device, design challenges and future additions should be considered. First, the Rankine Earth Pressure Theory assumes

the lateral earth pressure and the vertical stress can differ (Al-Agha, 2015). Therefore, since the design measures in 360° around a horizontal axis, the amount of stress measured by the device might depend on a soil's transformation factor. A second consideration, mentioned by Dr. Joe Maja, is the sensitivity of temperature on a pressure sensor. To mitigate this for future designs, we would recommend installing the pressure sensor to be at or below the ground surface in a recessed box. The box could be opened easily to apply maintenance on the sensor and riser. Third, Device 3.3 did include a ball valve, which was not shown in the conceptual CAD model in **Figure 2.4** and was covered by my hand in **Figure 2.5**. For future editions, Derek C. Justice recommended using a block and bleed valve on the arm that houses the pressure sensor. This would be to isolate the sensor housing to allow easy replacement of the sensor without losing pressure within the device. In addition to this, it has been considered to angle this arm downward, such as at a 45° angle. This would be to ensure that, when a sensor is replaced, any newly introduced air bubbles would rise away from the sensor to the top of the device. A fourth concern is that the delay in measuring soil wetting events may be due to the behavior described by the Boussinesq equation, which would limit the device's application.

Conclusions

The objectives of this study were to develop, fabricate, and test a pressure differential device (PDD) in its ability to determine crop ET, and to compare the performance of the PDD in measuring crop ET with ET measurements taken from a lysimeter. Although a pressure differential device was developed, fabricated, and tested, the device did not appear to measure crop ET accurately. When comparing its inferred

daily ET measurements to inferred daily ET measurements taken from a weighing lysimeter, the PDD performed poorly. This was despite agreement between the lysimeter and PDD profile moisture measurements. In the comparison, four behavior patterns were observed with the device in comparison to the lysimeter that might explain the weak agreement. These behaviors, in combination with theoretical approaches for estimating subsurface stress, may present an opportunity for the PDD to be useful for other applications; however, for measurement of Crop ET, the device was not as useful.

REFERENCES

Al-Agha, A. S. (2015). Chapter (7) lateral earth pressure. *Basics of foundation engineering* (pp. 157-175). Gaza:

Allen, R. G., Pereira, L. S., Howell, T. A., & Jensen, M. E. (2011). *Evapotranspiration information reporting: I. factors governing measurement accuracy* doi:https://doi.org/10.1016/j.agwat.2010.12.015

Bardsley, W. E., & Campbell, D. I. (2000). Natural geological weighing lysimeters: Calibration tools for satellite and ground surface gravity monitoring of subsurface water-mass change. *Natural Resources Research, 9*(2), 147-156. Retrieved from https://doi.org/10.1023/A:1010147527484

Beck, K. (2020). In Bandoim L. (Ed.), *How to find barometric pressure in my area* sciencing.com. Retrieved from https://sciencing.com/barometric-pressure-area-5877559.html

Borja, R. I. (2006). *On the mechanical energy and effective stress in saturated and unsaturated porous continua* doi:https://doi.org/10.1016/j.ijsolstr.2005.04.045

Cofield, C., & Ewing, A. C. (2019). *1st generation pressure differential device*. Clemson University Makerspace:

Evett, S. R., Warrick, A. W., & Matthias, A. D. (1995). Wall material and capping effects on microlysimeter temperatures and evaporation. *Soil Science Society of America Journal, 59*(2), 329-336. doi:10.2136/sssaj1995.03615995005900020009x

Hillel, D. (2003). In Hillel D. (Ed.), *13 - stress, strain, and strength of soil bodies*. Burlington: Academic Press. doi:https://doi.org/10.1016/B978-012348655-4/50014-9

Howell, T., Schneider, A. D., & Jensen, M. (1991). History of lysimeter design and use for evapotranspiration measurements. Paper presented at the *International Symposium on Lysimetry,* 1-9.

Justice, D. C. (2019). In Ewing A. C. (Ed.), *Piston accumulator design*

Justice, D. C. (2020). *Pressure differential device 3.3 CAD model*

Kirkham, M. B. (2014). In Kirkham M. B. (Ed.), *Chapter 4 - Soil–Water terminology and applications*. Boston: Academic Press. doi:https://doi.org/10.1016/B978-0-12-420022-7.00004-5

Kuang, X., Jiao, J. J., & Li, H. (2013). Review on airflow in unsaturated zones induced by natural forcings. *Water Resources Research, 49*(10), 6137-6165. doi:10.1002/wrcr.20416

Muir Wood, D., Davison, L. & Springman, S. (2000). GeotechniCAL reference package: Soil mechanics / water table. Retrieved from http://environment.uwe.ac.uk/geocal/SoilMech/water/water.htm

Neeper, D. (2002). Investigation of the vadose zone using barometric pressure cycles. *Journal of Contaminant Hydrology, 54*, 59-80. doi:10.1016/S0169-7722(01)00146-2

Occupational Safety and Health Administration. (2005). Trenching and excavation safety. Retrieved from https://www.osha.gov/Publications/trench_excavation_fs.html

Remson, I., & Randolph, J. R. (1962). *Review of some elements of soil-moisture theory* (FLUID MOVEMENT IN EARTH MATERIALS ed.). Washington, DC, USA: U.S. Government Printing Office: U.S. Geological Survey. Retrieved from https://books.google.com/books?id=GUIRAAAAIAAJ

Terzaghi, K., Peck, R. B., & Mesri, G. (1996). ARTICLE 15 EFFECTIVE STRESS, POREWATER PRESSURE, AND CRITICAL HYDRAULIC GRADIENT . *Soil mechanics in engineering practice (third edition)* (pp. 83). 605 Third Avenue, New York, NY, USA: John Wiley & Sons, Inc.

Todd, R. W., Evett, S. R., Howell, T. A., & Klocke, N. L. (2000). Soil temperature and water evaporation of small steel and plastic lysimeters replaced daily. *Soil Science, 165*(11) Retrieved from https://journals.lww.com/soilsci/Fulltext/2000/11000/SOIL_TEMPERATURE_AND_WATER_EVAPORATION_OF_SMALL.7.aspx

CHAPTER THREE

APPLICATION OF REFERENCE EVAPOTRANSPIRATION AND CROP COEFFICIENTS TO COTTON GROWING IN SOUTH CAROLINA

Introduction

Though there are many ways to measure evapotranspiration, one of the most common ways is to measure a standard reference evapotranspiration (ET_o) for an area based on local factors. ET_o is defined as the evapotranspiration of a reference crop, such as a short grass or alfalfa. It application is used to measure the atmospheric demand for water at a site. Two common methods used to measure ET_o are an Evaporation pan and the Penman-Monteith equation. An evaporation pan allows for a visual reference to be obtained by measuring the depth of water level in a pan and recording the change in depth over time intervals, such as a day. After multiplying this depth change by a coefficient, a pan ET_o measurement is obtained. In contrast to this, the Penman-Monteith equation allows for the use of climate-based variables to compute an ET_o, without needing the physical use of water.

Once ET_o is quantified, it can then be multiplied by a constant known as a crop coefficient (K_c) to predict the ET for a specific crop, such as cotton. This crop coefficient varies at different times of the season and for each crop.

With the measurement of ET_o in mind and its use in incorporating crop water demand, the objectives of this study were to:

1. Compare ET_o measurements obtained from a Class A evaporation pan with those obtained using the Penman-Monteith equation.

2. Develop K_p values based upon the Penman-Monteith ET_o comparison.
3. Develop a crop coefficient curve from lysimeter data for a cotton crop growing in the humid southeastern climate.

Background

ET_o Measurement

One method of measuring ET_o in this study was using an evaporation pan. In the United States, two common pans used for the measurement of pan evaporation are the Colorado Sunken Pan and the National Weather Service Class A Evaporation Pan. In this study, we used the National Weather Service Class A Evaporation pan, also referred to as the Class A evaporation pan. A Class A evaporation pan is a metal pan that has sides 0.25 m (10") tall and an inner pan diameter of 120.7 cm. It is commonly made of stainless steel or galvanized metal (Allen et al., 1998). Located within the pan is a stilling well, which the National Weather Service recommends siting 0.25 m away from the north side of the pan (Howell, Terry A. and Meron, 2007). The stilling well is used as a place to take water level measurements without the interference of waves that have been created by wind blowing across the water surface. The pan should be raised on a wooden platform, so that it is 15 cm above the ground (Allen et al., 1998). An image of a Class A Evaporation pan, with this siting and dimensions, is shown in **Figure 3.1**.

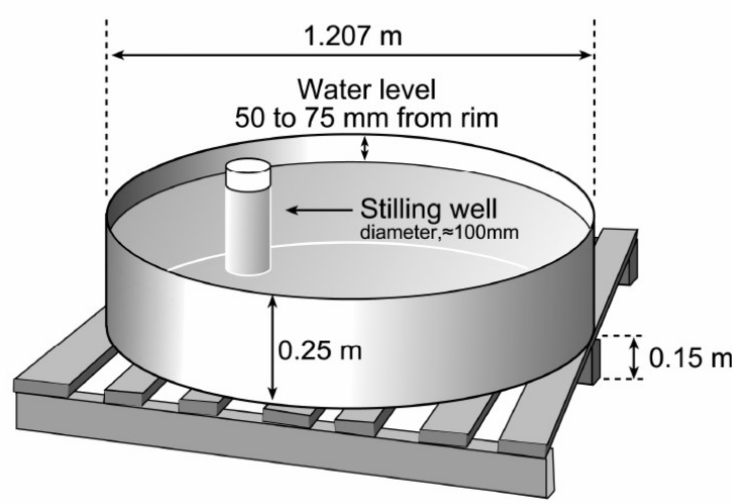

Figure 3.1. National Weather Service Class A Evaporation Pan Schematic with Dimensions (Howell, Terry A. and Meron, 2007)

The surroundings of a pan are important as it has been shown that pan evaporation is affected by local microclimate conditions. Allen et al. (1998) recommend siting a pan to be surrounded by a 20m by 20m short grass canopy, with all sides open to free air and with the pan sited downwind of a large cropped field. In addition, they recommend having the pan surrounded by a large wire enclosure to prevent animals from drinking from the pan. Although birds and other small wildlife may try to drink from the pan, it is best not to have the pan itself covered by a mesh screen, as it reduces the pan's evaporation rate (Allen et al., 1998). An example of a pan following these recommendations is shown in **Figure 3.2**.

Figure 3.2. Class A Evaporation Pan Surrounded by Wire Enclosure

(National Weather Service, 2015)

The evaporation pan allows for atmospheric evaporative demand to be directly quantified, though it requires regular maintenance to account for the effect of wind. With wind in mind, it is recommended to keep the pan water level within 50 to 75 mm (2" to 3") of the top of the pan (Howell, Terry A. and Meron, 2007). Otherwise, a pan maintained with water levels at a depth < 50 mm might allow the wind to play a larger role in measurements since the water surface is higher and closer to the air flowing over the top of the pan. Whereas, a pan maintained at a depth > 75 mm may not show effects of wind on the evaporative demand, since the water surface is further below the edge of the pan and removed from the air flowing over the top of the pan. Errors can be up to 15% when the water level falls 100 mm below the standard 50 to 75 mm (Allen et al., 1998).

Other seasonal or equipment dependent factors play a role in measurement. Seasonal factors such as air temperature raise and lower the pan temperature, causing increased and decreased rates of evaporation. To work around these concerns, a conversion coefficient— known as the pan coefficient (K_p)— is applied to account for the seasonal and site factors,

which include if the pan is surrounded by fallow soil or vegetation. The comparison is made by using the average daily ET across a time period using **equation 3.1**:

$$ET_0 = K_p * E_{pan} \quad (3.1)$$

Where:

ET_o = reference evapotranspiration (mm/day)
K_p = pan coefficient (unitless)
E_{pan} = pan evaporation (mm/day)

As previously discussed, the pan coefficient will vary depending upon site and seasonal factors. Typical values for K_p based on these factors are shown in **Table 3.1**, which has been taken directly from Allen et al. (1998) who obtained the data from the FAO Irrigation and Drainage Paper 24 (Doorenbos and Pruitt, 1977).

Table 3.1. Typical Pan Coefficients based on Site and Weather Factors

Class A pan	Case A: Pan placed in short green cropped area				Case B: Pan placed in dry fallow area			
RH mean (%) ®		low < 40	medium 40 - 70	high > 70		low < 40	medium 40 - 70	high > 70
Wind speed (m s^{-1})	Windward side distance of green crop (m)				Windward side distance of dry fallow (m)			
Light	1	.55	.65	.75	1	.7	.8	.85
< 2	10	.65	.75	.85	10	.6	.7	.8
	100	.7	.8	.85	100	.55	.65	.75
	1000	.75	.85	.85	1000	.5	.6	.7
Moderate	1	.5	.6	.65	1	.65	.75.	.8
2-5	10	.6	.7	.75	10	.55	.65	.7
	100	.65	.75	.8	100	.5	.6	.65
	1000	.7	.8	.8	1000	.45	.55	.6.
Strong	1	.45	.5	.6	1	.6	.65	.7
5-8	10	.55	.6	.65	10	.5	.55	.65
	100	.6	.65	.7	100	.45	.5	.6
	1000	.65	.7	.75	1000	.4	.45	.55
Very strong	1	.4	.45	.5	1	.5	.6	.65
> 8	10	.45	.55	.6	10	.45	.5	.55
	100	.5	.6	.65	100	.4	.45	.5
	1000	.55	.6	.65	1000	.35	.4	.45

(Allen et al., 1998; Doorenbos and Pruitt, 1977)

Using a regression analysis based on the values in **Table 3.1**, equations were developed for calculating K_p. These equations are provided in **Table 3.2.**

Table 3.2. Pan coefficients (K_p) Regression Equations

Class A pan with green fetch	$K_p = 0.108 - 0.0286 * u_2 + 0.0422 \ln(F) + 0.1434 \ln(RH_{mean}) - 0.000631 * [\ln(\text{FET})]^2 * \ln(\text{RH}_{\text{mean}})$
Class A pan with dry fetch	$K_p = 0.61 + 0.00341 * \text{RH}_{\text{mean}} - 0.000162 * u_2 * \text{RH}_{\text{mean}} - 0.00000959 * u_2 * \text{FET} + 0.00327 * u_2 * \ln(\text{FET}) - 0.00289 * u_2 * \ln(86.4 * u_2) - 0.0106 * \ln(86.4 * u_2) * \ln(\text{FET}) + 0.00063 * [\ln(\text{FET})]^2 * \ln(86.4 * u_2)$
Coefficients and parameters	K_p = the pan coefficient (unitless) u_2 = the average daily wind speed at 2 m height (m/s) RH_{mean} is the average daily relative humidity (%) which is $\text{RH}_{\text{mean}} = (\text{RH}_{\text{max}} + \text{RH}_{\text{min}})/2$ FET = fetch of the identified surface type
Range for variables	1 m ≤ FET ≤ 1000 m (these limits must be observed) 30% ≤ RH_{mean} ≤ 84% 1 m/s ≤ u_2 ≤ 8 m/s

(Allen et al., 1998)

An additional concern in using an evaporation pan for ET_o measurements is that the behavior of evapotranspiration differs from an open-water surface compared to a plant (Howell, Terry A. and Meron, 2007; Allen et al., 1998). With this in mind, Allen et al. (1998) recommend making the comparison shown in **Equation 3.1** across 10 + day time periods.

The FAO Penman-Monteith Equation is the United Nations Food and Agriculture Organization's (FAO) sole recommended method for determining ET_o. The equation was developed in 1990 by a panel organized by the FAO, the International Commission for Irrigation and Drainage, and the World Meteorological Organization in response to two studies that suggested the FAO's previously recommended Modified Penman equation overestimated ET in certain circumstances. The studies had used lysimeters in both arid and humid climates around the world and suggested the Penman-Monteith equation performed well in both climates (Allen et al., 1998).

The Penman-Monteith equation makes a few key assumptions in its measurement of ET_o. First, it is assumed that the meteorological measurements take place at a 2 m height

over a 0.12 m (4.7") tall green crop canopy, such as a short green grass cover. Second, it is assumed the surface resistance of the vegetation at this height is 70 s/m. Third, it is assumed the vegetation has adequate water and is actively growing. Fourth, it is assumed that the albedo of the groundcover is 23%. With these inputs considered, the measurement is to be taken at a 2 m height for windspeed (Allen et al., 1998).

Although some inputs are to be held constant, the Penman-Monteith equation itself can be varied to measure over different lengths of time. The equation can be used for four different time lengths: a month, ten days, one day, or an hour. For this study, we focused on the hourly computation using **Equation 3.2** (Allen et al., 1998):

$$ET_o = \frac{0.408\Delta(R_n - G) + \gamma \frac{37}{T_{hr}+273} * u_2 e^{\circ}(T_{hr})(1 - \frac{RH_{hr}}{100})}{\Delta + \gamma(1 + 0.34u_2)} \quad (3.2)$$

where

ET_o = Reference evapotranspiration (mm/hr)

R_n = Net radiation at the grass surface ($\frac{\text{MJ}}{m^2 * hr}$)

G = Soil heat flux density ($\frac{\text{MJ}}{m^2 * hr}$)

can be approximated during daylight periods as:

$$G = 0.1\ R_n \quad (3.3)$$

and during nighttime periods as:

$$G = 0.5\ R_n \quad (3.4)$$

T_{hr} = Mean hourly air temperature (°C)

Δ = Saturation slope vapor pressure curve at T_{hr} (kPa/°C)

where $\Delta = \frac{4098 * e^{\circ}(T_{hr})}{(T_{hr}+237.3)^2}$ (3.5)

γ = Psychrometric constant (kPa/°C)

where $\gamma = \frac{c_p P}{\varepsilon \lambda} = 0.665 * 10^{-3} * P$ (3.6)

P = Atmospheric pressure (kPa)

λ = Latent heat of vaporization, 2.45 (MJ/kg)

c_p = Specific heat at constant pressure, $1.013\ 10^{-3}$ ($\frac{\text{MJ}}{kg * °\text{C}}$)

ε = Ratio molecular weight of water vapor/dry air = 0.622

$e°(T_{hr})$ = Saturation vapor pressure at air temperature T_{hr} (kPa)

where $e^{\circ}(T_{hr}) = 0.6108 * e^{\left(\frac{17.27 * T_{hr}}{T_{hr}+237.3}\right)}$ (3.7)

u_2 = Average hourly wind speed at 2 m height (m/s)

Developing K_p from Penman-Monteith Equation

Even with the pan coefficients provided by **Table 3.1** and **Table 3.2**, it is still recommended to calibrate the pan evaporation with the Penman-Monteith equation locally to determine if local site factors are not accounted for in K_p (Allen et al., 1998). This calibration can be done using **Equation 3.1**, solving for K_p using the Penman-Monteith ET_o for the ET_0 input. E_{pan} would remain the same as the depth change in water measured over the period.

Comparing ET_o to Crop ET

Once ET_o has been calculated, it still needs a comparison with crop ET. Crop ET is dependent upon three major factors that differ from the reference ET_o of a short green crop canopy such as grass or alfalfa. First, the percentage of ground covered by a specific crop will often be less than a reference crop like grass. This can lead to an increased rate of soil evaporation compared to the reference crop due to the increased exposure of bare soil. Second, the crop will likely be taller and have more aerodynamic resistance than the reference crop, which makes it more susceptible to climatic conditions. Third, the crop phenology will lead to varying rates of water use depending upon the stage of growth. These three factors can be combined or separated into varying coefficients. In this study, we focused on one coefficient to keep the application simple. This one coefficient comparison is shown in **Equation 3.8**:

$$ET_c = K_c * ET_o \tag{3.8}$$

where
ET_c = Crop evapotranspiration (mm/day)

K_c = Crop coefficient (unitless)
ET_o= Reference crop evapotranspiration (mm/day)

This study incorporated Cotton in its comparison against the reference crop. Typical K_c values for each stage of Cotton growth are displayed in **Table 3.3** along with data that determines each stage of growth by heat units from research performed in Tifton, GA.

Table 3.3. Cotton Growth Stage Data

Growth Stage	Heat Units	K_c
Initial	0	0.35
Development	550	
Mid	950	1.15-1.20
Late	2150	0.50-0.70
Harvest	2600+	

(Ritchie et al., 2004; Allen et al., 1998)

As seen in **Table 3.3**, the crop coefficient depends upon the stage of growth. Each stage of growth has a different length depending upon the crop and climate-based variables. For Cotton, growth can be expressed based upon heat units, as shown in **Table 3.3**. The step-by-step way to calculate these heat units is shown from left to right in **Table 3.4,** which is an example taken directly from an Extension Service publication from The University of Georgia (UGA).

Table 3.4. Calculation of Cotton Heat Units

Day	Daily High Temperature ($°F_{max}$)	Daily Low Temperature ($°F_{min}$)	Average Daily Temperature ($°F_{max}+°F_{min}$)/2	Daily Heat Units ($°F_{max}+°F_{min}$)/2-60	Accumulated Heat Units
1	81	61	71	11	11
2	83	63	73	13	24
3	82	62	72	12	36
4	85	66	75.5	15.5	51.5
5	80	62	71	11	62.5

(Ritchie et al., 2004)

As seen in **Table 3.4**, heat unit calculation is a four-step process. First, one must obtain the daily high and low temperature. Second, one must take the average daily temperature by averaging the high and the low temperature for that day. Third, one must subtract 60°F from the average daily temperature to obtain the heat units. Fourth, one must sum the heat units for all the days of growth that lead up to the day being analyzed, which is referred to as accumulated heat units. Once the accumulated heat units have been calculated, the data for an experiment can be compared to the data presented in **Table 3.3** to estimate the stage of growth in the season.

As an example of what a crop coefficient curve should look like, **Figure 3.3** is shown below using the FAO data and UGA data presented in **Table 3.3**, as well as additional historical data presented in the original UGA publication.

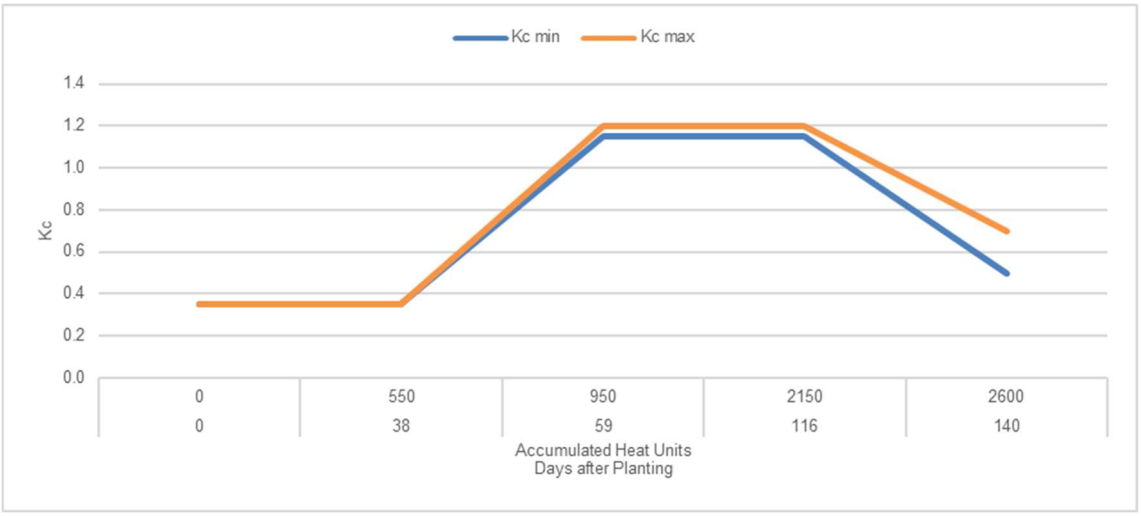

Figure 3.3. Cotton Crop Development K_c Curve

In **Figure 3.3**, $K_{c\,min}$ and $K_{c\,max}$ represent the minimum and maximum range values, respectively, given by the FAO data in **Table 3.3**. This reference curve or an average of the min and max FAO curves can be used at the end of the study to compare if our crop performed near the range expected for Cotton.

Methods and Materials

ET_o Measurement

For this study, a Class A evaporation pan was sited in a location surrounded by a short grass canopy. The pan was more than 15 m to the west of the cotton field being used in this study, and was more than 20 m east of the Edisto Bull Forage Test Facility. Combined together, this distance gives 35 m distance of short grass canopy in the east-west direction (Microsoft and Earth Zoom, 2019). To the North and South, there was much more fetch of short grass canopy (north: 40 to 75 m, depending on azimuth; south: 45 to 60 m). The siting does meet Allen et al.'s recommendation of siting a pan in an area surrounded by 20m by 20m of short grass canopy, with all sides are open to free air. Though, for this

study, a few conditions did not meet the recommendations provided in the Background section. First, the pan was sited upwind of the Cotton field used in this study. Second, the pan was not surrounded by a wire enclosure to keep animals from drinking the pan water. However, a copper-sulfate based algaecide was used to maintain clear water in the pan, which likely served as a deterrent to animals drinking the water. Third, a regular depth of 50 mm to 75 mm from the top of the pan was not maintained in the study. The pan maintained a wide range of depths during the growing season. The depth was maintained properly enough to allow the measurement equipment to continue measurements uninterrupted, though not at the 50 mm to 75 mm recommendation. The pan used for the study and its measurement equipment are shown in **Figure 3.4.**

Figure 3.4. Pan Siting of Class A Evaporation Pan

The water level in the Evaporation Pan was measured using several methods. These methods included a load cell supporting one side of a tri-pointed stand, a MiloneTech eTape measurement tape (Milone Technologies, Sewell, NJ, USA), a pressure sensor, and an Analog Output Evaporation Gauge (NovaLynx Corporation, Grass Valley, California,

USA). For this study, the data from the Evaporation Gauge will be used for the evaporation pan measurement. The Evaporation Gauge is shown in **Figure 3.5**.

Figure 3.5. NovaLynx 255-100 Analog Output Evaporation Gauge (NovaLynx Corporation, 2016)

The Evaporation Gauge connects to the evaporation pan via a hose to conduct measurements. The device is hollow and is similar to a stilling well in that it allows water in at the base of the Gauge to maintain a water level inside that is level with the evaporation pan. Measurements are taken by a float with a chain that rolls over a wheel at the top of the device. This can be seen in **Figure 3.5**. The float goes up and down as the water level changes inside the Gauge. Because its attached chain goes over the wheel, the wheel turns with these movements. The wheel is connected to a potentiometer, so that as the wheel turns, the potentiometer outputs different voltage outputs. Using these outputs, the potentiometer is calibrated to measure the depth level inside of the Evaporation Gauge, allowing for the calculation of changes over time.

Using data from the evaporation gauge, the analysis was conducted with the goal of averaging pan evaporation over 10+ day time periods. The depth level changes were

measured in 30-minute time intervals. The sum of these changes was taken as a sum over each 24-hour day (midnight to midnight). Following the recommendations in the background section, these daily ET rates were then combined and averaged to be across 10+ day time intervals.

K_p was derived using the directions given in **Table 3.2**. RH_{mean} was calculated for each day using the equation given in **Table 3.2**, taking the mean of RH_{min} and RH_{max}. u_2 was taken as the average wind speed for each day. Both RH_{mean} and u_2 were averaged over their analysis period (10+ day period), then used as the input to the equation for K_p with green fetch given in **Table 3.2**. This value was then multiplied to E_{pan} to obtain Pan ET_o measurements.

The meteorological variables that account for the pan coefficient and the Penman-Monteith ET_o, were measured by a weather sensor sited on a pole next to the Evaporation Gauge. The weather station used for this study was a ClimaVUE^{TM}50 (Campbell Scientific, Inc., Logan, Utah, USA)(**Figure 3.6**).

Figure 3.6. Campbell Scientific ClimaVUE ™50 Weather Sensor (Campbell Scientific, 2018)

The sensor was able to sample weather data using a CR6 datalogger (Campbell Scientific, Inc., Logan, Utah, USA) and automatically compute the hourly Penman-Monteith ET_o using this data. The computation was stored in a data table across the entire season. For the analysis, these hourly ET_o computations were summed over 24-hour periods to estimate the daily ET_o. Following the same procedure used for the evaporation pan, the daily ET_o was then averaged over 10+ day time periods to be over the same comparison periods as the evaporation pan.

For analysis in the results section, the comparison between the two datasets of pan ET_o and Penman-Monteith ET_o was made using a linear regression R^2 fit of the datasets.

Developing K_p from Penman-Monteith Equation

Following the background section, a calibration was made between the pan evaporation and the Penman-Monteith equation (Allen et al., 1998). This calibration was conducted using **Equation 3.1**, solving for K_p while using the Penman-Monteith ET_o in the equation for ET_o. E_{pan} remained the same as the depth change in water measured over the period. The comparison was conducted using a two-sample t-test using Minitab (Minitab

LLC, State College, PA, USA) with a level of significance of $\alpha = 0.05$. In addition, an R^2 linear regression was used to also compare the two K_p datasets.

Crop Coefficient Curve

The crop coefficient curve for cotton in a southeastern humid environment was developed using **Equation 3.8**. Measurements from the south lysimeter were used to obtain ET_c, and ET_o values were obtained using the Penman-Monteith equation.

The specifications for the lysimeter and its design are given in Chapter 1 of this Thesis. The specifications, as a basic review, are a 1 m wide by 1 m long by 1.5 m deep metal weighing lysimeter measured continuously using four Phidget S Type Load Cells (Phidgets, Calgary, Alberta, Canada). Sampling was made every five seconds and output as the average for each 10-minute time period. The measurements were taken using a 24-bit CR1000X datalogger (Campbell Scientific, Inc., Logan, Utah, USA).

The ET data used for this study from the lysimeter was the same data used in Chapter 1, with the exceptions of filtering and analyzing the data on different time intervals. The procedure for obtaining this data involved measuring lysimeter changes in 30-minute time intervals, discarding data that was believed to be collected during irrigation or precipitation events, and summing the changes into Daily ET. No daily ET values were discarded for significant differences in plant heights between the field and the south lysimeter. Using **Equation 3.8**, these daily ET values were used to obtain the daily K_c values. The K_c values were then compiled into crop growth stage based upon calculations of temperature data recorded at the neighboring Edisto Bull Forage Test facility (Sell, 2019) and the accumulated heat unit changepoints given in **Table 3.3**. Any gaps in

temperature data were filled by data obtained from the ClimaVUE^{TM}50 weather sensor. The daily K_c values were analyzed to filter out any values that were more than 2 standard deviations from its crop growth stage's average K_c. The data analysis for the K_c curve ended on the Friday of the week the cotton crop was defoliated (18 Oct). After defoliation, it was assumed that crop growth ended. Two K_c curves, a daily plot and a crop growth stage plot, were created to display how the cotton crop performed against FAO data.

A statistical comparison was made using the crop growth stage K_c curve versus the midpoint of each FAO recommended K_c range given in **Table 3.3**. The data was compared using one-sample t-tests to analyze if the average K_c during each growth stage fitted the midpoint FAO K_c data using an α level of significance of 0.05.

Results

The cotton was planted in the Lysimeter on 24 May and harvested on 11 November, which included 171 days. To avoid interference of ET measurements from planting and harvesting, the analysis period was conducted from 25 May to 10 November. Dates in June were excluded from the analysis period due to two different causes: floating of the south lysimeter, and missing weather data. The dates excluded for each analysis are mentioned in each subsection.

ET_o Measurement

For this analysis, data was lost when setting up a cellular module for the datalogger. Therefore, the dates from 17 to 22 June were excluded from the analysis. The Pan and Penman-Monteith ET_o plots are shown in **Figure 3.7.**

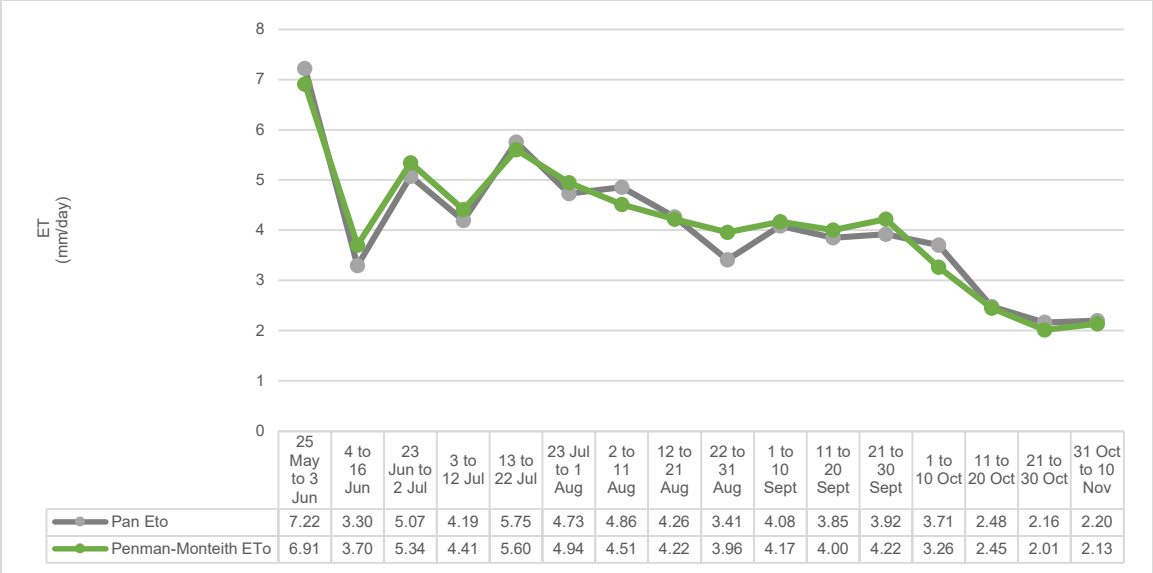

	25 May to 3 Jun	4 to 16 Jun	23 Jun to 2 Jul	3 to 12 Jul	13 to 22 Jul	23 Jul to 1 Aug	2 to 11 Aug	12 to 21 Aug	22 to 31 Aug	1 to 10 Sept	11 to 20 Sept	21 to 30 Sept	1 to 10 Oct	11 to 20 Oct	21 to 30 Oct	31 Oct to 10 Nov
Pan Eto	7.22	3.30	5.07	4.19	5.75	4.73	4.86	4.26	3.41	4.08	3.85	3.92	3.71	2.48	2.16	2.20
Penman-Monteith ETo	6.91	3.70	5.34	4.41	5.60	4.94	4.51	4.22	3.96	4.17	4.00	4.22	3.26	2.45	2.01	2.13

Figure 3.7. Pan and Penman-Monteith ET_o

For the data in **Figure 3.7**, visually there is much agreement between the two plotted values. Numerically, the two datasets show an $R^2 = 0.95$. As seen in the data, both ET_o plots tend to decrease towards the end of the season.

Developing K_p Values from Penman-Monteith Equation

Following the ET_o comparison, the dates 17 to 22 June were excluded from the analysis. The data for K_p throughout the season are shown in **Figure 3.8**.

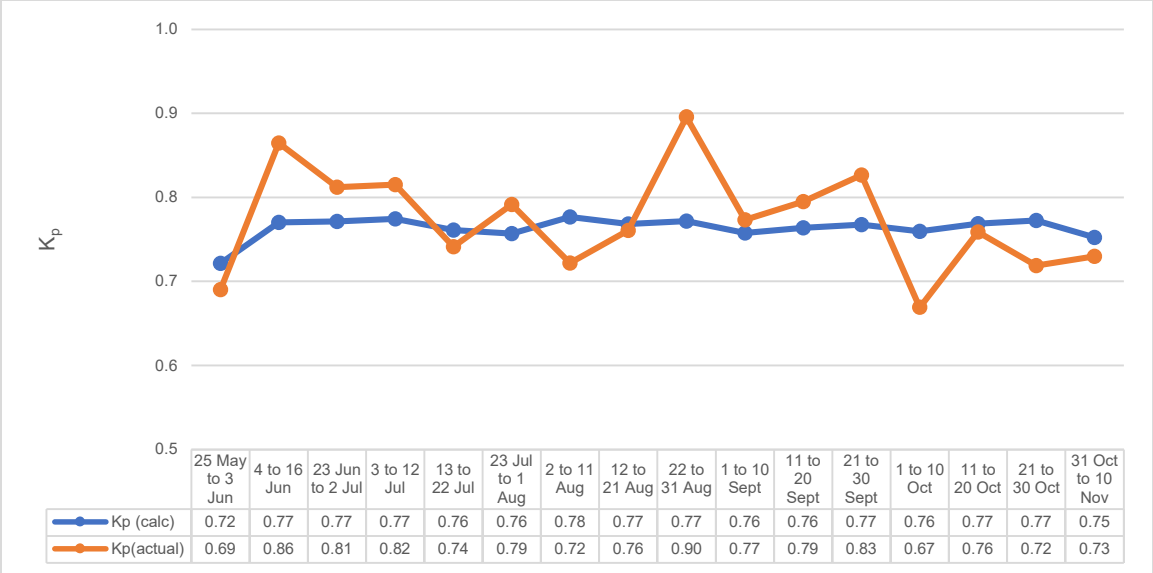

	25 May to 3 Jun	4 to 16 Jun	23 Jun to 2 Jul	3 to 12 Jul	13 to 22 Jul	23 Jul to 1 Aug	2 to 11 Aug	12 to 21 Aug	22 to 31 Aug	1 to 10 Sept	11 to 20 Sept	21 to 30 Sept	1 to 10 Oct	11 to 20 Oct	21 to 30 Oct	31 Oct to 10 Nov
Kp (calc)	0.72	0.77	0.77	0.77	0.76	0.76	0.78	0.77	0.77	0.76	0.76	0.77	0.76	0.77	0.77	0.75
Kp(actual)	0.69	0.86	0.81	0.82	0.74	0.79	0.72	0.76	0.90	0.77	0.79	0.83	0.67	0.76	0.72	0.73

Figure 3.8. Pan Coefficients for Different Comparison Periods throughout the Season

As seen in **Figure 3.8**, the pan coefficient values for the season lie in the range of 0.69 to 0.90. The average for $K_p(calc)$ was 0.76 and $K_p(actual)$ was 0.77. A two-sample t-test was performed (N=16) and the two K_p values were found to not be significantly different (p-value=0.56). An R^2 linear regression was also performed between the two K_p values, and was found to be 0.22. This shows a poor agreement between the K_p values, which should be factored into the discussion of whether to retain the FAO derived K_p values.

Crop Coefficient Curve

For the season, the lysimeter experienced floating from a high water-table from 14 to 25 June. With the exception of these dates, the data was analyzed up to October 18th – which was the Friday of the week the crop was defoliated. **Figure 3.9** shows a plot of the midpoint FAO values expected for each growth stage compared to daily K_c values and a 5-day moving average of these daily K_c values.

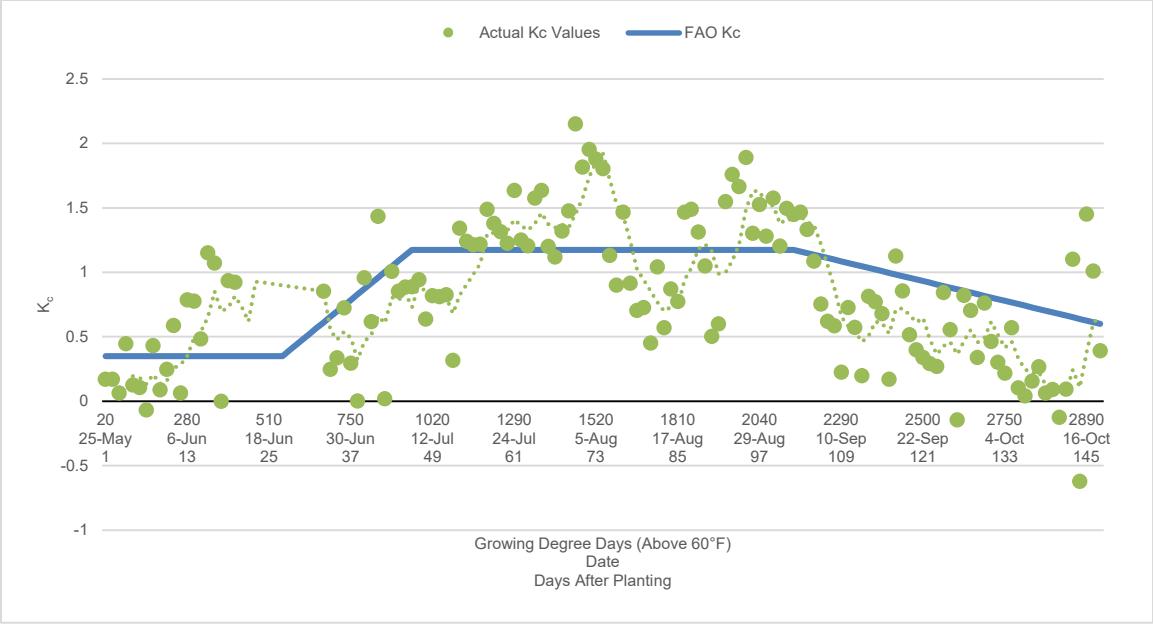

Figure 3.9. Plot of Season's K_c data in comparison to FAO data

Using the data from **Figure 3.9**, it was determined that none of the three growth stages analyzed differed significantly from the FAO provided crop coefficient recommendations. **Table 3.5** shows the results from this analysis:

Table 3.5. One-Sample T-test Results

Growth Stage	Hypothesis (H_0)	P-value
Initial	$K_c = 0.35$	0.270
Mid	$K_c = 1.175$	0.277
Late	$K_c = 0.6$	0.206

Taking the data in **Figure 3.9** a new K_c curve was developed for this study. This curve is shown in **Figure 3.10**:

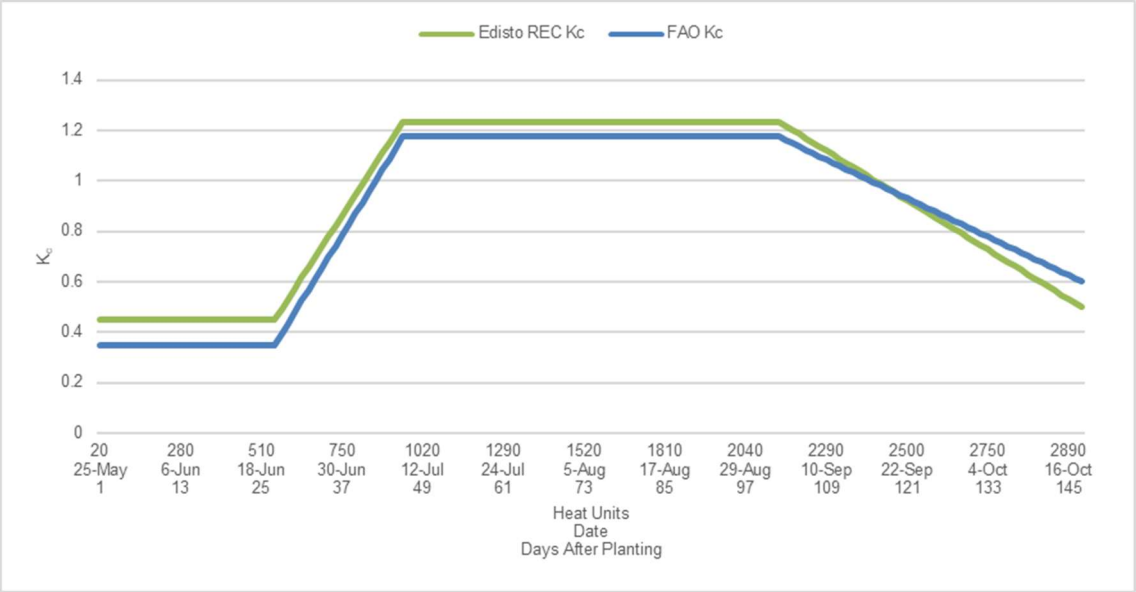

Figure 3.10. Crop Coefficients for Different Comparison Periods Throughout the Season

The coefficients for the new K_c curve are shown in **Table 3.6**. These values are the averages across each growth stage based on the 147-day growing season used in the analysis**.**

Table 3.6. New K_c Values

	Initial	Mid	Late
Average	0.45	1.23	0.50

The values in **Table 3.6** are near the values expected from FAO data. As it can be seen, the Initial K_c is 0.45, which is slightly but not significantly higher than the FAO value of 0.35. The mid-season K_c of 1.23 is near the FAO expected range of 1.15 to 1.2. While the Late stage K_c of 0.50, is just within the FAO expected late-season range of 0.50 to 0.70.

Discussion

ET_o Measurement

The ET_o measurements from the evaporation pan and those derived from weather data using the Penman-Monteith equation showed good agreement with each other at R^2 = 0.95. Therefore, either method should provide relatively good results throughout different times of year for producing ET_o values at this site.

Developing K_p Values from the Penman-Monteith Equation

The results for K_p were satisfactory. The K_p values obtained from the FAO regression equations and the K_p values obtained from the Penman-Monteith ET_o data were not significantly different (p-value=0.56). Although the agreement between the two datasets is poor at $R^2 = 0.22$, the high R^2 agreement found in Objective 1's ET_o comparison and an insignificant t-test suggest that the FAO K_p regression equations perform well enough for continued use at the Edisto REC site.

Crop Coefficient Curve

For the K_c curve analysis, the data performed quite similarly to the FAO recommended K_c values for the three growth stages compared. For the initial stage, there was no statistical difference between the FAO value (0.35) and the data obtained in our study (Avg. = 0.45). This is encouraging as the FAO writes that $K_{c\ ini}$ can be highly variable (0.1 to 1.15) depending upon soil wetting events. This is because the crop has not grown enough to shield the surface from the sun, which causes high rates of soil evaporation when there are frequent soil wetting events. As the crop begins to grow and shield the ground,

these values should normalize. In addition, the mid-season K_c data was not significantly different from the FAO recommended values; and with an average of 1.23, it was near the FAO range of 1.15 to 1.20. Lastly, the late season K_c data (Avg. = 0.50) did not significantly differ from the FAO midpoint value (0.60) and the average was within the FAO range of 0.50 to 0.70. With the similarity between the average K_c values obtained in this study and the FAO K_c recommendations given for Cotton, it could be recommended to continue using FAO K_c values for cotton in South Carolina's humid southeastern climate. The study did yield site-specific data that could be applied for future use, though the south lysimeter data used did differ significantly from the field at points in the growing season (see Chapter 1).

Conclusions

In conclusion, there were three objectives which were accomplished in this study. The first objective was to compare ET_o measurements obtained from a Class A evaporation pan with those obtained using the Penman-Monteith equation. For the first objective, both methods performed well compared to one another (R^2=0.95). The second objective was to develop K_p values based upon Objective 1's ET_o comparison. The newly developed K_p values did not significantly differ from K_p values obtained from the Penman-Monteith ET_o. The third objective was to develop a crop coefficient (K_c) curve from lysimeter data for a cotton crop growing in the southeastern humid climate. The results obtained from this third objective reveal that the K_c curve for the southeastern humid climate did not significantly differ from the recommended FAO values for cotton. Therefore, it can be recommended to continue using the FAO K_c values for South Carolina's humid southeastern climate, though the K_c curve obtained in this study may better predict Cotton water usage in South Carolina.

REFERENCES

Allen, R. G., Pereira, L. S., Raes, D., & Smith, M. (1998). *Crop evapotranspiration - guidelines for computing crop water requirements - FAO irrigation and drainage paper 56* [FAO Irrigation and drainage paper 56]. Rome, Italy: Food and Agriculture Organization of the United Nations. Retrieved from http://www.fao.org/3/X0490E/x0490e00.htm

Campbell Scientific, I. (2018). *ClimaVUE^{TM}50 compact digital weather sensor* Campbell Scientific, Inc. Retrieved from https://www.campbellsci.com/climavue-50

Doorenbos, J., & Pruitt, W. O. (1977). *FAO irrigation and drainage paper 24: Crop water requirements*
(Revised ed.). Rome, Italy: Food and Agriculture Organization (FAO).

Howell, T. A., & Meron, M. (2007). 3. irrigation scheduling. In F. R. Lamm, J. E. Ayars & F. S. Nakayama (Eds.), *Developments in agricultural engineering* (pp. 61-130) Elsevier. doi:https://doi.org/10.1016/S0167-4137(07)80006-0 " Retrieved from http://www.sciencedirect.com/science/article/pii/S0167413707800060

Microsoft, & Earth Zoom. (2019). *Edisto research and education center*
Zoom Earth.

National Weather Service. (2015). *Class A evaporation pan with wire fence in background*
National Weather Service. Retrieved from https://www.weather.gov/images/box/coop/coop_evap.jpg

NovaLynx Corporation. (2016). 255-100 analog output evaporation gauge. Retrieved from https://novalynx.com/store/pc/255-100-Analog-Output-Evaporation-Gauge-20p802.htm

Ritchie, G. L., Bednarz, C. W., Jost, P. H., & Brown, S. M. (2004). *Cotton growth and development.* ().The University of Georgia College of Agricultural and Environmental Sciences Cooperative Extension Service. Retrieved from https://www.spar.msstate.edu/class/EPP-2008/Chapter%201/Reading%20material/Temperature%20including%20Extremes/cotton_heat_Units1.pdf

Sell, S. (2019).
Davis vantage pro weather station - 2019 EDISTO REC WX DATA. Edisto Research and Education Center, 3.5 miles West of Blackville, SC: Clemson University.

APPENDICES

Appendix A

Wiring for Surface Renewal 2 Setup

Table A.1. Wiring for Surface Renewal 2 Datalogger

Sensor	Sensor Wire	Datalogger Connection	Comments
Sonic Anemometer (Gill Windmaster)	White[TXA(-)]	RX(C2)	
	Yellow[RXA(-)]	TX(C1)	
	Red+Blue (Power V+)	12V	
	Black (Power 0V)	Power GND	
	Brown	Signal GND	
	Orange	"Chassis" GND	
Stevens Hydraprobe II	Blue	C3	SN 247853
	Red	12V	
	Black	Power GND	
Stevens Hydraprobe II	Blue	C5	SN 247622
	Red	12V	
	Black	Power GND	
Thermocouple (FW3)-1	Signal (purple)	1H	
	Signal Ref (red)	1L	
	Shield	AG	
Thermocouple (FW3)-2	Signal (purple)	2H	
	Signal Ref (red)	2L	
	Shield	AG	
Net Radiometer (NR Lite 2)	Signal (red)	3H	SN 191530
	Signal Ref (blue)	3L	
	Short jumper to 3L	AG	
Temp/RH sensor (CS215)	Power (red)	12V	
	SDI-12 Signal (green)	C7	
	Black, White, Clear	G	
Huskeflux Soil Heat Flux Plate 1	White	4H	SN 15678
	Green	4L	
	Black	AG	
Huskeflux Soil Heat Flux Plate 2	White	5H	SN 15679

	Green	5L	
	Black	AG	
Solar Radiation Pyranometer (Apogee SP-110)	Signal (red or white)	6H	SN 45173
	Signal Ref Jumper to AG (black)	6L	
	Shield (clear)	AG	
Tipping Bucket Rain Gauge (TE-525)	Precipitation signal (black)	P1	135 ms needed for switch closure, 0.75 ms settling time
	Signal Ref (white)	AG	
	Shield (clear)	AG	
Cell 210 module	CS I/O	CS I/O	

Appendix B

Fetch Dimensions of Cotton Field

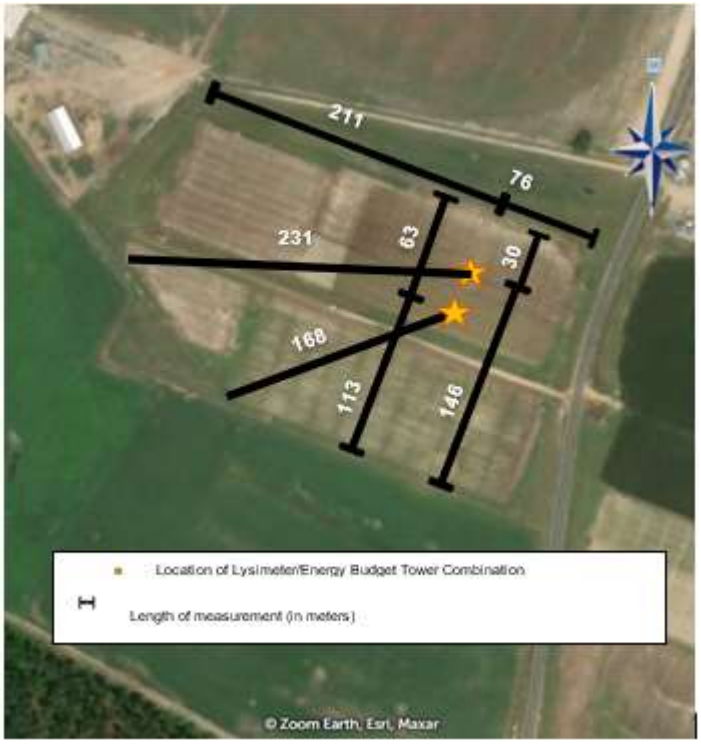

Figure B.1. Fetch Dimensions of Cotton
Used with permission and modified from (Zoom Earth et al., 2018)

Appendix C

Wind Rose of Growing Season Data

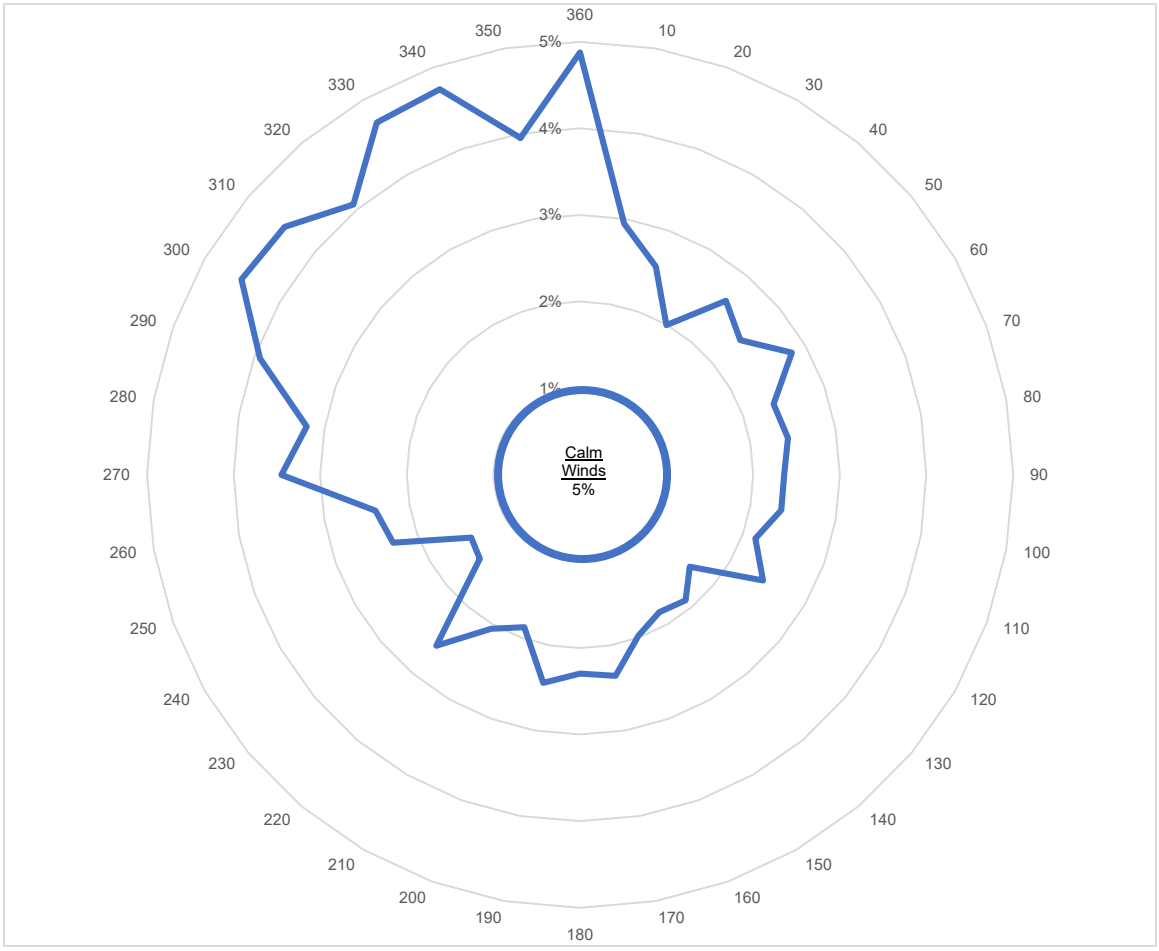

Figure C.1. Wind Rose of South Tower

Calm Winds are < 1 mph (0.447 m/s)
Filtered to include data only from 6:00 am to 9:30 pm

Appendix D

Scatter Plots of Surface Renewal Fetch Analysis

	T1 ET Comparison (Uncalibrated)	T2 ET Comparison (Uncalibrated)
North Lysimeter (n=12)	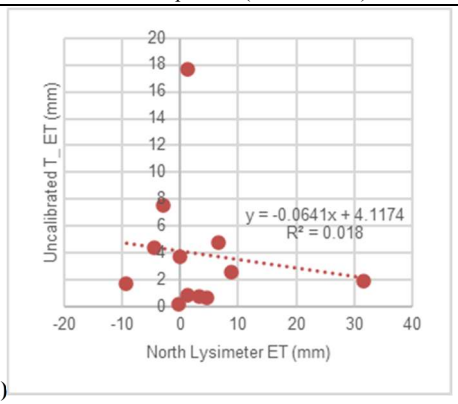 a)	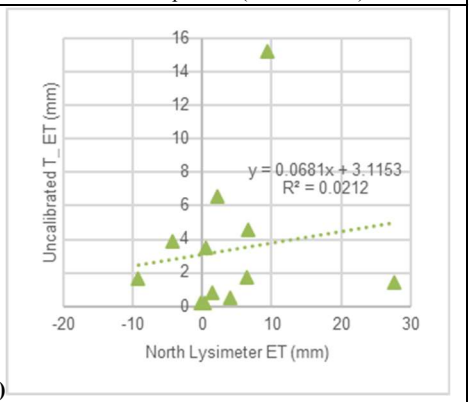 b)
South Lysimeter (n=23)	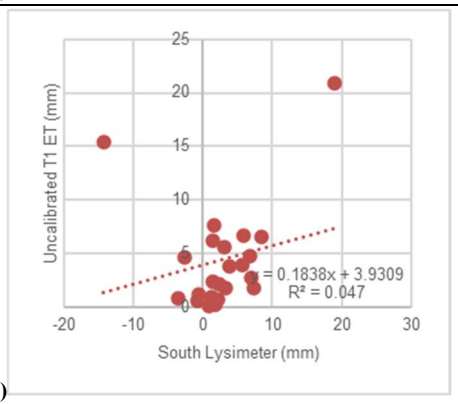 c)	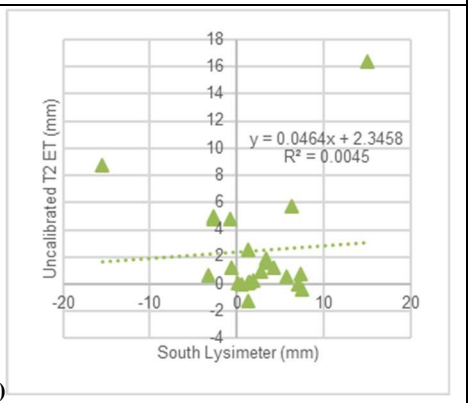 d)

Figure D.1. Comparison of Uncalibrated Surface Renewal ET with Lysimeter ET using Fetch requirements

	T1 Castellví ET Comparison	T2 Castellví ET Comparison
North Lysimeter (n=12)	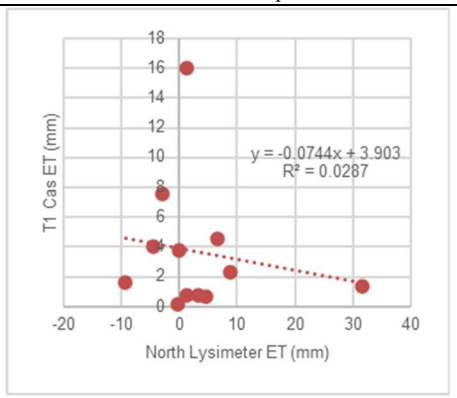 a)	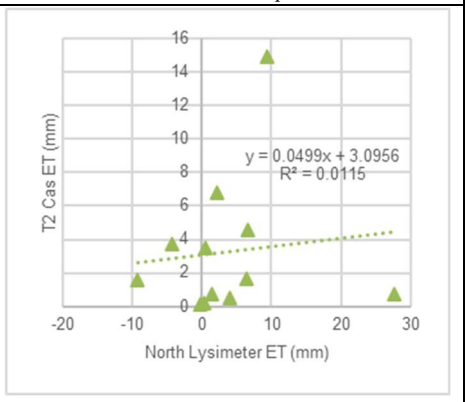 b)
South Lysimeter (n=15)	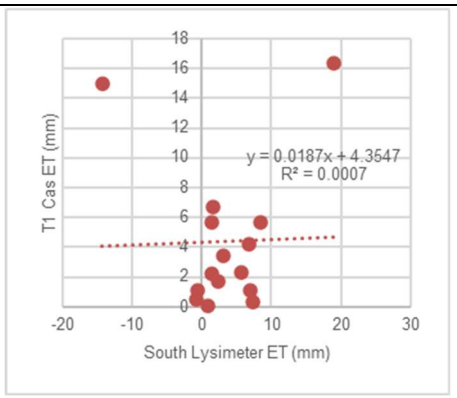 c)	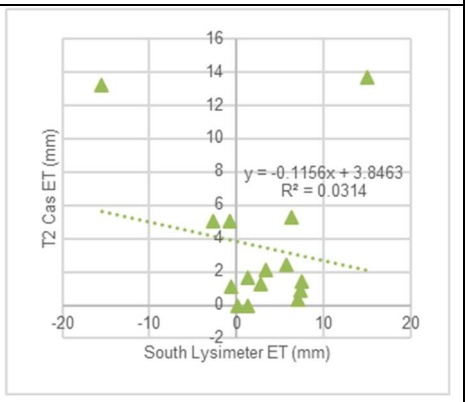 d)

Figure D.2. Comparison of Castellví method ET with Lysimeter ET using Fetch Requirements

Appendix E

Cotton Plants' Height Data

Table E.1 Cotton Plants' Height Data

	For South Tower			For North Tower			
Date	All Plants Average(m)	South Lysimeter Avg. (m)	p-value	All Plants Average (m)	North Lysimeter Avg. (m)	p-value	Commentary
17-Jun	0.12	0.06	#DIV/0!	0.12	0.18	#DIV/0!	
21-Jun	0.13	0.10	0.043	0.13		#DIV/0!	
24-Jun	0.16		#DIV/0!	0.16		#DIV/0!	
28-Jun	0.19		#DIV/0!	0.20		#DIV/0!	
1-Jul	0.21	0.23	#DIV/0!	0.23	0.30	#DIV/0!	
5-Jul	0.26	0.32	#DIV/0!	0.26	0.41	#DIV/0!	
8-Jul	0.29	0.41	#DIV/0!	0.29	0.48	#DIV/0!	
12-Jul	0.38	0.41	0.614	0.40	0.53	0.016	
15-Jul	0.38	0.41	0.666	0.43	0.57	0.016	
19-Jul	0.52	0.65	0.102	0.48	0.69	0.001	
22-Jul	0.54	0.70	0.047	0.58	0.75	0.014	
29-Jul	0.63	0.88	0.000	0.68	0.87	0.005	
2-Aug	0.69	0.93	0.006	0.76	0.91	0.022	
5-Aug	0.70	0.86	0.036	0.76	0.93	0.018	
9-Aug	0.76	0.95	0.014	0.85	1.01	0.004	
12-Aug	0.87	1.04	0.003	0.87	1.03	0.019	
16-Aug	0.88	1.05	0.001	0.93	1.07	0.003	*Growth retardant sprayed 8/14/2019
19-Aug	0.87	0.94	0.341	0.94	1.00	0.283	
23-Aug	0.85	0.99	0.062				*North half was not measured due to lighting.
26-Aug	0.89	0.91	0.868	0.95	0.96	0.966	
30-Aug	0.82	0.98	0.036	1.00	1.08	0.025	
3-Sep	0.92	1.01	0.190	1.03	1.08	0.095	
13-Sep	0.90	1.17	0.007	0.95	1.02	0.198	
20-Sep	0.90	0.98	0.268	1.01	1.07	0.129	
27-Sep	0.92	0.97	0.537	1.01	1.07	0.176	
4-Oct	0.94	1.05	0.103	1.03	1.08	0.264	*Additional Growth retardant sprayed. Did not measure plant heights after Oct. 4th

*P-value was obtained using a 2-tailed T-test assuming different variances

Appendix F

Pressure Differential Device Materials

2 Devices

First device was built using the following materials:

- Plastiflex 6’ by 1.5” Magnum Filter/Pump Connection Hose
- Used pvc adapters to connect the 1.5” Plastiflex hose to the 1” riser pvc pipe at a 90-degree angle
- 6-foot length of a 1” pvc pipe as a riser to the surface.
- Sensor: Currently using a milontech eTape for depth level measurement. Original plan was to use an ultrasonic depth-level sensor

Second device was built using the following materials:

- 78” of Angus Premium 200 4” diameter Irrigation hose
    - Material: “Nitrile rubber extruded through-the-weave.” -source: http://angusfire.com/industrial-hose/agricultural/premium-200/
- 3/4” riser piece

P-7100-132A-R1 Pressure Transducer from Nidec Copal Electronics

Appendix G

Pressure Differential Device Data compared with Rainfall

Table G.1 Lysimeter Rainfall/Irrigation Data and PDD ET

Date	Rain / Irr. (mm)	PDD ET (mm)
6/8	35.14	-152.03
6/9	25.79	57.79
6/10	9.73	86.88
6/11	1.04	10.68
6/12	7.58	-24.42
6/13	0	-6.57
6/14	0	2.19
6/15	0	1.31
6/16	0	1.75
6/17	0	7.22
6/18	0	-4.37
6/19	0	-0.10
6/20	5.08	6.09
6/21		5.30
6/22	7.27	8.41
6/23	8.87	10.07
6/24	0	-8.70
6/25	0	-6.07
6/26		6.43
6/27		0.63
6/28		1.54
6/29	1.66	2.90
6/30		-1.33
7/1	6.47	7.16
7/2		-0.89
7/3		-0.32
7/4	2.39	2.06
7/5	5.31	5.39
7/6		1.28
7/7		1.82
7/8		0.22
7/9		0.73
7/10	1.80	1.79
7/11		-0.88
7/12		-0.04
7/13		2.38
7/14		-0.45
7/15	20.25	23.04
7/16		1.77
7/17		1.26
7/18		1.47
7/19	11.81	13.78
7/20		1.42
7/21		0.33
7/22		-0.53
7/23	5.30	6.52
7/24	0.14	2.15
7/25		2.22
7/26	11.78	17.14
7/27		2.89
7/28		3.23
7/29		-0.92
7/30	17.68	19.93
7/31	10.10	12.43
8/1		2.74
8/2		3.38
8/3		1.66
8/4	5.24	9.78
8/5		1.82
8/6		0.90
8/7		-0.79
8/8	11.77	11.35
8/9		0.24
8/10		-1.84
8/11		4.63
8/12		8.38
8/13	10.72	23.32
8/14		10.45
8/15		4.41
8/16	12.37	20.37
8/17	18.76	18.93
8/18		-0.16
8/19		2.45
8/20		3.38
8/21		7.25
8/22	9.2	17.55
8/23	49.89	45.75
8/24	23.82	-19.38
8/25		-10.20
8/26		-0.55
8/27		-8.71
8/28		3.77
8/29		4.17
8/30		3.50
8/31		5.68
9/1	4.92	8.66
9/2		2.38
9/3		4.65
9/4		6.00
9/5		5.59
9/6		11.12
9/7		15.12
9/8		9.13
9/9		4.70
9/10	9.38	11.16
9/11		-2.11
9/12		-1.82
9/13	11.9	12.09
9/14		-0.42
9/15		1.71
9/16		1.86
9/17	6.27	7.78
9/18		-0.25
9/19		4.69
9/20		4.82
9/21		4.08
9/22		2.52
9/23		1.81
9/24	12.33	14.18
9/25		0.18
9/26		-1.93
9/27	8.39	8.16
9/28		-1.43
9/29		-1.35
9/30	1.29	0.48
10/1		0.32
10/2		-0.76
10/3		-2.38
10/4		-1.72
10/5		-0.72
10/6		-1.22
10/7		-0.41
10/8		2.76
10/9		1.97
10/10		1.65
10/11		2.30
10/12		1.79
10/13	5.26	5.65
10/14	4.22	8.13
10/15	6.15	5.09
10/16	11.77	15.33
10/17		5.40
10/18		5.27
10/19	23.94	29.07
10/20	2.62	9.98
10/21		4.93
10/22	1.21	5.80
10/23		2.37
10/24		1.74
10/25		1.90
10/26	20.12	20.72
10/27	5.90	6.46
10/28		-6.24
10/29	12.78	8.30
10/30		-5.01
10/31	8.73	5.99
11/1		-5.07
11/2		-4.36
11/3		0.87
11/4		1.50
11/5		1.97
11/6		0.58
11/7	1.62	-0.91
11/8	14.70	14.45
11/9		-1.00
11/10		1.91
11/11		3.59

Appendix H

Month by Month Comparison of PDD and Lysimeter

Week	Data Picture
June	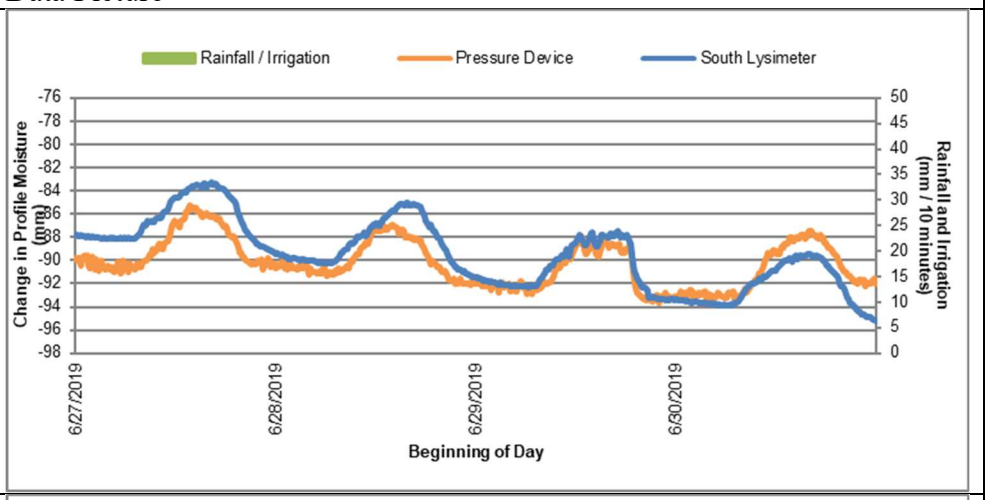
July	

August	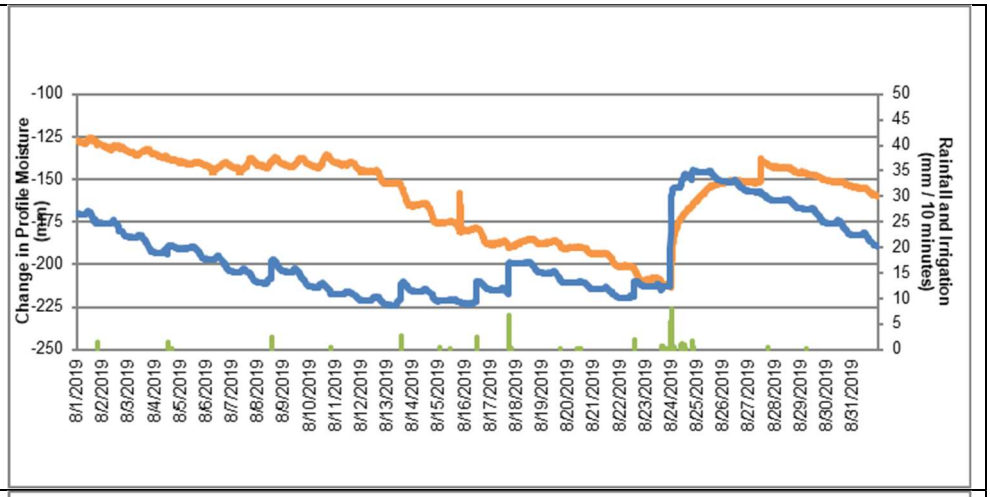
September	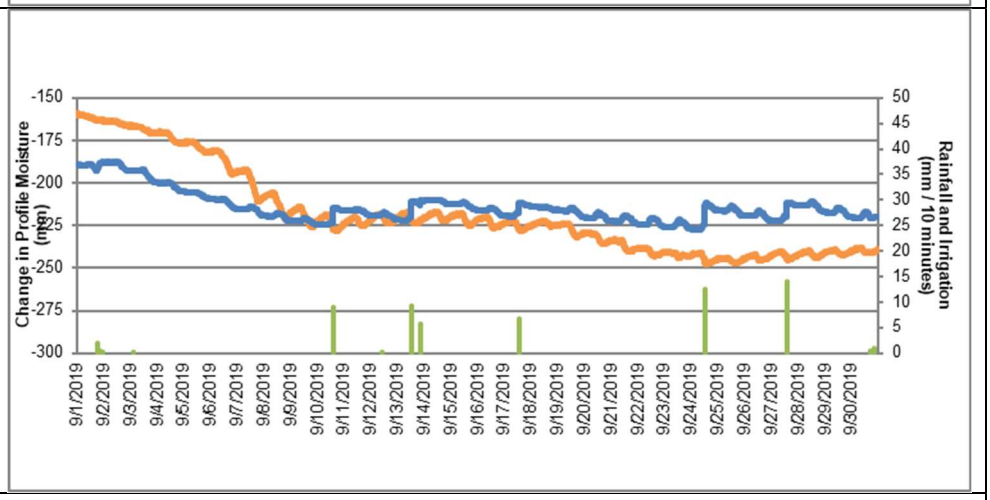
October	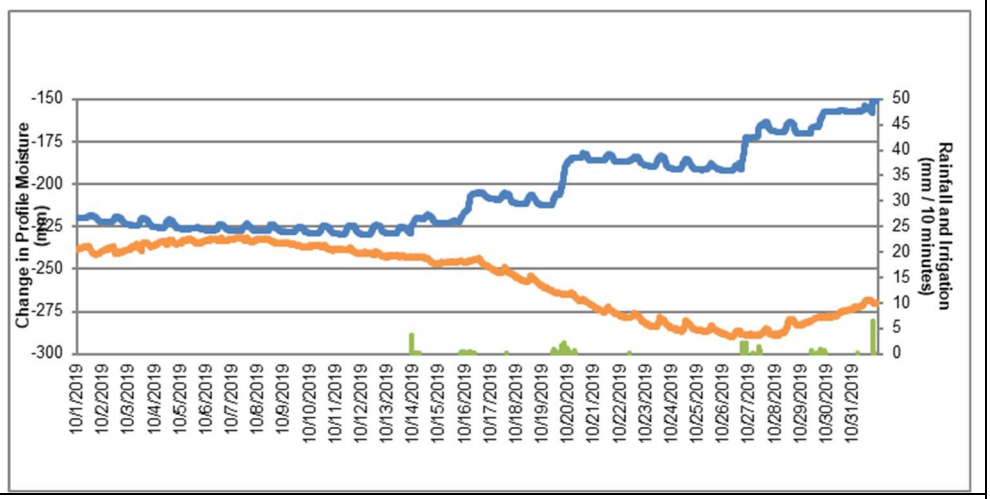

November	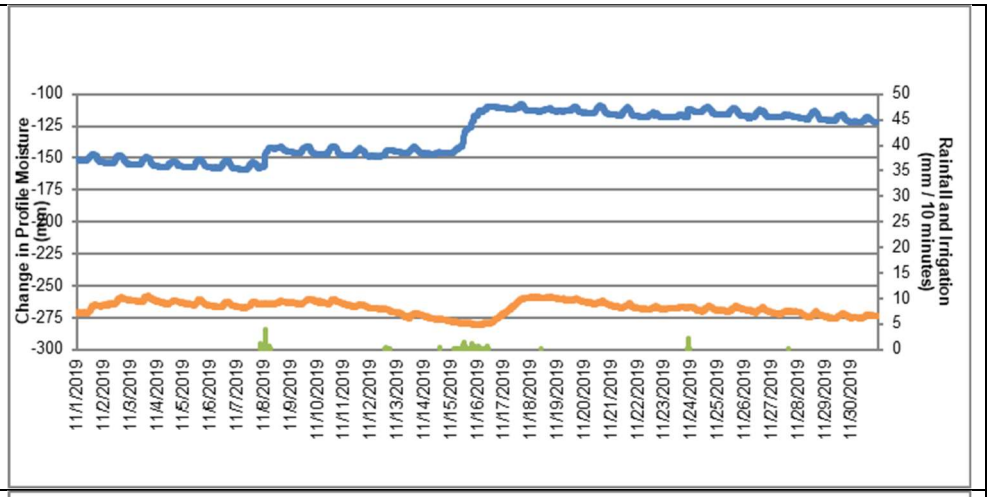
December	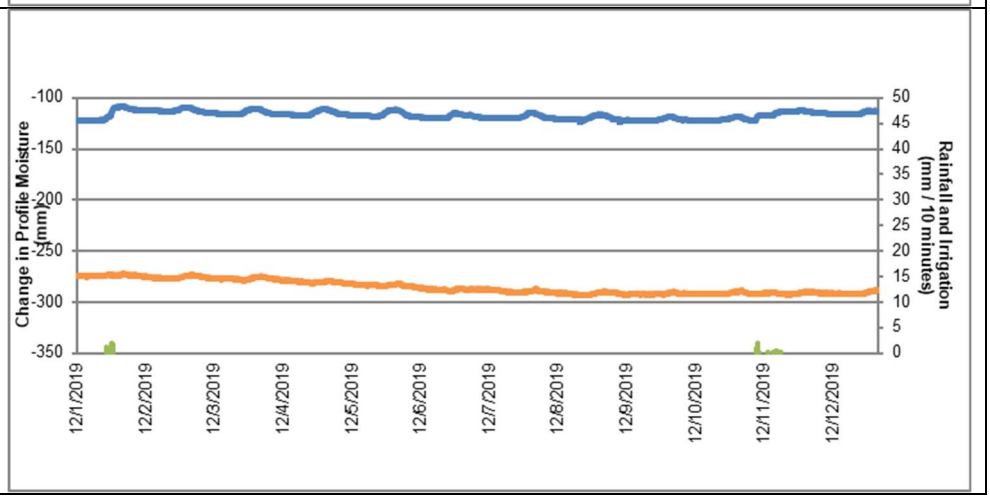

Figure H.1. Month by Month Comparison of PDD and Lysimeter

Appendix I

South Lysimeter / Pressure Differential Device Datalogger Program

```
'CR1000X Series
'Created by Short Cut (4.0)

'Declare Variables and Units
Public BattV
Public PTemp_C
Public DiffVolt(4)
Public Total_mV
Public Total_mm
Public Total_in
Public SoilMoist(7)
Public Mult(4)={1,1,1,1}
Public Offs(4)={0,0,0,0}
Public OutString As String * 2000
Public OutArray(20)
Public PMult(2)={1,1}
Public POffs(2)={0,0}
Public Rain_mm

Public eTape
Public Pressure(2)

Dim X

Units BattV=Volts
Units PTemp_C=Deg C
Units DiffVolt=mV
Units Total_mV=mV
Units Total_mm=mm
Units Total_in=in
Units SoilMoist =VWC
Units Pressure=mV
Units Rain_mm=mm
Units eTape=arb

'Define Data Tables
DataTable(Table1,True,-1)
		DataInterval(0,10,Min,10)
		CardOut(0,-1)
		Sample(4,DiffVolt(1),IEEE4)
		Sample(1,Total_mV,IEEE4)
		Sample(1,Total_mm,IEEE4)
		Sample(1,Total_in,IEEE4)
  Sample(1,BattV,FP2)
		Sample(7,SoilMoist(1),FP2)
		'Sample(2,Pressure(1),IEEE4)
		Average (2,Pressure(1),IEEE4,False)
		Average(1,eTape,IEEE4, False)
		Totalize (1,Rain_mm,FP2,False)
		Sample(1, OutString, String)

EndTable

DataTable(Table2,True,-1)
		DataInterval(0,1440,Min,10)
		CardOut(0,-1)
		Minimum(1,BattV,FP2,False,False)
		Sample(4,DiffVolt(1),IEEE4)
		Sample(1,Total_mV,IEEE4)
		Sample(1,Total_mm,IEEE4)
		Sample(1,Total_in,IEEE4)
		Sample(1,BattV,FP2)
		Sample(7,SoilMoist(1),FP2)
		Sample(2,Pressure(1),IEEE4)
		Sample(1,eTape,IEEE4)
		Totalize (1,Rain_mm,FP2,False)
EndTable
```

```
'Main Program
BeginProg

 SerialOpen (ComC1,9600,0,0,10000)

            'Main Scan
            Scan(10,Sec,1,0)
                        'Default CR1000X Datalogger Battery Voltage measurement 'BattV'
                        Battery(BattV)
                        'Default CR1000X Datalogger Wiring Panel Temperature measurement 'PTemp_C'
                        PanelTemp(PTemp_C,60)

  'Preload inactive moisture sensor error (cover all missing sensors)
  For X=1 To 7 Step 1
    SoilMoist(X)=-1000
  Next X

  SW12 (SW12_1,1 )

                        'Generic Differential Voltage measurements 'DiffVolt()'
                        VoltDiff(DiffVolt(),4,mV5000,1,True,500,60,Mult(),Offs())
                        Total_mV=DiffVolt(1)+DiffVolt(2)+DiffVolt(3)+DiffVolt(4)
                        Total_mm=31.449*Total_mV + 104.55    'Calibration for South Lysimeter-Jan 31 2019
                        Total_in=Total_mm/25.4

  SW12 (SW12_1,0)

  'Measure EnvironScan Probe with 7 sensors and 5 retries
  For X=1 To 5 Step 1
  SDI12Recorder (SoilMoist(),C7,0,"M!",1.0,0)
  Next X

  'Load moisture measurement failure errors
  If SoilMoist(1)=NAN Then   'If probe fails(NAN at first sensor), load -99999 to all sensors
    For X=1 To 7 Step 1
      SoilMoist(X)=-99999
    Next X
  EndIf

            'Measure 2 pressure sensors-Generic Single-Ended Voltage measurements 'SEVolt()'
            VoltSe(Pressure(),2,mV5000,9,True,500,60,PMult(),POffs())

            'Generic Single-Ended Voltage measurements 'eTape'
            VoltSe(eTape,1,mV5000,11,True,500,60,1,0)
            eTape = 1500/eTape  ' convert eTape Voltage to Resistance (Ohm)              .... 1500 is the resistance (Ohm) of the resistor in the eTape


  '--------------------------------------------------------------------------------------------------
  ' 1. Sample the rain gauge
  '--------------------------------------------------------------------------------------------------
  PulseCount(Rain_mm,1,P1,1,0,0.254,0)     'Used multiplier 0.254 for PulseCount instruction for mm and 0.01 for Inches

                        'Call Data Tables and Store Data
                        CallTable Table1
                        CallTable Table2
            NextScan

'Everything in the slow sequence runs in the background
 SlowSequence
    Scan(10,min,3,0)

       GetRecord (OutArray(),Table1,1)
       'OutString="7,"+OutArray(5)+","+OutArray(6)+","+OutArray(7)+","+OutArray(8)

OutString="7,"+FormatFloat(OutArray(5),"%f")+","+FormatFloat(OutArray(6),"%f")+","+FormatFloat(OutArray(7),"%f")+","+FormatFloat(OutArray(8
),"%f")+","+FormatFloat(OutArray(10),"%f")+","+FormatFloat(OutArray(16),"%f")
       SerialOut (ComC1,OutString,"",0,100)
    NextScan
 EndSequence



EndProg
```

Appendix J

Edisto Bull Forage Test Facility Rain Data

Table J.1. Edisto Bull Forage Test Facility Rainfall Data

Date	Rain (mm)
5/25/2019	0
5/26/2019	0
5/27/2019	0
5/28/2019	0
5/29/2019	0
5/30/2019	0
5/31/2019	0
6/1/2019	0
6/2/2019	0
6/3/2019	0
6/4/2019	1.0
6/5/2019	18.3
6/6/2019	0.5
6/7/2019	19.6
6/8/2019	36.3
6/9/2019	26.4
6/10/2019	11.2
6/11/2019	0.3
6/12/2019	9.9
6/13/2019	0
6/14/2019	0
6/15/2019	0
6/16/2019	0
6/17/2019	0
6/18/2019	14.0
6/19/2019	1.0
6/20/2019	9.9
6/21/2019	0
6/22/2019	9.7
6/23/2019	10.7
6/24/2019	6.9
6/25/2019	0.3
6/26/2019	0
6/27/2019	0
6/28/2019	0
6/29/2019	0.8
6/30/2019	0
7/1/2019	7.6
7/2/2019	0
7/3/2019	0
7/4/2019	0.5
7/5/2019	6.9
7/6/2019	0
7/7/2019	0
7/8/2019	0
7/9/2019	0
7/10/2019	0.5
7/11/2019	0
7/12/2019	0
7/13/2019	0
7/14/2019	0
7/15/2019	6.1
7/16/2019	0
7/17/2019	0
7/18/2019	2.5
7/19/2019	0.3
7/20/2019	0
7/21/2019	0
7/22/2019	0
7/23/2019	6.6
7/24/2019	0.3
7/25/2019	0
7/26/2019	0
7/27/2019	0
7/28/2019	0
7/29/2019	0
7/30/2019	0
7/31/2019	11.9
8/1/2019	0
8/7/2019	0
8/8/2019	0
8/9/2019	0
8/10/2019	1.3
8/11/2019	0.3
8/12/2019	0
8/13/2019	0
8/14/2019	0.3
8/15/2019	0.3
8/16/2019	0
8/17/2019	13.0
8/18/2019	0
8/19/2019	0
8/20/2019	0.5
8/21/2019	0
8/22/2019	0
8/23/2019	59.9
8/24/2019	22.6
8/25/2019	0
8/26/2019	0
8/27/2019	0.8
8/28/2019	0
8/29/2019	0
8/30/2019	0
8/31/2019	0
9/1/2019	4.8
9/2/2019	0.3
9/3/2019	0
9/4/2019	0
9/5/2019	0.5
9/6/2019	0
9/7/2019	0
9/8/2019	0
9/9/2019	0
9/10/2019	0
9/11/2019	0
9/12/2019	0
9/13/2019	2.8
9/14/2019	0
9/15/2019	0
9/16/2019	0
9/17/2019	0
9/18/2019	0.5
9/19/2019	0
9/20/2019	0
9/21/2019	0
9/22/2019	0
9/23/2019	0
9/24/2019	0
9/25/2019	0
9/26/2019	0
9/27/2019	0
9/28/2019	0
9/29/2019	0
9/30/2019	4.0
10/1/2019	0
10/2/2019	0
10/3/2019	0
10/4/2019	0
10/5/2019	0
10/6/2019	0
10/7/2019	0
10/8/2019	0
10/9/2019	0
10/10/2019	0
10/11/2019	0
10/12/2019	0
10/13/2019	5.6
10/14/2019	4.1
10/15/2019	6.4
10/16/2019	10.4
10/17/2019	0
10/18/2019	0
10/19/2019	24.1
10/20/2019	2.8
10/21/2019	0
10/22/2019	0.8
10/23/2019	0
10/24/2019	0
10/25/2019	0
10/26/2019	18.5
10/27/2019	7.1
10/28/2019	0
10/29/2019	13.7
10/30/2019	0
10/31/2019	8.4
11/1/2019	0
11/2/2019	0
11/3/2019	0
11/4/2019	0
11/5/2019	0
11/6/2019	0
11/7/2019	9.4
11/8/2019	6.1
11/9/2019	0
11/10/2019	0
11/11/2019	0

(Sell, 2019)

Appendix K

Cost Comparison Analysis of Each Method

Table K.1. Total Equipment Cost

Part	Cost Per Part	# of Parts per Setup	Total Costs per Setup	# of Setups	Total Equipment Costs
In-Field Weighing Lysimeters					
Box Assembly / Drainage System / Soil Volumetric Water Sensor	$ 1,418.75	1	$ 1,418.75		
*Using CPI Inflation Adjustment from Fisher's 2001 Costs					
Load Cells	$ 50.00	4	$ 200.00		
			$ 1,618.75	2	$ 3,237.49
Pressure Differential Device (Device 3.3)					
Irrigation Hose	$ 46.00	1	$ 46.00		
PVC Riser	$ 3.29	1	$ 3.29		
90 Degree Elbow Adapter	$ 0.44	1	$ 0.44		
Worm-Drive Hose Clamps	$ 1.46	1	$ 1.46		
4" End Cap	$ 5.89	1	$ 5.89		
4" Reducing Assembly to 3/4"	$ 24.26	1	$ 24.26		
Ball Valve	$ 10.06	1	$ 10.06		
Sensor Housing	$ 0.53	1	$ 0.53		
Pressure Transducers	$ 147.04	2	$ 294.08		
3/4" Threaded Plug	$ 0.85	1	$ 0.85		
			$ 386.86	1	$ 386.86
Eddy Covariance Method					
3D Sonic Anemometer	$ 3,000.00	1	$ 3,000.00		
Total			$ 3,000.00	2	$ 6,000.00
Surface Renewal Method					
Fine-Wire Thermocouples	$ 225.00	2	$ 450.00		
Total			$ 450.00	2	$ 900.00
Eddy Covariance/Surface Renewal (Shared) Cost					
Net Radiometer	$ 1,300.00	1	$ 1,300.00		
Rain gauge	N/A	1	N/A		
Soil Heat Flux Plate Pair	$ 700.00	2	$ 1,400.00		
Soil Moisture and Temperature Probe	$ 300.00	2	$ 600.00		
Tower	$ 700.00	1	$ 700.00		
Relative Humidity Sensor	$ 400.00	1	$ 400.00		
Pyranometer	$ 300.00	1	$ 300.00		
Total			$ 4,700.00	2	$ 9,400.00
Additional Needs for all setups					
Datalogger	$ 1,700.00			2	$ 3,400.00
Loggernet Software	$ 724.80				$ 724.80
Solar Panel	$ 50.00			2	$ 100.00
12V Battery	$ 120.00			2	$ 240.00
Total Expenses listed					$ 24,389.15

Table K.2. Lysimeter Design Material Costs as of 2001

1m x 1m Surface Area Lysimeter

assembly	description	size			qty	price
			in	cm		
inner tank	steel plate	3/16 thick	59.3 x 39.4	150 x 100	4	
	steel plate	3/16 thick	39.4 x 39.4	100 x 100	1	
	steel structural channel	3 x 1.6 flange x 0.36 web	39	99	10	
outer tank	steel plate	3/16 thick	65.1 x 40.9	165.3 x 104	4	
	steel plate	3/16 thick	40.9 x 40.9	104 x 104	1	$750
	steel structural channel	3 x 1.6 flange x 0.36 web	41.3	105	8	
	steel structural channel	3 x 1.6 flange x 0.36 web	40.5	103	2	
	steel bar	1.5 x 1	2.2	5.7	4	
loadcell	loadcells	2000 lb			4	$205 ea
	leveling mounts	½ - 20 UNF			4	$25 ea
	bolts	½ - 20 UNF	2.5		8	
drain	PVC pipe, perforated	4 in OD	36	91	1	$30 est
	PVC pipe	4 in OD	43	110	1	
	PVC pipe	2 in OD	12	31	1	
	PVC pipe cap	2 in OD			1	
	PVC reducer	4 x 2			1	
moisture sensors	Watermark sensors	3 inside, 3 outside			6	$200

Parts list and approximate cost (excluding labor to fabricate) of 1m x 1m lysimeter

Source: (Fisher, 2003)

Fisher, K. (2003). *Lysimeter work at stoneville, mississippi*. Jamie Whitten Delta States Research Center, 141 Experiment Station Road Stoneville, Mississippi 38776: USDA Agricultural Research Service.

Appendix L

Irrigation Log Data

Table L.1. Edisto REC Field A12 Irrigation Data

Activity Date	Employee	Field	Irrigation Depth
5/21/2019	Becky Davis	A12A; A12D	.5 in.
5/22/2019	Becky Davis	A12A; A12D	.25 in.
5/28/2019	Becky Davis	A12A; A12D	.75 in.
6/3/2019	Becky Davis	A12A; A12D	.75 in.
7/19/2019	[Other: Bayleah Cooper]	A12A	.75 in.
7/15/2019	Becky Davis	A12A	1 in.
7/30/2019	Becky Davis	A12A	1 in.
8/8/2019	Becky Davis	A12A	1 in.
8/13/2019	Becky Davis	A12A	1 in.
8/16/2019	[Other: Bayleah Cooper]	A12A	1 in.
8/22/2019	Becky Davis	A12A	1 in.
9/10/2019	Becky Davis	A12A	1 in.
9/17/2019	Becky Davis	A12A	1 in.
9/24/2019	Becky Davis	A12A	1 in.

Appendix M

Coursework

Table M.1 Master's GS2 Coursework

	Fall 2018	Spring 2019	Summer 2019	Fall 2019	Spring 2020	Summer 2020	Totals
Remedial Course:	CE 2080-Dynamics (2)	CE 3410/3411-Fluid Mechanics (4)			BE 3220-Small Watershed Hydrology and Sedimentology (3)		9
Graduate Courses:	STAT 8010-Statistical Methods I (3)	STAT 8050-Design and Analysis of Experiments (3)		GEOL 8080-Groundwater Modeling (3)	EES 8200-Environmental Systems Analysis (3)		> 8000: 15
	BE 8710-Geomatics (3)	BE 6150/6151-Instrumentation and Controls for Biosystems Engineers (3)		BE 6210/6211-Engineering Systems for Soil Water Management (2)	BE 6240-Ecological Engineering (3)		< 8000: 11
				GEOL 6820-Ground Water and Contaminant Transport (3)			
Research Hours:	2	2	3			6	> 6
Seminar	EEES (1)	Newman (1)		EEES (1)	Newman (1)		
TOTAL	11	13	3	9	10		42